Prof. Yu Huang
State Key Lab of Loess and Quaternary Geology
Institute of Earth Environment, Chinese Academy of Sciences, Xi'an, 710061, China
Tel./Fax: (86) 29-62336261
E-mail: huangyu@ieecas.cn

Jan. 27, 2022

Dear Prof. Chan,

Revision for Manuscript acp-2021-890

We thank you very much for giving us the opportunity to revise our manuscript. We highly appreciate the reviewers for their comments and suggestions on the manuscript entitled "**OH-initiated atmospheric degradation of hydroxyalkyl hydroperoxides: mechanism, kinetics, and structure-activity relationship**". We have made revisions of our manuscript carefully according to the comments and suggestions of reviewers. The revised contents are marked in blue color. The response letter to reviewers is attached at the end of this cover letter.

We hope that the revised manuscript can meet the requirement of Atmospheric Chemistry & Physics. Any further modifications or revisions, please do not hesitate to contact us.

Look forward to hearing from you as soon as possible.

Best regards,

Yu Huang

Comments of reviewer #1

1. The investigated HHPs are generated from the reactions of CH_2OO, anti-CH_3CHOO and $(CH_3)_2COO$ with water vapor, not considering the HHP from the bimolecular reaction of syn-CH_3CHOO with water. This should be stated.

Response: Based on the Reviewer's suggestion, OH-initiated oxidation of hydroxyalkyl hydroperoxide (HHP), generated from the bimolecular reaction of *syn*-CH_3CHOO with water, has been added in the revised manuscript. The corresponding free-energy and electronic-energy potential energy surface (PES) are displayed in Figures S4 and S5, respectively. As shown in Figure S4, the H-abstraction by OH radical from $HOCH(CH_3)OOH$ has six kinds of pathways. For each pathway, a per-reactive complex is formed prior to the corresponding transition state, and then it overcomes modest barrier to reaction. The $\Delta G_a^{\#}$ of R6' and R8' are 2.3 and 1.8 kcal mol^{-1}, respectively, which are ~ 5 kcal mol^{-1} lower than those of R5' and R7'. This result shows that H-abstraction from the -CH (R6') and -OOH (R8') groups are preferable kinetically. Same conclusion is also derived from the energy barriers $\Delta E_a^{\#}$ that R6' and R8' the most favourable H-abstraction pathways (Figure S5). It should be noted that although the barriers of R6' and R8' are comparable, the exoergicity of the former case is significantly lower than that of the latter case. The above-mentioned conclusions are consistent with the results derived from the OH-initiated oxidation of $HOCH(CH_3)OOH$ from the *anti*-CH_3CHOO + H_2O reaction. Zhou et al. has demonstrated that the bimolecular reaction of *syn*-CH_3CHOO with water leading to the formation of $HOCH(CH_3)OOH$ is of less importance in the atmosphere, while the unimolecular decay to OH radical is the major loss process of *syn*-CH_3CHOO (Zhou et al., 2019). Therefore, in the present study, we mainly focus on the subsequent mechanism of intermediate generated from OH-initiated oxidation of $HOCH(CH_3)OOH$ from the *anti*-CH_3CHOO + H_2O reaction.

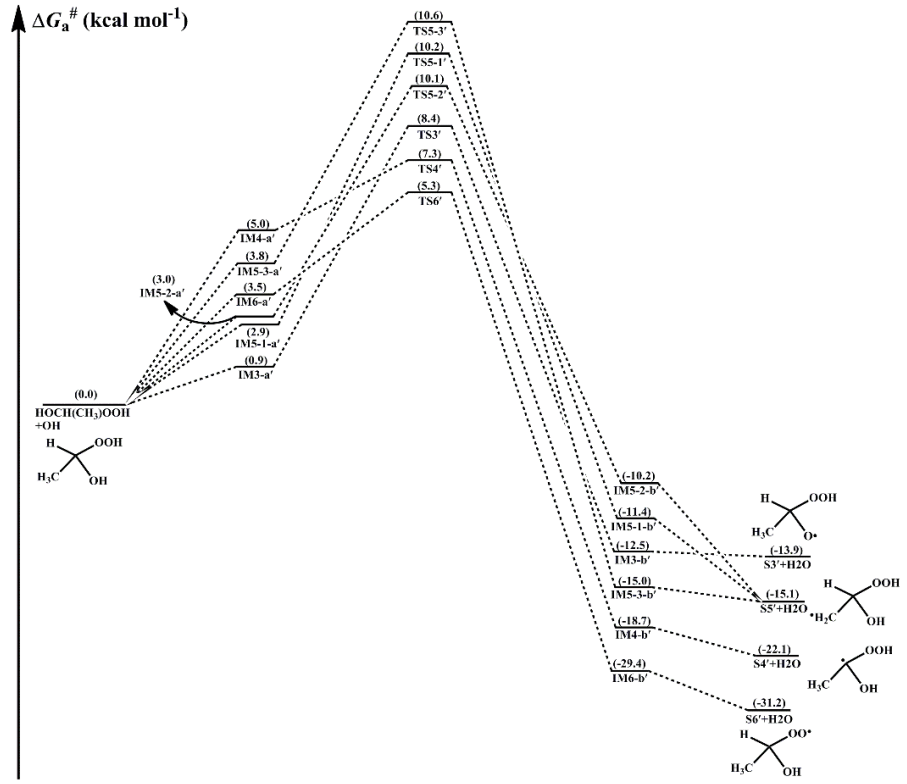

Figure S4. PES ($\Delta G_a^{\#}$) for the OH-initiated reactions of $HOCH(CH_3)OOH$ from the *syn*-CH_3CHOO + H_2O reaction predicted at the M06-2X/ma-TZVP//M06-2X/6-311+G(2df,2p) level of theory (a and b represent the pre-reactive and post-reactive complexes)

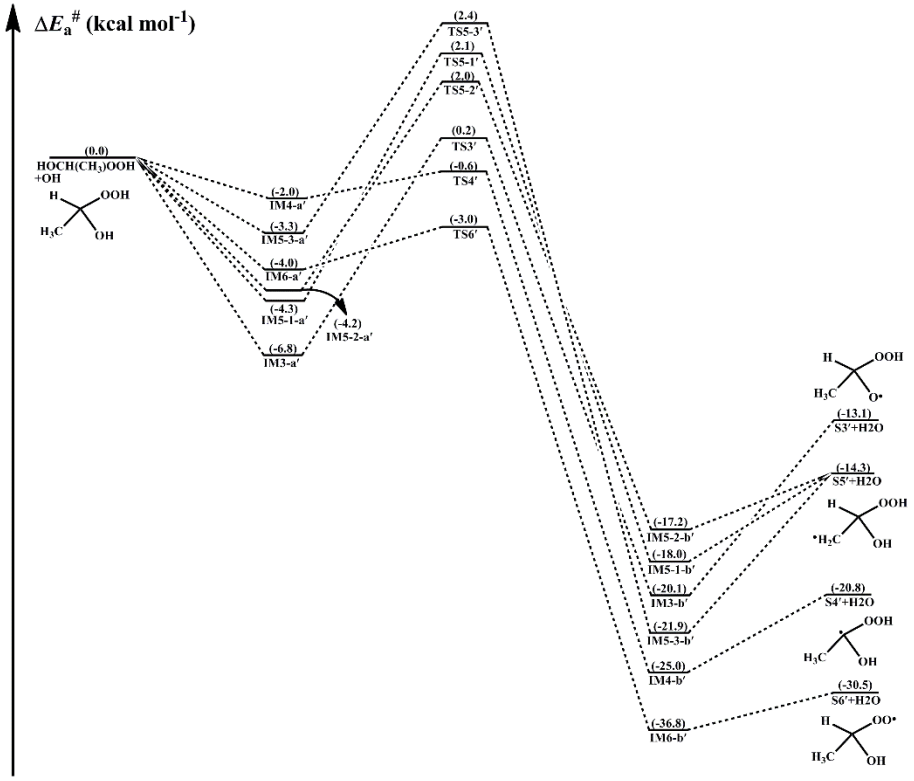

Figure S5. PES ($\Delta E_a^{\#}$) for the OH-initiated reactions of $HOCH(CH_3)OOH$ from the *syn*-CH_3CHOO + H_2O reaction predicted at the M06-2X/ma-TZVP//M06-2X/6-311+G(2df,2p) level of theory (a and b represent the pre-reactive and post-reactive complexes)

Corresponding descriptions have been added in the page 11 line 289-308 of the revised manuscript:

For the OH-initiated oxidation of $HOCH(CH_3)OOH$ from the syn-CH_3CHOO + H_2O reaction, the corresponding free-energy and electronic-energy PESs are displayed in Figures S4 and S5, respectively. From Figure S4, it can be seen the H-abstraction by OH radical from $HOCH(CH_3)OOH$ has six kinds of pathways. For each pathway, a per-reactive complex is formed prior to the corresponding transition state, and then it overcomes modest barrier to reaction. The $\Delta G_a^{\#}$ of R6' and R8' are 2.3 and 1.8 kcal mol^{-1}, respectively, which are about 5 kcal mol^{-1} lower than those of R5' and R7'. This result shows that H-abstraction from the -CH (R6') and -OOH (R8') groups are preferable kinetically. Same conclusion is also derived from the energy barriers $\Delta E_a^{\#}$ that the R6' and R8' the most favourable H-abstraction pathways (Figure S5). It should be noted that although the barriers of R6' and R8' are comparable, the exoergicity of the former case is significantly lower than that of the latter case. The above-mentioned conclusions are consistent with the results derived from the OH-initiated oxidation of $HOCH(CH_3)OOH$ from the anti-CH_3CHOO + H_2O reaction. Zhou et al. has demonstrated that the bimolecular reaction of syn-CH_3CHOO with water leading to the formation of $HOCH(CH_3)OOH$ is of less importance in the atmosphere, while the unimolecular decay to OH radical is the major loss process of syn-CH_3CHOO (Zhou et al., 2019). Therefore, in the present study, we mainly focus on the subsequent mechanism of intermediate generated from OH-initiated oxidation of $HOCH(CH_3)OOH$ from the anti-CH_3CHOO + H_2O reaction.

2. Line 226-228, the reaction barriers are reduced in the order of 6.4 (R1) > 5.8 (R3) ≈ 5.4 (R2) > 1.5 (R4) kcal mol^{-1}, indicating that H-abstraction from the -OOH group is the most favorable. The authors should explain the order of TS1, TS3, TS2, and TS4 in the initial H-abstraction reactions.

Response: Based on the Reviewer's suggestion, the corresponding explanations on the order of barrier heights of H-abstraction reactions have been added in the revised manuscript. A schematic PES for the initiation reactions of OH radical with $HOCH_2OOH$ is drawn in Figure 2. As can be seen in Figure 2, the reaction for $HOCH_2OOH$ with OH radical proceeds via four distinct pathways: H-abstraction from the -O_1H_1 (R1), -C_1H_3 (R2), -C_1H_4 (R3) and -$O_2O_3H_2$ groups (R4). For each pathway, a pre-reactive complex with a six- or seven-membered ring

structure is formed in the entrance channel, which is stabilized by hydrogen bond interactions between the oxygen atom of OH radical and the abstraction hydrogen atom of $HOCH_2OOH$, and the remnant hydrogen atom of OH radical and one of oxygen atoms of $HOCH_2OOH$. Then, it surmounts modest barrier that is higher in energy than the reactants to reaction. The reaction barrier $\Delta G_a^{\#}$ are reduced in the order of 6.4 (R1) > 5.8 (R2) ≈ 5.4 (R3) > 1.5 (R4) kcal mol^{-1}, indicating that H-abstraction from the $-O_2O_3H_2$ group (R4) is more preferable than those from the $-O_1H_1$, $-C_1H_3$ and $-C_1H_4$ groups (R1-R3). Same conclusion is also derived from the energy barriers $\Delta E_a^{\#}$ that R4 is the most favorable H-abstraction pathway (Figure S1). The difference of barrier heights can be attributed to the bond dissociation energy (BDE) of different types of bonds in $HOCH_2OOH$ molecule. The BDE are decreased in the order of 103.7 (O_1-H_1) > 98.2 (C_1-H_3) ≈ 97.4 (C_1-H_4) > 87.2 (O_3-H_2) kcal mol^{-1}, which are in good agreement with the order of barrier heights of H-abstraction reactions.

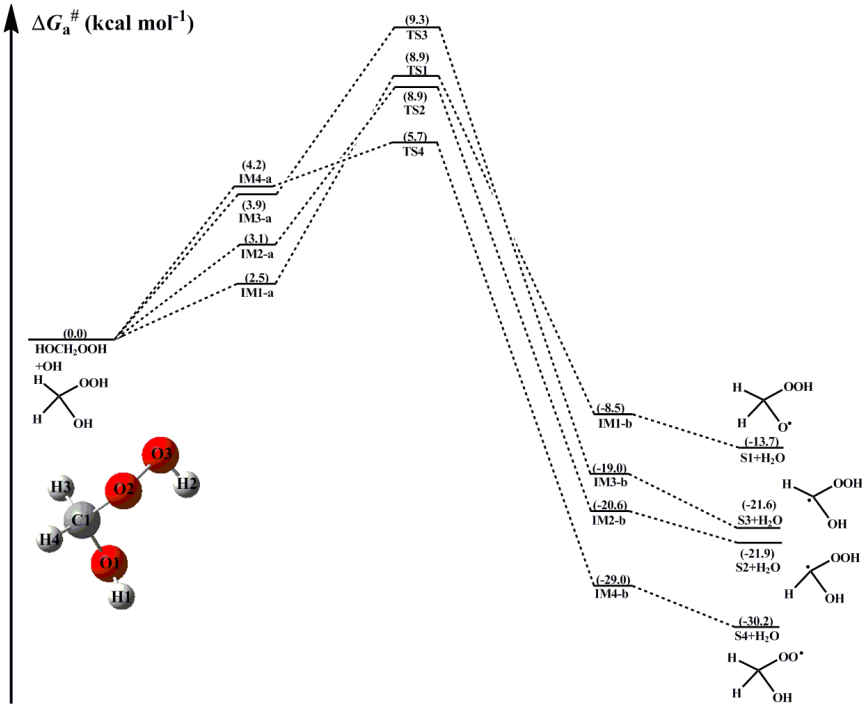

Figure 2. PES ($\Delta G_a^{\#}$) for the OH-initiated reactions of $HOCH_2OOH$ from the CH_2OO + H_2O reaction predicted at the M06-2X/ma-TZVP//M06-2X/6-311+G(2df,2p) level of theory (a and b represent the pre-reactive and post-reactive complexes)

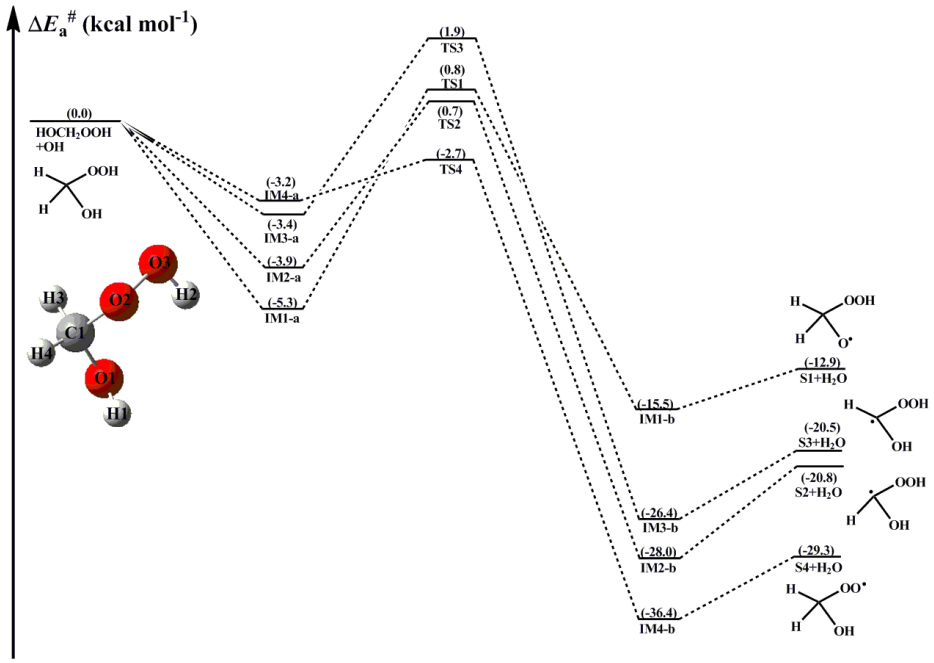

Figure S1. PES ($\Delta E_a^{\#}$) for the OH-initiated reactions of $HOCH_2OOH$ from the CH_2OO + H_2O reaction predicted at the M06-2X/ma-TZVP//M06-2X/6-311+G(2df,2p) level of theory (a and b represent the pre-reactive and post-reactive complexes)

Corresponding descriptions have been added in the page 10 line 253-269 of the revised manuscript:

As can be seen in Figure 2, the reaction for $HOCH_2OOH$ with OH radical proceeds via four distinct pathways: H-abstraction from the -O_1H_1 (R1), -C_1H_3 (R2), -C_1H_4 (R3) and -$O_2O_3H_2$ groups (R4). For each pathway, a pre-reactive complex with a six- or seven-membered ring structure is formed in the entrance channel, which is stabilized by hydrogen bond interactions between the oxygen atom of OH radical and the abstraction hydrogen atom of $HOCH_2OOH$, and the remnant hydrogen atom of OH radical and one of oxygen atoms of $HOCH_2OOH$. Then, it surmounts modest barrier that is higher in energy than the reactants to reaction. The reaction barrier $\Delta G_a^{\#}$ are reduced in the order of 6.4 (R1) > 5.8 (R2) ≈ 5.4 (R3) > 1.5 (R4) kcal mol^{-1}, indicating that H-abstraction from the -$O_2O_3H_2$ group (R4) is more preferable than those from the -O_1H_1, -C_1H_3 and -C_1H_4 groups (R1-R3). Same conclusion is also derived from the energy barriers $\Delta E_a^{\#}$ that R4 is the most favorable H-abstraction pathway (Figure S1). The difference of barrier heights can be attributed to the bond dissociation energy (BDE) of different types of bonds in $HOCH_2OOH$ molecule. The BDE are decreased in the order of 103.7 (O_1-H_1) > 98.2 (C_1-H_3) ≈ 97.4 (C_1-H_4) > 87.2 (O_3-H_2) kcal mol^{-1}, which are in good agreement with the order of barrier heights of H-abstraction reactions.

3. The authors discuss the mechanism of RO_2 reactions with HO_2. But there is no information provided on HO_2. They must describe how HO_2 is formed in the atmosphere, what is its concentration, and where this reaction could be relevant.

Response: Based on the Reviewer's suggestion, the relevant information on the production of HO_2 radical has been added in the revised manuscript. The main sources of HO_2 radcial involve the photo-oxidation of oxygenated volatile organic compounds (OVOCs) and the ozonolysis reaction, as well as senondary sources include the reactions of OH radical with CO, ozone and volatile organic compounds (VOCs), the reaction of alkoxy radcial RO with O_2 and the red-light-induced decomposition of α-hydroxy methylperoxy radical $OHCH_2OO$ (Stone et al., 2012; Hofzumahaus et al., 2009; Kumar et al., 2015). The atmospheric concentration of HO_2 radical is 1.5-10 $\times 10^8$ molecules cm^{-3} at ground level in polluted urban environments (Stone et al., 2012).

Corresponding descriptions have been added in the page 21 line 496-503 of the revised manuscript:

The main sources of HO_2 radical involve the photo-oxidation of oxygenated volatile organic compounds (OVOCs) and the ozonolysis reaction, as well as senondary sources include the reactions of OH radical with CO, ozone and volatile organic compounds (VOCs), the reaction of alkoxy radical RO with O_2 and the red-light-induced decomposition of α-hydroxy methylperoxy radical $OHCH_2OO$ (Kumar et al., 2015; Stone et al., 2012; Hofzumahaus et al., 2009). The atmospheric concentration of HO_2 radical is 1.5-10 $\times 10^8$ molecules cm^{-3} at ground level in polluted urban environments (Stone et al., 2012).

4. Authors should compare $k_{MC\text{-}TST}$ and the pseudo first-order rates (k'_{HO2} and k'_{NO}) for the bimolecular processes (HO_2 reaction and NO reaction) as a function of concentration. See the recent review of autoxidation by Bianchi et al. (Chem. Rev. 2019, 119, 6, 3472-3509).

Response: As the Reviewer's said, the relative importance of different transformation pathways (unimolecular, $HO_2\cdot$ and NO reactions) of peroxy radicals RO_2 is significantly dependent on the rate coefficients and coreactant concentrations. For the H-shift reaction of RO_2 radicals, the multi-conformer rate coefficient $k_{MC\text{-}TST}$ can be calculated by the weighted sum of the single-conformer rate coefficient $k_{IRC\text{-}TST}$. At room temperature, $k_{MC\text{-}TST}$ of first H-shift reaction of

$HOCH_2OO$ radical is calculated to be 4.4×10^{-16} s^{-1}. The room temperature rate coefficient of $HOCH_2OO$ radical reaction with HO_2 radical is estimated to be 1.7×10^{-11} cm^3 $molecule^{-1}$ s^{-1}. The typical atmospheric concentrations of HO_2 radical are 5, 20 and 50 pptv in the urban, rural and forest environments (Bianchi et al., 2019), translating into the pseudo-first-order rate constants $k'_{HO2} = k_{HO2}[HO_2]$ of 1.1×10^{-3}, 4.2×10^{-3} and 1.1×10^{-2} s^{-1}, respectively.

The typical atmospheric concentrations of NO are about 10 ppbv, 1 ppbv and 20 pptv in the urban, rural and forest environments (Bianchi et al., 2019). The rate coefficient of $HOCH_2OO$ radical reaction with NO is calculated to be 4.3×10^{-12} cm^3 $molecule^{-1}$ s^{-1} at room temperature, resulting in the pseudo-first-order rate constants $k'_{NO} = k_{NO}[NO]$ of 6.5×10^{-1}, 6.5×10^{-2}, and 1.3×10^{-3}, respectively, in the urban, rural and forest environments. It is of interest to assess the relative importance for the H-shift reaction of $HOCH_2OO$ radical and bimolecular reactions with HO_2 ·and NO based on the calculated $k_{MC\text{-}TST}$, k'_{HO2} and k'_{NO}. It can be found that the H-shift reaction is of less importance, the HO_2 radical reaction is favourable in the forest environment, the NO reaction is predominant in the urban and rural regions. Similar conclusion is also obtained from the cases of $HOCH(CH_3)OO$ and $HO(CH_3)_2CHOO$ radicals.

Corresponding descriptions have been added in the page 22 line 525-531 and page 27 line 653-664 of the revised manuscript:

At ambient temperature, k_{R31} is estimated to be 1.7×10^{-11} cm^3 $molecule^{-1}$ s^{-1}, which is in good agreement with the value of ~2×10^{-11} cm^3 $molecule^{-1}$ s^{-1} for the reaction of acyl peroxy radicals with HO_2 radical (Wennberg et al., 2018). The typical atmospheric concentrations of HO_2 radical are about 5, 20 and 50 pptv in the urban, rural and forest environments (Bianchi et al., 2019), translating into the pseudo-first-order rate constants $k'_{HO2} = k_{HO2}[HO_2]$ of 1.1×10^{-3}, 4.2×10^{-3} and 1.1×10^{-2} s^{-1}, respectively.

The typical atmospheric concentrations of NO are about 10 ppbv, 1 ppbv and 20 pptv in the urban, rural and forest environments (Bianchi et al., 2019). The rate coefficient of $HOCH_2OO$ · reaction with NO is calculated to be 4.3×10^{-12} cm^3 $molecule^{-1}$ s^{-1} at room temperature, resulting in the pseudo-first-order rate constants $k'_{NO} = k_{NO}[NO]$ of 6.5×10^{-1}, 6.5×10^{-2}, and 1.3×10^{-3}, respectively, in the urban, rural and forest environments. It is of interest to assess the relative importance for the H-shift reaction of $HOCH_2OO$ radical and bimolecular reactions with HO_2 ·and NO based on the calculated $k_{MC\text{-}TST}$, k'_{HO2} and k'_{NO}. It can be found that

the H-shift reaction is of less importance, the HO_2 radical reaction is favorable in the forest environment, while the NO reaction is predominant in the urban and rural regions. Similar conclusion is also obtained from the cases of $HOCH(CH_3)OO$ and $HO(CH_3)_2CHOO$ radicals.

5. For the alkoxy radical fragmentation, the author should calculate rate constants in the temperature range studied.

Response: Based on the Reviewer's suggestion, the rate coefficients of the dominant pathways of alkoxyl radical fragmentation have been calculated over the temperature range of 273-400 K. The corresponding results are listed in Table S12 of the revised manuscript. For the fragmentation of $HOCH_2O$ radical, the dominant pathway is H-abstraction by O_2 from $HOCH_2O$ radical resulting in formation of HCOOH and HO_2 radical (R41). For the fragmentation of $HOCH(CH_3)O$ and $HOC(CH_3)_2O$ radicals, the dominant pathways are β-site C-C bond scission leading to the formation of HCOOH + $CH_3\cdot$(R45) and CH_3COOH + $CH_3\cdot$(R51). As can be seen in Table S12, k_{R41} is slightly increased with the temperature increasing, and the discrepancy is about a factor of 12 at the two extremes of temperature. At ground level with $[O_2]$ = ~ 5.0×10^{18} molecule cm^{-3}, the pseudo-first-order rate constant $k'_{O2} = k_{R41}[O_2]$ is estimated to be 38.0 s^{-1} at room temperature. k_{R45} vary significantly from 2.0×10^6 (273 K) to 3.1×10^8 (400 K) s^{-1}, and they exhibit a marked positive temperature dependence. Similar phenomenon is also observed from k_{R51} that k_{R51} is significantly increased with the temperature increasing. k_{R51} is a factor of ~ 1.3 greater than k_{R45} in the temperature range studied, implying that the rate coefficient of β-site C-C bond scission is slightly increased as the number of methyl group is increased.

Table S12 Rate coefficients of the dominant pathways of the fragmentation of $HOCH_2O\cdot$(R41), $HOCH(CH_3)O\cdot$(R45) and $HO(CH_3)_2CO\cdot$(R51) computed at different temperatures

T/K	k_{R41}(cm^3 $molecule^{-1}$ s^{-1})	k_{R45}(s^{-1})	k_{R51}(s^{-1})
273	4.3×10^{-18}	2.0×10^6	2.6×10^6
280	5.0×10^{-18}	2.9×10^6	3.8×10^6
298	7.6×10^{-18}	7.3×10^6	9.5×10^6
300	7.9×10^{-18}	8.1×10^6	1.0×10^7
320	1.2×10^{-17}	1.9×10^7	2.5×10^7
340	1.8×10^{-17}	4.4×10^7	5.6×10^7
360	2.6×10^{-17}	9.0×10^7	1.1×10^8

380	3.7×10^{-17}	1.7×10^{8}	2.2×10^{8}
400	5.1×10^{-17}	3.1×10^{8}	3.8×10^{8}

Corresponding descriptions have been revised in the page 26 line 625-629, page 27 line 633-640, page 27 line 648-652 and page 28 line 655-675 of the revised manuscript:

The formed $HOCH_2O$ radical has two kinds of pathways: (1) it directly decomposes into CH_2O and OH radical (R40) via β-site C_1-O_1 bond scission with the barrier of 52.4 kcal mol^{-1}; (2) it converts into HCOOH and HO_2 radical (R41) through H-abstraction by O_2 with the barrier of 26.4 kcal mol^{-1}. This result reveals that R41 is the most feasible channel in the fragmentation of $HOCH_2O$ radical.

The resulting $HOCH(CH_3)O$ radical has three types of pathways. The first one is β-site C_1-C_2 bond scission leading to the formation of HCOOH + CH_3 (R45) with the barrier of 8.3 kcal mol^{-1}. The second one is β-site C_1-O_1 bond cleavage resulting in formation of CH_3COH + OH (R46) with the barrier of 26.7 kcal mol^{-1}. The third one is H-abstraction by O_2 leading to CH_3COOH + HO_2 ·(R47) with the barrier of 26.2 kcal mol^{-1}. Based on the calculated reaction barriers, it can be found that β-site C_1-C_2 bond scission is the dominant pathway in the fragmentation of $HOCH(CH_3)O$ radical.

The formed $HO(CH_3)_2CO$ radical can either dissociate to CH_3COOH + CH_3 ·(R51) via the C_1-C_3 bond scission with the barrier of 8.2 kcal mol^{-1}, or decompose into CH_3COCH_3 + OH (R52) through the C_1-O_1 bond breaking with the barrier of 24.3 kcal mol^{-1}. The result again shows that the β-site C-C bond scission is the dominate pathway.

The rate coefficients of the dominant pathways of $HOCH_2O$, $HOCH(CH_3)O$ and $HO(CH_3)_2CHO$ radicals fragmentation are summarized in Table S12. As can be seen in Table S12, k_{R41} is slightly increased with the temperature increasing, and the discrepancy is about a factor of 12 at the two extremes of temperature. At ground level with $[O_2]$ = ~ 5.0×10^{18} molecule cm^{-3}, the pseudo-first-order rate constant $k'_{O2} = k_{R41}[O_2]$ is estimated to be 38.0 s^{-1} at room temperature. k_{R45} vary significantly from 2.0×10^{6} (273 K) to 3.1×10^{8} (400 K) s^{-1}, and they exhibit a marked positive temperature dependence. Similar phenomenon is also observed from k_{R51} that k_{R51} is significantly increased with increasing temperature. k_{R51} is a factor of ~ 1.3 greater than k_{R45} in the temperature range studied, implying that the rate coefficient of β-site C-C bond scission is slightly increased as the number of methyl group is increased.

6. The prefix ‘anti’ should be italicized throughout the manuscript.

Response: Based on the Reviewer’s suggestion, the prefix ‘anti’ is italicized throughout the manuscript.

7. The italics/non-italics energies in Fig. S13 and S14 in the supplement are not always in the same vertical order.

Response: Based on the Reviewer’s suggestion, the non-italics energies have been placed in the upper number in Figures S13 and S14.

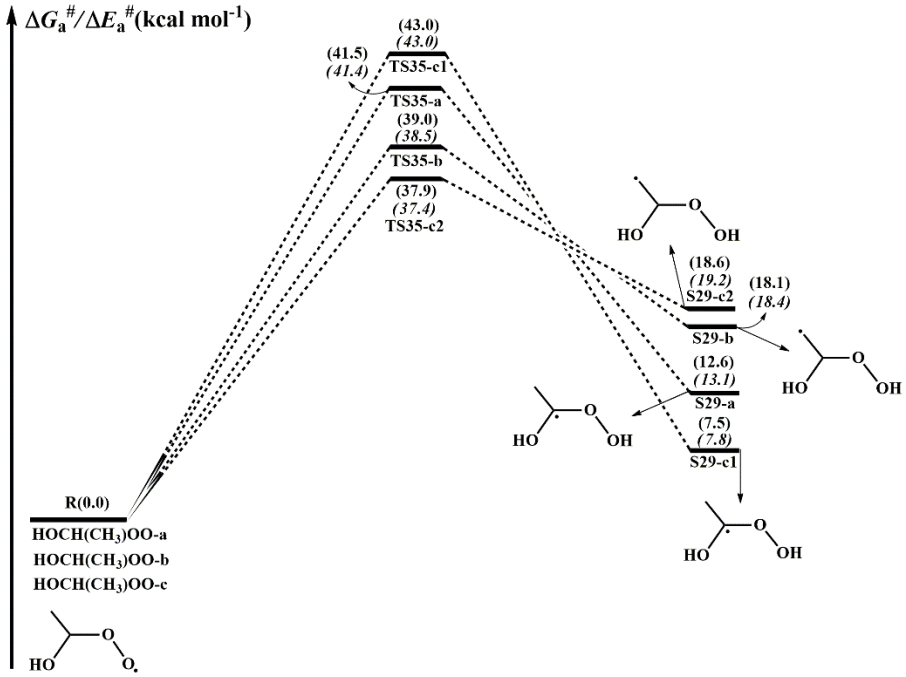

Figure S13. PES ($\Delta G_a^{\#}$ and $\Delta E_a^{\#}$, in italics) for the autoxidation of $HOCH_3CHOO$ radical predicted at the M06-2X/ma-TZVP//M06-2X/6-311+G(2df,2p) level of theory

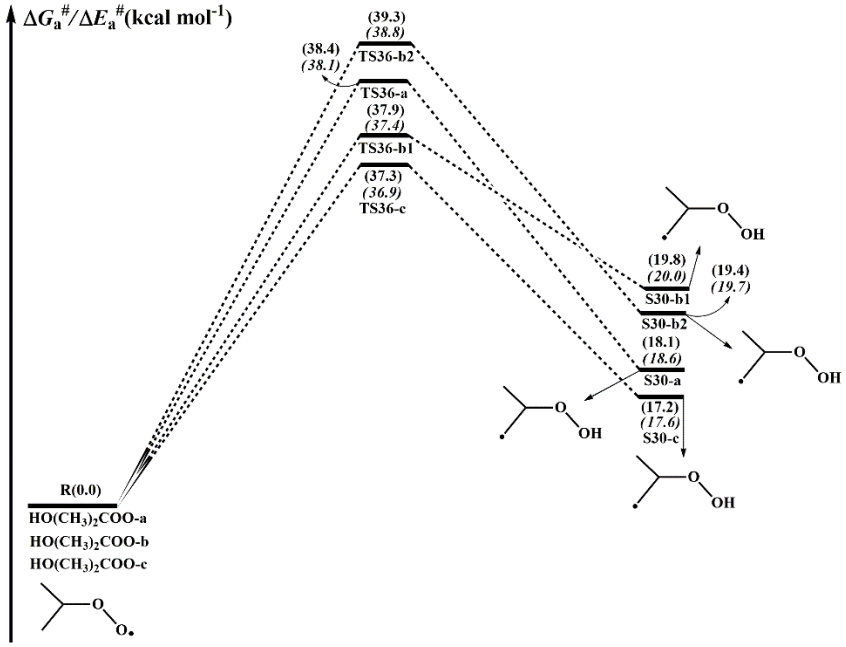

Figure S14. PES ($\Delta G_a^{\#}$ and $\Delta E_a^{\#}$, in italics) for the autoxidation of $HO(CH_3)_2COO$ radical predicted at the M06-2X/ma-TZVP//M06-2X/6-311+G(2df,2p) level of theory

8. There are some grammatical and logical errors in this manuscript. I suggest revising the grammatical errors accordingly.

Response: Based on the Reviewer's suggestion, the sentences/phrases, missing words, and the grammatically confusing sentences have been corrected carefully in the revised manuscript.

References

Bianchi, F., Kurten, T., Riva, M., Mohr, C., Rissanen, M. P., Roldin, P., Berndt, T., Crounse, J. D., Wennberg, P. O., Mentel, T. F., Wildt, J., Junninen, H., Jokinen, T., Kulmala, M., Worsnop, D. R., Thornton, J. A., Donahue, N., Kjaergaard, H. G., and Ehn, M.: Highly oxygenated organic molecules (HOM) from gas-phase autoxidation involving peroxy radicals: a key contributor to atmospheric aerosol, Chem. Rev., 119, 3472-3509, https://doi.org/10.1021/acs.chemrev.8b00395, 2019.

Hofzumahaus, A., Rohrer, F., Lu, K., Bohn, B., Brauers, T., Chang, C. C., Fuchs, H., Holland, F., Kita, K., Kondo, Y., Li, X., Lou, S., Shao, M., Zeng, L., Wahner, A., and Zhang, Y.: Amplified trace gas removal in the troposphere, Science, 324, 1702-1704, https://doi.org/10.1126/science.1164566, 2009.

Kumar, M., and Francisco, J. S.: Red-light-induced decomposition of an organic peroxy radical: a new source of the HO_2 radical, Angew. Chem. Int. Ed., 54, 15711-15714, https://doi.org/10.1002/anie.201509311, 2015.

Stone, D., Whalley, L. K., and Heard, D. E.: Tropospheric OH and HO_2 radicals: field measurements and model comparisons, Chem. Soc. Rev., 41, 6348-6404, https://doi.org/10.1039/c2cs35140d, 2012.

Zhou, X., Liu, Y., Dong, W., and Yang, X.: Unimolecular reaction rate measurement of *syn*-CH_3CHOO, J. Phys. Chem. Lett., 10, 4817-4821, https://doi.org/10.1021/acs.jpclett.9b01740, 2019.

Comments of reviewer #2

1. Authors discuss the transformation mechanism of HHPs. But there is no information on the concentration of HHPs (in forested regions?).

Response: Based on the Reviewer's suggestion, the concentrations of hydroxyalkyl hydroperoxides (HHPs) have been added in the revised manuscript. Hydroxymethyl hydroperoxide (HMHP, $HOCH_2OOH$), the simplest HHPs from the ozonolysis of ethene in the presence of water, is observed in significant abundance in the atmosphere (Allen et al., 2018). The measured concentration of HMHP is varied considerably depending on the location, season and altitude, and its concentration is measured to be up to 5 ppbv in forested regions (Allen et al., 2018; Francisco and Eisfeld, 2009). Recently, the concentration of HMHP was measured during the summer 2013 in the southeastern United States, and found that the average mixing ratio of HMHP is 0.25 ppbv with a maximum of 4.0 ppbv in the boundary layer (Allen et al., 2018).

Corresponding descriptions have been added in the page 4 line 98-106 of the revised manuscript:

Hydroxymethyl hydroperoxide (HMHP, $HOCH_2OOH$), the simplest HHPs from the ozonolysis of ethene in the presence of water, is observed in significant abundance in the atmosphere (Allen et al., 2018). The measured concentration of HMHP is varied considerably depending on the location, season and altitude, and its concentration is measured to be up to 5 ppbv in forested regions (Allen et al., 2018; Francisco and Eisfeld, 2009). Recently, the concentration of HMHP was measured during the summer 2013 in the southeastern United States, and found that the average mixing ratio of HMHP is 0.25 ppbv with a maximum of 4.0 ppbv in the boundary layer(Allen et al., 2018).

2. The lifetimes of distinct HHPs with respect to OH should be estimated under atmospheric conditions.

Response: Based on the Reviewer's suggestion, the lifetime of distinct HHPs reactivity toward OH radical has been added in the revised manuscript. The atmospheric lifetime is expressed as eqn (1): (Long et al., 2017)

$$\tau = \frac{1}{k[\mathrm{X}]} \quad (1)$$

where *k* is the rate coefficient of distinct HHPs reactions with OH radical. [X] is the concentration of OH radical, which varies from 5 to 15 $\times 10^6$ molecules cm^{-3} during daylight (Tan et al., 2017). At ambient temperature, the total rate coefficients of OH radical reactions with $HOCH_2OOH$, $HOCH(CH_3)OOH$ and $HOC(CH_3)_2OOH$ are 3.3 $\times 10^{-11}$, 3.0 $\times 10^{-11}$ and 1.6 $\times 10^{-11}$ cm^3 $molecule^{-1}$ s^{-1}, respectively. The atmospheric lifetime of $HOCH_2OOH$, $HOCH(CH_3)OOH$ and $HOC(CH_3)_2OOH$ reactivity toward OH radical are estimated to be 0.58-1.74 h, 0.60-1.79 h and 1.23-3.69 h at room temperature.

Corresponding descriptions have been added in the page 13 line 348-352 of the revised manuscript:

The concentrations of OH radical vary from 5 to 15 $\times 10^6$ molecules cm^{-3} during daylight (Long et al., 2017), resulting in the atmospheric lifetime of $HOCH_2OOH$, $HOCH(CH_3)OOH$ and $HOC(CH_3)_2OOH$ reactivity toward OH radical are estimated to be 0.58-1.74 h, 0.60-1.79 h and 1.23-3.69 h at room temperature.

3. $\Delta E_a^{\#}$, $\Delta G_a^{\#}$ and ΔG are employed in the manuscript, the author should explain the meaning of each item in detail.

Response: Based on the Reviewer's suggestion, the explanations on the meaning of $\Delta E_a^{\#}$, $\Delta G_a^{\#}$ and ΔG have been added in the revised manuscript. The Gibbs free energy (*G*) for each species is obtained by combining the single-point energy with the Gibbs correction ($G = G_{corr} + E$). The electronic energy ($\Delta E_a^{\#}$) and free energy ($\Delta G_a^{\#}$) barriers are defined as the difference in energy between transition state and pre-reactive complex ($\Delta E_a^{\#} = E_{TS} - E_{RC}$ and $\Delta G_a^{\#} = G_{TS} - G_{RC}$). The reaction free energy (ΔG) is referred to the difference in energy between product and reactant ($\Delta G = G_P - G_R$).

Corresponding descriptions have been added in the page 7 line 178-183 of the revised manuscript:

Herein, the Gibbs free energy (G) for each species is obtained by combining the single-point energy with the Gibbs correction ($G = G_{corr} + E$). The electronic energy ($\Delta E_a^{\#}$) and free energy ($\Delta G_a^{\#}$) barriers are defined as the difference in energy between transition state and pre-reactive complex ($\Delta E_a^{\#} = E_{TS} - E_{RC}$ and $\Delta G_a^{\#} = G_{TS} - G_{RC}$). The reaction free energy (ΔG) is referred to the difference in energy between product and reactant ($\Delta G = G_P - G_R$).

4. Author should compare the barriers of the gas phase decomposition of $HOCH_2OO$ radical with the barrier of self-reaction of $HOCH_2OO$ radical. Kumar and Francisco reported the unimolecular decay of $HOCH_2OO$ radical could be a new source of HO2 radical (Angew. Chem. Int. Ed. 2015, 54, 15711-15714; J. Phys. Chem. A 2016, 120, 2677-2683).

Response: Based on the Reviewer's suggestion, the comparation on the barriers of the gas phase decomposition of $HOCH_2OO$ radical and its self-reaction has been added in the revised manuscript. As can be seen in Figure 5, the self-reaction of $HOCH_2OO$ radical proceeds via oxygen-to-oxygen coupling leading to the formation of tetroxide intermediate S14 with the electronic energy and free energy barriers of 7.3 and 19.6 kcal mol^{-1}. Kumar and Francisco reported that the electronic energy barrier of the gas phase decomposition of $HOCH_2OO$ radical is 14.0 kcal mol^{-1} and it could be a new source of HO_2 radical in the troposphere (Kumar and Francisco, 2015, 2016). Compared with the electronic energy barriers of unimolecular decomposition of $HOCH_2OO$ radical and its self-reaction, it can be found that the self-reaction of $HOCH_2OO$ radical resulting in formation of tetroxide intermediate S14 is significantly feasible. The related reference has been cited in the revised manuscript.

Corresponding descriptions have been added in the page 16 line 412-420 of the revised manuscript:

The self-reaction of $HOCH_2OO$ radical proceeds via oxygen-to-oxygen coupling leading to the formation of tetroxide intermediate S14 with the electronic energy and free energy barriers of 7.3 and 19.6 kcal mol^{-1}. Kumar and Francisco reported that the electronic energy barrier of the gas phase decomposition of $HOCH_2OO$ radical is 14.0 kcal mol^{-1} and it could be a new source of HO_2 radical in the troposphere (Kumar and Francisco, 2015, 2016). Compared with the electronic energy barriers of unimolecular dissociation of $HOCH_2OO$ radical and its self-reaction, it can be found that the self-reaction of $HOCH_2OO$ radical resulting in formation of S14 is significantly feasible.

5. Author should provide the pseudo first order rates for the reactions of distinct RO_2 radicals with HO_2 and NO under the urban, rural and forest environments.

Response: Based on the Reviewer's suggestion, the pseudo-first-order rate constants of distinct RO_2 radicals reactions with HO_2 radical and NO have been added in the revised

manuscript. The typical atmospheric concentrations of HO_2 radical are 5, 20 and 50 pptv in the urban, rural and forest environments (Bianchi et al., 2019). At ambient temperature, the rate coefficient k_{R31} of $HOCH_2OO\cdot + HO_2\cdot$ reaction (R31) is estimated to be 1.7×10^{-11} cm^3 $molecule^{-1}$ s^{-1}, translating into the pseudo-first-order rate constants $k'_{HO2} = k_{HO2}[HO_2]$ of 1.1×10^{-3}, 4.2×10^{-3} and 1.1×10^{-2} s^{-1}, respectively, in the urban, rural and forest environments. The pseudo-first-order rate constants of $HOCH(CH_3)OO\cdot + HO_2\cdot$ (R32) and $HOC(CH_3)_2OO\cdot + HO_2\cdot$ (R33) reactions are predicted to be 3.0×10^{-3} and 4.8×10^{-3} (urban), 1.1×10^{-2} and 1.8×10^{-2} (rural), 3.0×10^{-2} and 4.8×10^{-2} s^{-1} (forest) at room temperature.

The typical atmospheric concentrations of NO are about 10 ppbv, 1 ppbv and 20 pptv in the urban, rural and forest environments (Bianchi et al., 2019). The rate coefficient k_{R39} of $HOCH_2OO$ radical reaction with NO is estimated to be 4.3×10^{-12} cm^3 $molecule^{-1}$ s^{-1} at ambient temperature, resulting in the pseudo-first-order rate constants $k'_{NO} = k_{NO}[NO]$ of 6.5×10^{-1}, 6.5×10^{-2}, and 1.3×10^{-3}, respectively, in the urban, rural and forest environments. For the bimolecular reaction of $HOCH(CH_3)OO$ radical with NO, the predicted pseudo-first-order rate constants are 6.7×10^{-1}, 6.7×10^{-2}, and 1.3×10^{-3}, respectively, in the urban, rural and forest environments. The pseudo-first-order rate constants of $HOC(CH_3)_2OO$ radical reaction with NO are 7.3×10^{-1}, 7.3×10^{-2}, and 1.5×10^{-3}, respectively, in the urban, rural and forest environments.

Corresponding descriptions have been added in the page 22 line 525-533 and page 27 line 653-658 of the revised manuscript:

At ambient temperature, k_{R31} is estimated to be 1.7×10^{-11} cm^3 $molecule^{-1}$ s^{-1}, which is in good agreement with the value of ~2×10^{-11} cm^3 $molecule^{-1}$ s^{-1} for the reaction of acyl peroxy radicals with HO_2 radical (Wennberg et al., 2018). The typical atmospheric concentrations of HO_2 radical are about 5, 20 and 50 pptv in the urban, rural and forest environments (Bianchi et al., 2019), translating into the pseudo-first-order rate constants $k'_{HO2} = k_{HO2}[HO_2]$ of 1.1×10^{-3}, 4.2×10^{-3} and 1.1×10^{-2} s^{-1}, respectively. The pseudo-first-order rate constants of R32 and R33 are predicted to be 3.0×10^{-3} and 4.8×10^{-3} (urban), 1.1×10^{-2} and 1.8×10^{-2} (rural), 3.0×10^{-2} and 4.8×10^{-2} s^{-1} (forest) at room temperature.

The typical atmospheric concentrations of NO are about 10 ppbv, 1 ppbv and 20 pptv in the urban, rural and forest environments (Bianchi et al., 2019). The rate coefficient of $HOCH_2OO\cdot$ reaction with NO is calculated to be 4.3×10^{-12} cm^3 $molecule^{-1}$ s^{-1} at room

temperature, resulting in the pseudo-first-order rate constants $k'_{NO} = k_{NO}[NO]$ of 6.5×10^{-1}, 6.5×10^{-2}, and 1.3×10^{-3}, respectively, in the urban, rural and forest environments. For the bimolecular reaction of $HOCH(CH_3)OO$ radical with NO, the predicted pseudo-first-order rate constants are 6.7×10^{-1}, 6.7×10^{-2}, and 1.3×10^{-3}, respectively, in the urban, rural and forest environments. The pseudo-first-order rate constants of $HOC(CH_3)_2OO$ radical reaction with NO are 7.3×10^{-1}, 7.3×10^{-2}, and 1.5×10^{-3}, respectively, in the urban, rural and forest environments.

6. In Fig. 2, the text (mentioned structural parameters) overlaps with the structures.

Response: Based on the Reviewer's suggestion, the Figure 2 has been redrawn in the revised manuscript. For clarity, the 2D drawings of some important species are labeled in Figure 2. The optimized geometries of all the stationary points involved in the initial reactions of OH radical with $HOCH_2OOH$ are displayed Figure S6.

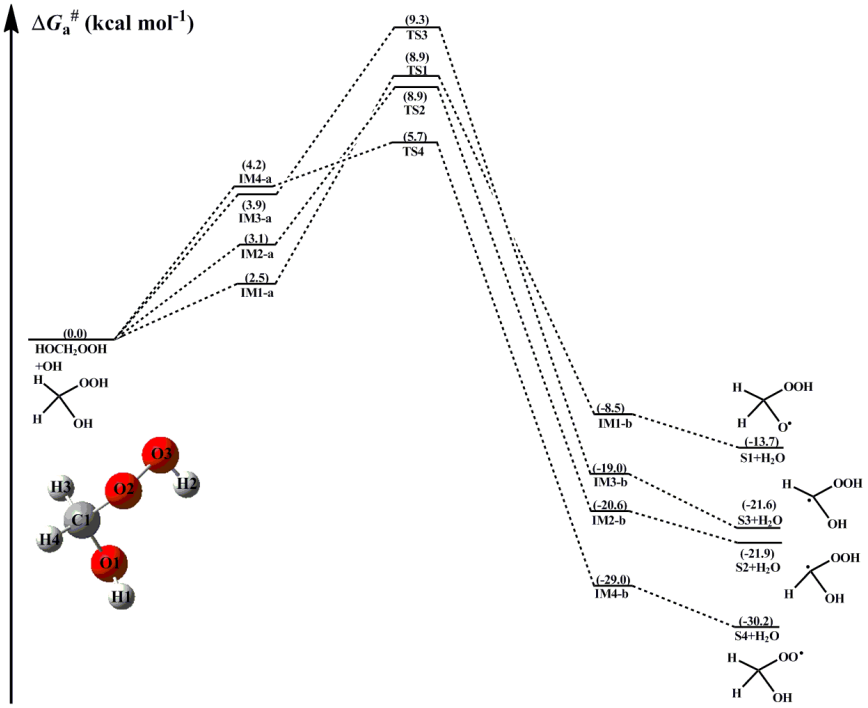

Figure 2. PES ($\Delta G_a^{\#}$) for the OH-initiated reactions of $HOCH_2OOH$ from the CH_2OO + H_2O reaction predicted at the M06-2X/ma-TZVP//M06-2X/6-311+G(2df,2p) level of theory (a and b represent the pre-reactive and post-reactive complexes)

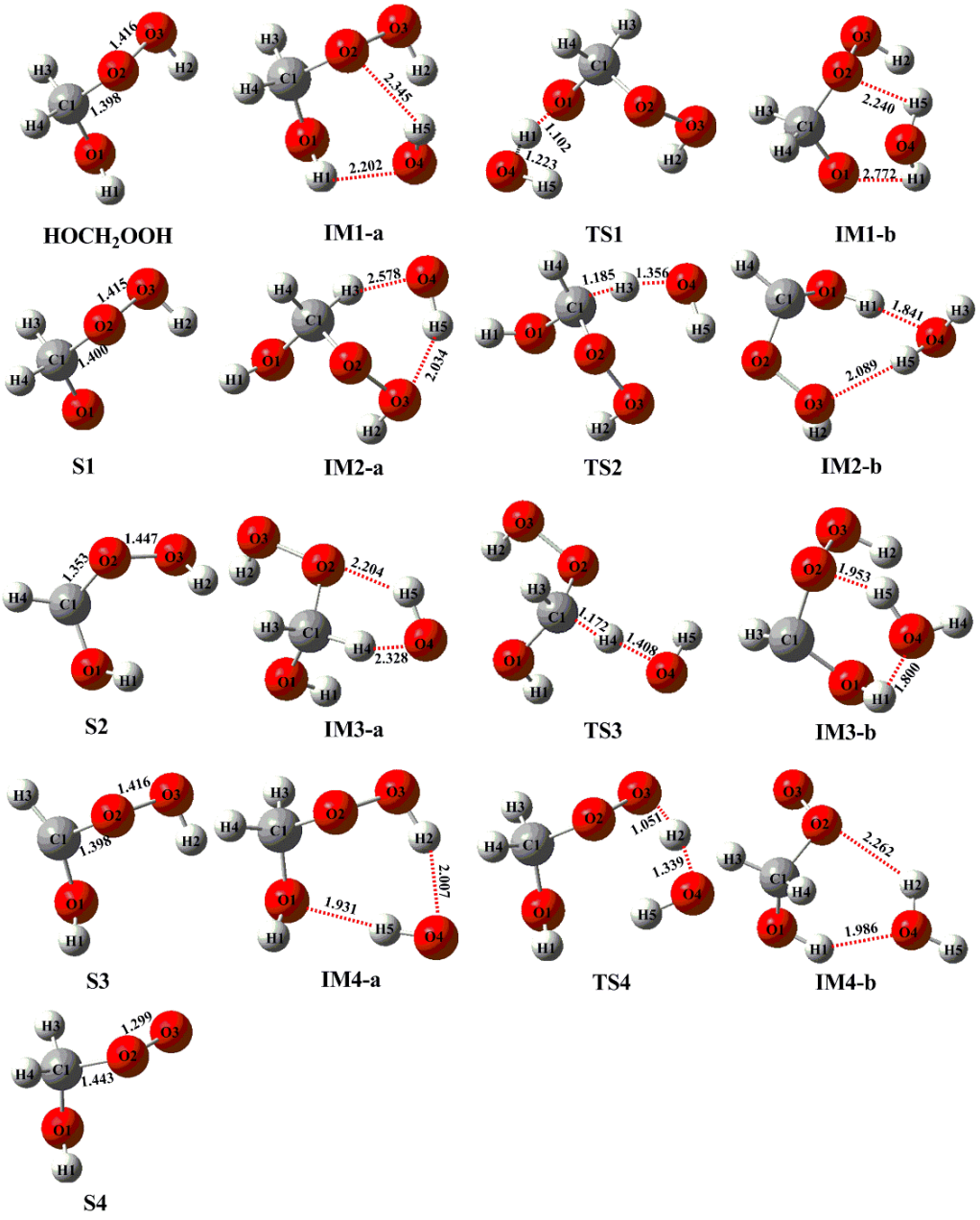

Figure S6. Geometries of all the stationary points for the initial reaction of $HOCH_2OOH$ with OH radical optimized at the M06-2X/6-311+G(2df,2p) level of theory

Reference

Allen, H. M., Crounse, J. D., Bates, K. H., Teng, A. P., Krawiec-Thayer, M. P., Rivera-Rios, J. C., Keutsch, F. N., Clair, J. M. S., Hanisco, T. F., Møller, K. H., Kjaergaard, H. G., and Wennberg, P. O.: Kinetics and product yields of the OH initiated oxidation of hydroxymethyl hydroperoxide, J. Phys. Chem. A, 122, 6292-6302, https://doi.org/10.1021/acs.jpca.8b04577, 2018.

Bianchi, F., Kurten, T., Riva, M., Mohr, C., Rissanen, M. P., Roldin, P., Berndt, T., Crounse, J. D., Wennberg, P. O., Mentel, T. F., Wildt, J., Junninen, H., Jokinen, T., Kulmala, M., Worsnop, D. R., Thornton, J. A., Donahue, N., Kjaergaard, H. G., and Ehn, M.: Highly oxygenated organic molecules (HOM) from gas-phase autoxidation involving peroxy radicals: a key contributor to atmospheric aerosol, Chem. Rev., 119, 3472-3509, https://doi.org/10.1021/acs.chemrev.8b00395, 2019.

Francisco, J. S., and Eisfeld, W.: Atmospheric oxidation mechanism of hydroxymethyl hydroperoxide, J. Phys. Chem. A, 113, 7593-7600, https://doi.org/10.1021/jp901735z, 2009.

Kumar, M., and Francisco, J. S.: Red-light initiated decomposition of α-hydroxy methylperoxy radical in the presence of organic and inorganic acids: implications for the HO_x formation in the lower stratosphere, J. Phys. Chem. A, 120, 2677-2683, https://doi.org/10.1021/acs.jpca.6b01515, 2016.

Kumar, M., and Francisco, J. S.: Red-light-induced decomposition of an organic peroxy radical: a new source of the HO_2 radical, Angew. Chem. Int. Ed., 54, 15711-15714, https://doi.org/10.1002/anie.201509311, 2015.

Long, B., Bao, J. L., and Truhlar, D. G.: Reaction of SO_2 with OH in the atmosphere, Phys. Chem. Chem. Phys., 19, 8091-8100, https://doi.org/10.1039/C7CP00497D, 2017.

Tan, Z., Fuchs, H., Lu, K., Hofzumahaus, A., Bohn, B., Broch, S., Dong, H., Gomm, S., Häseler, R., He, L., Holland, F., Li, X., Liu, Y., Lu, S., Rohrer, F., Shao, M., Wang, B., Wang, M., Wu, Y., Zeng, L., Zhang, Y., Wahner, A., and Zhang, Y.: Radical chemistry at a rural site (Wangdu) in the North China Plain: observation and model calculations of OH, HO2 and RO2 radicals, Atmos. Chem. Phys., 17, 663–690, https://doi.org/10.5194/acp-17-663-2017, 2017.

Comments of reviewer #3

1. I see two major issues with the work. First, it is generally known that the internal H-shift isomerizations become important only at larger carbon structures than studied here. The rather extensive previous literature amply points out that the H-shifts (discussed in older literature often as H transfer) are not competitive from the same, or adjacent, C-bearing functional groups. Thus it is rather surprising this was even considered here, and I think the whole discussion about RO_2 autoxidation does not make any sense for these small systems. Additionally, the resulting accretion products ROOR are important for aerosol growth only at larger sizes. Thus, these small systems are not expected to play any practical role in atmospheric particulate matter formation (unless the second RO_2 forming the ROOR is a very big and polar molecule). Moreover, one H-shift reaction does not really constitute autoxidation sequence, but is rather just a single isomerization/ rearrangement reaction. Thus the whole word "autoxidation" should not be associated with the current work. All that said, for the sake of completeness, the current calculations could/should be left in, but it has to be made crystal clear that autoxidation is not expected here, and these are only common isomerization (by H-shift) reactions.

Response: Extensive previous literatures have demonstrated the autoxidation of peroxy radical RO_2 plays an important role in the oxidation of volatile organic compounds (VOCs) with high molecular weight in the atmosphere (Bianchi et al., 2019; Ehn et al., 2017). The autoxidation of RO_2 radical includes sequential intramolecular H-shifts and O_2 additions, in which the first H-shift is strongly rate-limiting reaction (Nozière and Vereecken, 2019; Crounse et al., 2013). In the present study, we mainly focus on the mechanism of isomerization reactions of $HOCH_2OO$, $HOCH(CH_3)OO$, and $HO(CH_3)_2COO$ radicals. The corresponding potential energy surfaces (PES) are shown in Figures 9, S13 and S14, respectively. As can be seen in Figure 9, the lowest-energy conformer $HOCH_2OO$-a can proceed via a 1,3-H shift from the $-CH_2$ group to the terminal oxygen leading to S28-a (HO CHOOH) with the barrier of 41.6 kcal mol^{-1}. $HOCH_2OO$-b can isomerize to S28-b1 and S28-b2 via the four-membered ring transition states TS34-b1 and TS34-b2 (1,3-H shifts) with the barriers of 41.6 and 45.0 kcal mol^{-1}. But these three 1,3-H shift reactions have comparatively high barriers, making them irrelevant in the atmosphere. Equivalent to the case of $HOCH_2OO$ radical, the isomerization of $HOCH(CH_3)OO$ radical proceeds via the 1,3- and 1,4-H shifts from the -CH or $-CH_3$ groups to the terminal oxygen resulting in formation of

hydroperoxyalkyl radicals (Figure S13). These 1,3- and 1,4-H shift reactions accompany with the extremely high barriers (> 37.9 kcal mol^{-1}), implying that they are of less importance in the atmosphere. Similar conclusion is also derived from the isomerization of $HO(CH_3)_2COO$ radical that 1,4-H shift reactions are unfavourable kinetically (Figure S14). The high barriers of 1,3- and 1,4-H shifts can be interpreted as the result of the large ring strain energy (RSE) in the cyclic transition state geometries. As a consequence, the isomerization reactions of $HOCH_2OO$, $HOCH(CH_3)OO$ and $HO(CH_3)_2COO$ radicals are not likely to proceed in the atmosphere.

The accretion products ROOR are of less importance in the self-reactions of small RO_2 radicals (e.g. CH_3OO, C_2H_5OO, $CH_3C(O)OO$ radicals), while they are characterized as an effective source of secondary organic aerosol (SOA) in the self-reactions of large RO_2 radicals (Berndt et al., 2018; Zhang et al., 2012; Liang et al., 2011). Although the ROOR formed from the self-reactions of small RO_2 radicals is unimportant, the present mechanism investigation is meaningful to understand the self-reactions of complex RO_2 radicals. In the present study, the schematic PESs for the self-reactions of $HOCH_2OO$, $HOCH(CH_3)OO$ and $HO(CH_3)_2COO$ radicals are shown in Figures 5-7, respectively. As can be seen in Figure 5a, the self-reaction of $HOCH_2OO$ radical starts with the formations of tetroxide complexes IM13-a and IM14-a in the entrance channel, with 2.9 and 3.4 kcal mol^{-1} stability. Then they fragment into dimer S13 + $^1O_2$ (R13) and $HOCH_2OOH$ + HOCHOO (R14) via transition states TS13 and TS14 with the barriers of 43.3 and 51.5 kcal mol^{-1}. But the barriers of R13 and R14 are extremely high, making them irrelevant in the atmosphere.

From Figure 5b, it is seen that the self-reaction of $HOCH_2OO$ radical proceeds via oxygen-to-oxygen coupling leading to the formation of tetroxide intermediate S14 with the electronic energy and free energy barriers of 7.3 and 19.6 kcal mol^{-1}. The formed S14 can fragment into $HOCH_2O\cdot$ + HCOOH + $HO_2\cdot$ via a concerted process of O_2-O_3 and O_5-O_6 bonds rupture and O_3-H_6 bond forming with the barrier of 29.8 kcal mol^{-1}. Alternatively, S14 can convert into the caged tetroxide intermediate S16 through the asymmetric two step O_2-O_3 and O_5-O_6 bonds scission with the barriers of 19.1 and 3.1 kcal mol^{-1}, respectively. The result shows that the latter pathway is more preferable than the former channel owing to its lower barrier. The overall spin multiplicity of S16 is singlet, in which the O_2 moiety maintains the triplet ground state (spin up) and is very loosely bound. In order to preserve the overall singlet multiplicity, the two $HOCH_2O$

radical pairs (^{3}(HOCH$_2$O ··HOCH$_2$O)) must have the triplet multiplicity (spin down). S16 could be regarded as the ground state $^3O_2$ moving away from the two HOCH$_2$O radical pairs that keep interacting. Due to the difficulty in performing the constrained optimization for the dissociation of S16, the $^3O_2$ moiety is considered as a leaving moiety away from two HOCH$_2$O radical pairs, and merely the dissociation of ^{3}(HOCH$_2$O ··HOCH$_2$O) is taken into consideration in the present study. It has three types of pathways: (1) it yields HOCH$_2$OH and excited-state ^{3}HCOOH through the hydrogen transfer step with the barrier of 14.0 kcal mol^{-1} and 10.2 kcal mol^{-1} exothermicity, followed by the excited ^{3}HCOOH to go back to the ground-state ^{1}HCOOH; (2) it generates two HOCH$_2$O radicals via the barrierless process with the exoergicity of 16.9 kcal mol^{-1}; (3) it produces dimer S17 with the exoergicity of 32.1 kcal mol^{-1}. Based on the calculated reaction barriers, it can be found that the rate-limiting step is the scission of O_2-O_3 bond (R17) in the unimolecular decay processes of S14.

As can be seen in Figure 6a, the self-reaction of HOCH(CH$_3$)OO radical can either produce dimer S18 along with $^1O_2$ via transition state TS20 with the barrier of 44.4 kcal mol^{-1}, or generate HOCH(CH$_3$)OOH and HOC(CH$_3$)OO though transition state TS21 with the barrier of 54.3 kcal mol^{-1}. But the barriers of R20 and R21 are significantly high, making them are of less importance in the atmosphere. Alternatively, the self-reaction of HOCH(CH$_3$)OO radical proceeds via an oxygen-to-oxygen coupling resulting in formation of tetroxide intermediate S19 with the barrier of 19.9 kcal mol^{-1} (Figure 6b). The formed S19 proceeds through the asymmetric two step O_2-O_3 and O_5-O_6 bonds scission to produce a caged tetroxide intermediate S21 of overall singlet multiplicity comprising two same-spin alkoxyl radicals (spin down) and triplet oxygen (spin up). These two processes accompany with the barriers of 21.4 and 1.3 kcal mol^{-1}, respectively. Then it decomposes into the propagation (2HOCH(CH$_3$)O· + $^3O_2$) and termination products (HOCH(CH$_3$)OH + ^{3}CH$_3$OOH + $^3O_2$ and dimer S22 + $^3O_2$) with the exoergicity of 12.5, 11.7 and 33.0 kcal mol^{-1}. The rate-determining step is the rupture of O_2-O_3 bond (R24) in the dissociation processes of S19.

As shown in Figure 7, the dominant pathway for the self-reaction of HO(CH$_3$)$_2$COO radical begins with the formation of tetroxide intermediate S24 via an oxygen-to-oxygen coupling transition state TS28 with the barrier of 20.4 kcal mol^{-1}; then it transforms into the caged tetroxide intermediate S26 of overall singlet spin multiplicity through the asymmetric two-step O-O bond

cleavage with the barriers of 22.0 and 3.4 kcal mol^{-1}; finally, S26 can either produce two HO(CH$_3$)$_2$CO radicals with the exoergicity of 10.3 kcal mol^{-1}, or generate dimer S27 with the exothermicity of 31.5 kcal mol^{-1}. Different the self-reactions of HOCH$_2$OO and HOCH(CH$_3$)OO radicals, the termination product of the self-reaction of HOC(CH$_3$)$_2$OO radical is exclusively dimer S27. The reason is due to the absence of alpha hydrogen atom in HOC(CH$_3$)$_2$OO radical.

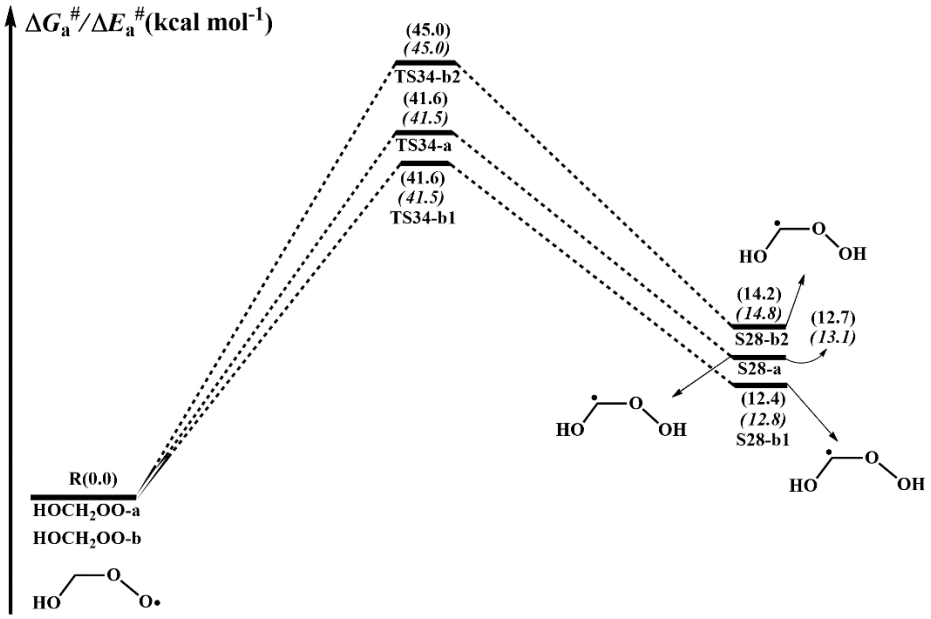

Figure 9. PES ($\Delta G_a^{\#}$ and $\Delta E_a^{\#}$, in italics) for the autoxidation of HOCH$_2$OO radical predicted at the M06-2X/ma-TZVP//M06-2X/6-311+G(2df,2p) level of theory

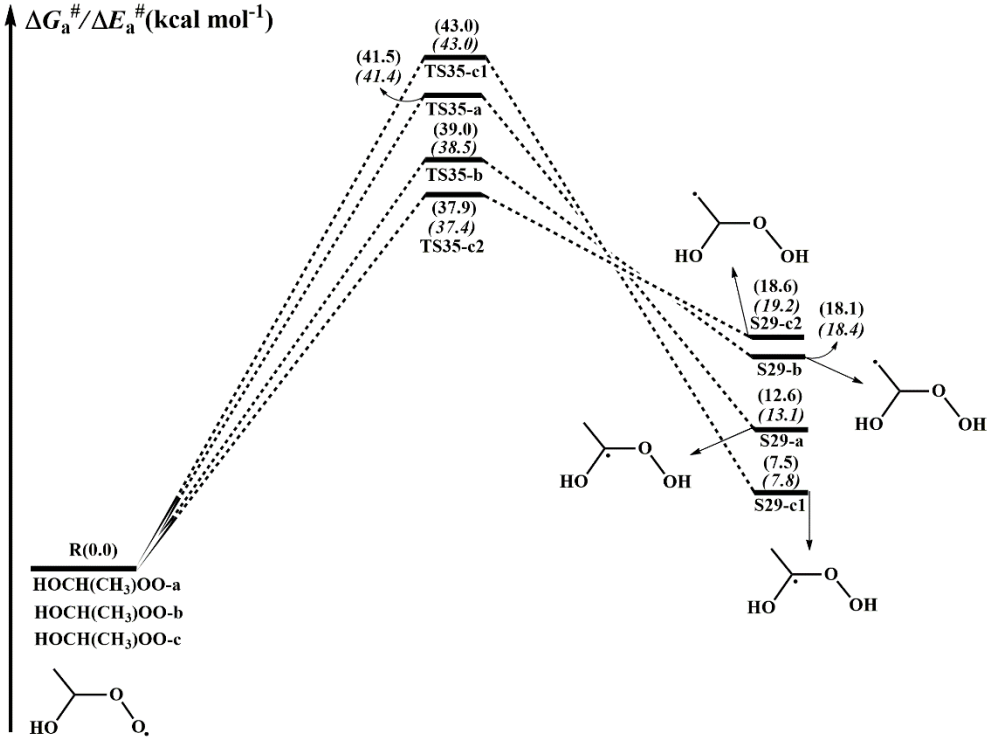

Figure S13. PES ($\Delta G_a^{\#}$ and $\Delta E_a^{\#}$, in italics) for the autoxidation of HOCH$_3$CHOO radical predicted at the M06-2X/ma-TZVP//M06-2X/6-311+G(2df,2p) level of theory

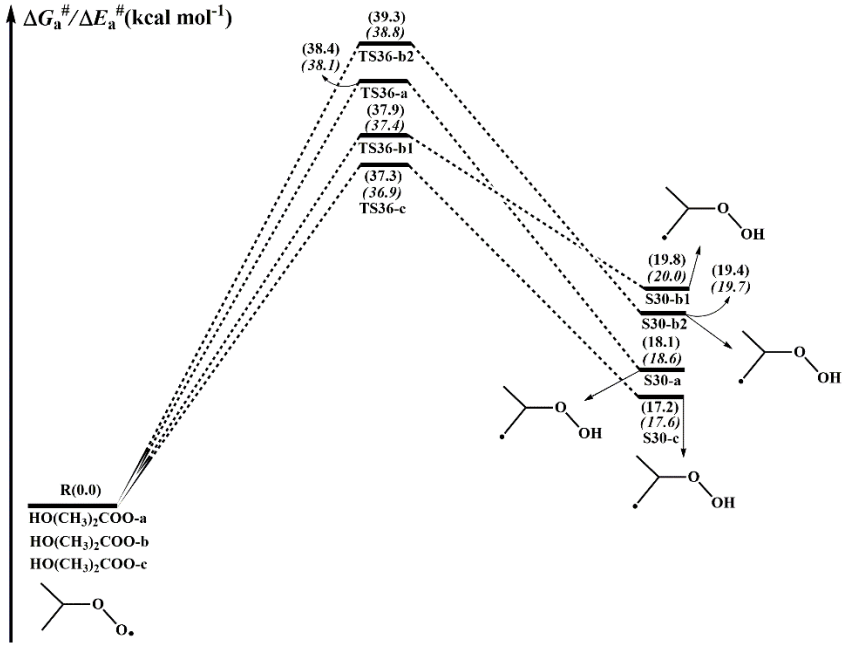

Figure S14. PES ($\Delta G_a^{\#}$ and $\Delta E_a^{\#}$, in italics) for the autoxidation of $HO(CH_3)_2COO$ radical predicted at the M06-2X/ma-TZVP//M06-2X/6-311+G(2df,2p) level of theory

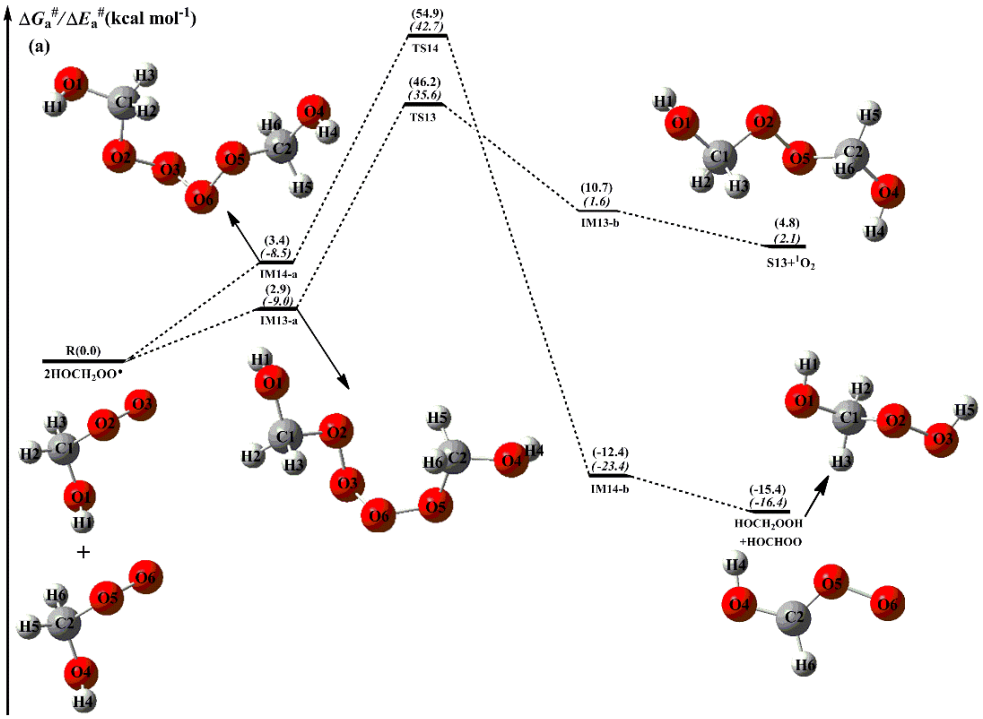

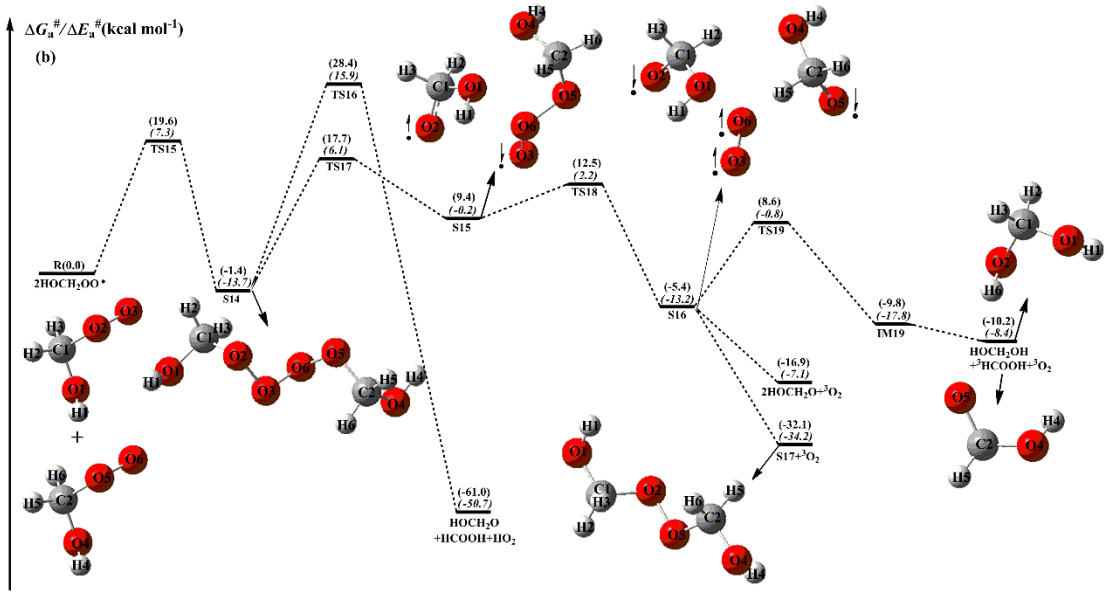

Figure 5. PES ($\Delta G_a^{\#}$ and $\Delta E_a^{\#}$, in italics) for the self-reaction of $HOCH_2OO$ radicals predicted at the M06-2X/ma-TZVP//M06-2X/6-311+G(2df,2p) level of theory

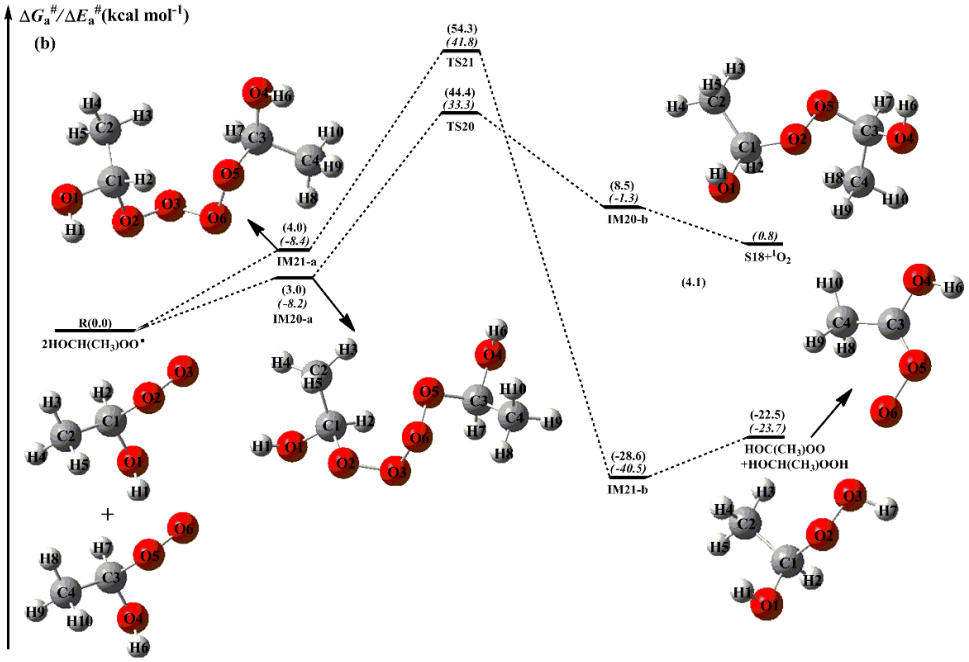

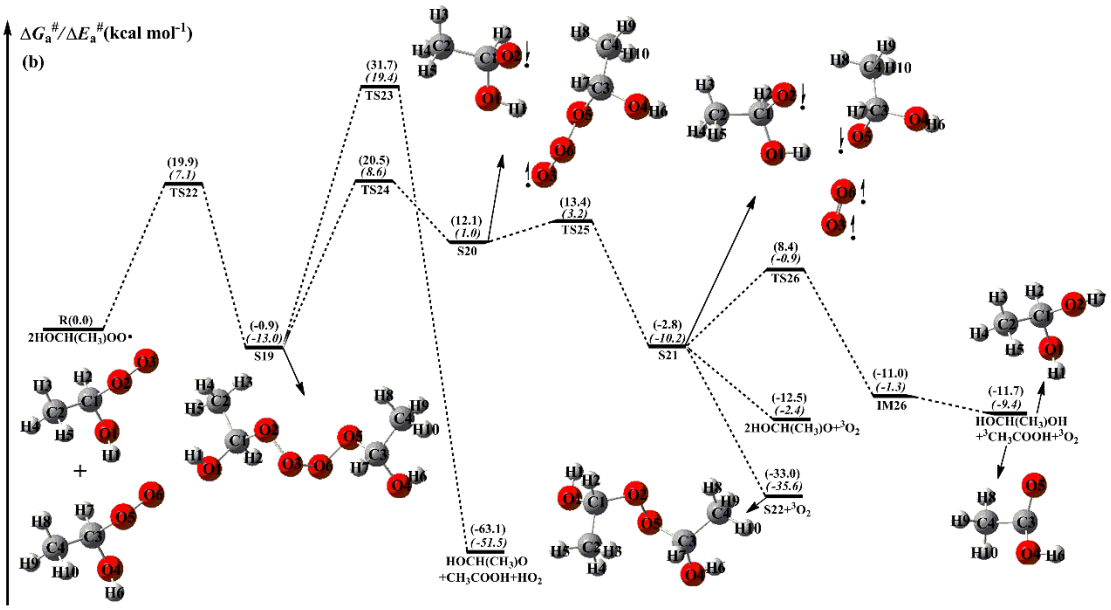

Figure 6. PES ($\Delta G_a^{\#}$ and $\Delta E_a^{\#}$, in italics) for the self-reaction of $HOCH(CH_3)OO$ radicals predicted at the M06-2X/ma-TZVP//M06-2X/6-311+G(2df,2p) level of theory

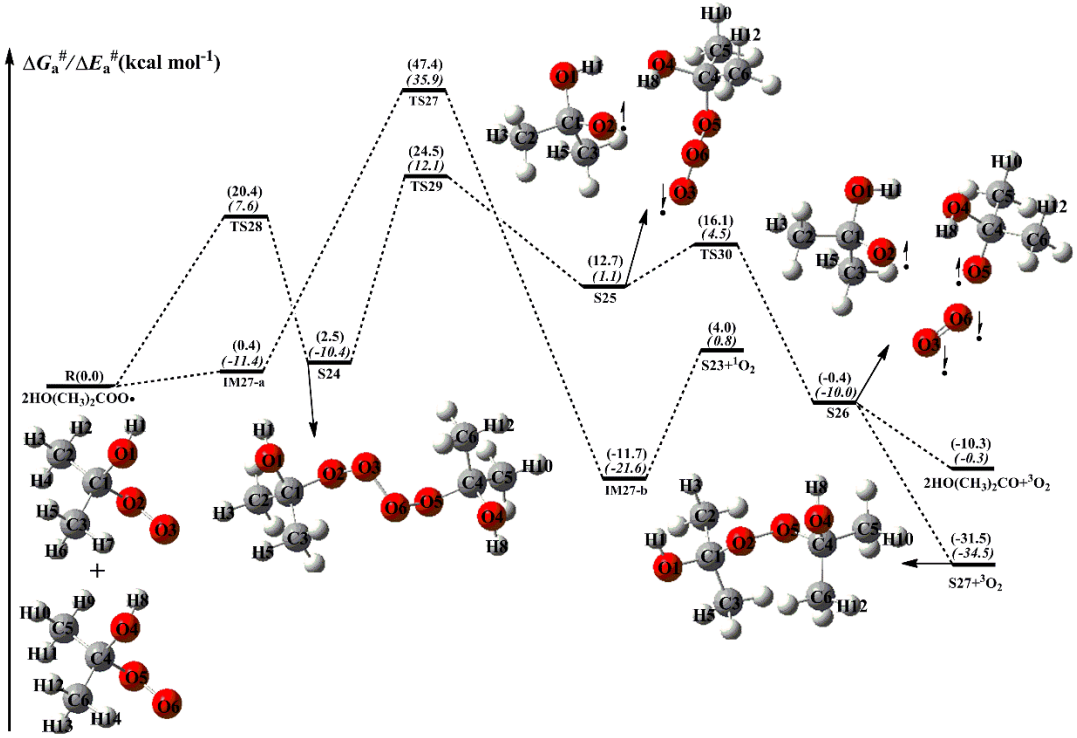

Figure 7. PES ($\Delta G_a^{\#}$ and $\Delta E_a^{\#}$, in italics) for the self-reaction of $HO(CH_3)_2COO$ radicals predicted at the M06-2X/ma-TZVP//M06-2X/6-311+G(2df,2p) level of theory

Corresponding descriptions have been added in the page 23 line 553-560, page 24 line 565-575, page 16 line 405-425, page 17 line 426-454, page 18 line 455-475 of the revised manuscript:

A schematic PES for the H-shift reactions of $HOCH_2OO$ radical is displayed in Figure 9. As can be seen in Figure 9, the lowest-energy conformer $HOCH_2OO$-a can proceed via a 1,3-H shift

from the -CH_2 group to the terminal oxygen leading to the formation of S28-a (HO CHOOH) with the barrier of 41.6 kcal mol^{-1}. $HOCH_2OO$-b can isomerize to S28-b1 and S28-b2 via the four-membered ring transition states TS34-b1 and TS34-b2 (1,3-H shifts) with the barriers of 41.6 and 45.0 kcal mol^{-1}. But these three 1,3-H shift reactions have comparatively high barriers, making them irrelevant in the atmosphere. Equivalent to the case of $HOCH_2OO$ radical, the isomerization of $HOCH(CH_3)OO$ radical proceeds via the 1,3- and 1,4-H shifts from the -CH or -CH_3 groups to the terminal oxygen resulting in formation of hydroperoxyalkyl radicals (Figure S13). These 1,3- and 1,4-H shift reactions accompany with the extremely high barriers (> 37.9 kcal mol^{-1}), implying that they are of less importance in the atmosphere. Similar conclusion is also derived from the isomerization of $HO(CH_3)_2COO$ radical that 1,4-H shift reactions are unfavourable kinetically (Figure S14). The high barriers of 1,3- and 1,4-H shifts can be interpreted as the result of the large ring strain energy (RSE) in the cyclic transition state geometries. As a consequence, the isomerization reactions of $HOCH_2OO$, $HOCH(CH_3)OO$ and $HO(CH_3)_2COO$ radicals are not likely to proceed in the atmosphere.

As can be seen in Figure 5a, the self-reaction of $HOCH_2OO$ radical starts with the formations of tetroxide complexes IM13-a and IM14-a in the entrance channel, with 2.9 and 3.4 kcal mol^{-1} stability. Then they fragment into dimer S13 + $^1O_2$ (R13) and $HOCH_2OOH$ + HOCHOO (R14) via transition states TS13 and TS14 with the barriers of 43.3 and 51.5 kcal mol^{-1}. But the barriers of R13 and R14 are extremely high, making them irrelevant in the atmosphere. From Figure 5b, it is seen that the self-reaction of $HOCH_2OO$ radical proceeds via oxygen-to-oxygen coupling leading to the formation of tetroxide intermediate S14 with the electronic energy and free energy barriers of 7.3 and 19.6 kcal mol^{-1}. The formed S14 can fragment into $HOCH_2O\cdot$ + HCOOH + $HO_2\cdot$ via a concerted process of O_2-O_3 and O_5-O_6 bonds rupture and O_3-H_6 bond forming with the barrier of 29.8 kcal mol^{-1}. Alternatively, S14 can convert into the caged tetroxide intermediate S16 through the asymmetric two step O_2-O_3 and O_5-O_6 bonds scission with the barriers of 19.1 and 3.1 kcal mol^{-1}, respectively. The result shows that the latter pathway is more preferable than the former channel owing to its lower barrier. The overall spin multiplicity of S16 is singlet, in which the O_2 moiety maintains the triplet ground state (spin up) and is very loosely bound. In order to preserve the overall singlet multiplicity, the two $HOCH_2O$ radical pairs ($^3(HOCH_2O\cdot\cdot HOCH_2O)$) must have the triplet multiplicity (spin down). S16 could be

regarded as the ground state $^3O_2$ moving away from the two $HOCH_2O$ radical pairs that keep interacting. Due to the difficulty in performing the constrained optimization for the dissociation of S16, the $^3O_2$ moiety is considered as a leaving moiety away from two $HOCH_2O$ radical pairs, and merely the dissociation of $^3(HOCH_2O \cdots HOCH_2O)$ is taken into consideration in the present study. It has three types of pathways: (1) it yields $HOCH_2OH$ and excited-state ^3HCOOH through the alpha hydrogen transfer with the barrier of 14.0 kcal mol^{-1} and 10.2 kcal mol^{-1} exothermicity, followed by the excited ^3HCOOH to go back to the ground-state ^1HCOOH; (2) it generates two $HOCH_2O$ radicals via the barrierless process with the exoergicity of 16.9 kcal mol^{-1}; (3) it produces dimer S17 with the exoergicity of 32.1 kcal mol^{-1}. Based on the calculated reaction barriers, it can be found that the rate-limiting step is the cleavage of O_2-O_3 bond (R17) in the unimolecular decay processes of S14.

Figure 6 depicts a schematic PES for the self-reaction of $HOCH(CH_3)OO$ radical. As shown in Figure 6a, the self-reaction of $HOCH(CH_3)OO$ radical can either produce dimer S18 along with $^1O_2$ via transition state TS20 with the barrier of 44.4 kcal mol^{-1}, or generate $HOCH(CH_3)OOH$ and $HOC(CH_3)OO$ though transition state TS21 with the barrier of 54.3 kcal mol^{-1}. But the barriers of R20 and R21 are significantly high, making them are of less importance in the atmosphere. Alternatively, the self-reaction of $HOCH(CH_3)OO$ radical proceeds via an oxygen-to-oxygen coupling resulting in formation of tetroxide intermediate S19 with the barrier of 19.9 kcal mol^{-1} (Figure 6b). The formed S19 proceeds through the asymmetric two step O_2-O_3 and O_5-O_6 bonds scission to produce a caged tetroxide intermediate S21 of overall singlet multiplicity comprising two same-spin alkoxyl radicals (spin down) and triplet oxygen (spin up). These two processes accompany with the barriers of 21.4 and 1.3 kcal mol^{-1}, respectively. Then it decomposes into the propagation ($2HOCH(CH_3)O\cdot + {}^3O_2$) and termination products ($HOCH(CH_3)OH + {}^3CH_3OOH + {}^3O_2$ and dimer S22 $+ {}^3O_2$) with the exoergicity of 12.5, 11.7 and 33.0 kcal mol^{-1}. The rate-determining step is the rupture of O_2-O_3 bond (R24) in the dissociation processes of S19.

As shown in Figure 7, the dominant pathway for the self-reaction of $HO(CH_3)_2COO$ radical begins with the formation of tetroxide intermediate S24 via an oxygen-to-oxygen coupling transition state TS28 with the barrier of 20.4 kcal mol^{-1}; then it transforms into the caged tetroxide intermediate S26 of overall singlet spin multiplicity through the asymmetric two-step

O-O bond cleavage with the barriers of 22.0 and 3.4 kcal mol^{-1}; finally, S26 can either produce two HO(CH$_3$)$_2$CO radicals with the exoergicity of 10.3 kcal mol^{-1}, or generate dimer S27 with the exothermicity of 31.5 kcal mol^{-1}. Different the self-reactions of HOCH$_2$OO and HOCH(CH$_3$)OO radicals, the termination product of the self-reaction of HOC(CH$_3$)$_2$OO radical is exclusively dimer S27. The reason is due to the absence of alpha hydrogen atom in HOC(CH$_3$)$_2$OO radical.

2. Another major issue connects to Figure 2: Are you sure you get the RC's and PC's right in the mechanism shown? Seems strange that such analogous reactions with so similar reaction partners (i.e., substituting -H with -CH_3 in adjacent sp3 C-atom is not expect have a profound influence) would have so different pre-reaction complexes. How was this specifically verified. I mean, is it possible you were doing a too constrained original conformer search/optimization and missed certain RC's? Did you try what the energetics would be if the RC spatial structure would be close to identical in every system? Especially RC3 really stands out, but others differ too. The whole issue might be better visualized, if you would show these with the actual reagent structures, and not just with grey symbols. After all there is only 3 systems, so this would not increase the space demands much.

Response: Based on the Reviewer's suggestion, the pre-reactive complexes (RCs) and post-reactive complexes (PCs) considered in the OH-initiated oxidation of the three smallest hydroxyalkyl hydroperoxides (HHPs) have been rechecked in the revised manuscript. Due to the representation way of presented RCs in Figure 2 of the original manuscript, the structure of RCs is misleading. In the revised manuscript, the original Figure 2 is divided into three figures. The free-energy and electronic-energy PESs for the initiation reactions of OH radical with HOCH$_2$OOH, HOCH(CH$_3$)OOH and HOC(CH$_3$)$_2$OOH are presented in Figures 2-4 and S1-S3 of the revised manuscript. And the optimized geometries of all the stationary points, including reactants, RCs, transition states, PCs, and products, are displayed in Figures S6-S8.

In the present study, the structures of distinct HHPs are displayed in Figure 1. The equilibrium geometries of all the stationary points on the PESs are fully optimized at the M06-2X/6-311+G(2df,2p) level of theory, rather than the constrained optimization. For each pre-reactive complex, a conformer search is employed to search the stable conformers of HHPs with OH radical. The structures obtained from the conformer search are initially optimized at the

B3LYP/6-31G(d) level of theory, since the B3LYP functional has been shown to yield reliable relative energies between conformers (Møller et al., 2016). Then, all unique conformers with electronic energies within 5.0 kcal mol^{-1} with respect to the lowest-energy conformer are further optimized at the M06-2X/6-311+G(2df,2p) level of theory. Based on the obtained conformers, the transition states of various possible H-abstraction reactions between OH radical and distinct HHPs are located at the M06-2X/6-311+G(2df,2p) level of theory. The intrinsic reaction coordinate (IRC) calculations are performed in both directions at the M06-2X/6-311+G(2df,2p) level of theory, and then the forward and reverse IRC endpoints are optimized at the same level. For improved energies, the single-point calculations are performed at the M06-2X/ma-TZVP level of theory

A schematic PES for the reaction of OH radical with $HOCH_2OOH$ is shown in Figure 2. As can be seen in Figure 2, the reaction for $HOCH_2OOH$ with OH radical proceeds via four distinct pathways: H-abstraction from the $-O_1H_1$ (R1), $-C_1H_3$ (R2), $-C_1H_4$ (R3) and $-O_2O_3H_2$ groups (R4). For each pathway, a pre-reactive complex with a six- or seven-membered ring structure is formed in the entrance channel, which is stabilized by hydrogen bond interactions between the oxygen atom of OH radical and the abstraction hydrogen atom of $HOCH_2OOH$, and the remnant hydrogen atom of OH radical and one of oxygen atoms of $HOCH_2OOH$ (Figures S6). Then, it surmounts modest barrier that is higher in energy than the reactants to reaction. The reaction barrier $\Delta G_a^{\#}$ are reduced in the order of 6.4 (R1) > 5.8 (R2) ≈ 5.4 (R3) > 1.5 (R4) kcal mol^{-1}, indicating that H-abstraction from the $-O_2O_3H_2$ group (R4) is more preferable than those from the $-O_1H_1$, $-C_1H_3$ and $-C_1H_4$ groups (R1-R3). Same conclusion is also derived from the energy barriers $\Delta E_a^{\#}$ that R4 is the most favorable H-abstraction pathway (Figure S1). The difference of barrier heights can be attributed to the bond dissociation energy (BDE) of different types of bonds in $HOCH_2OOH$ molecule. The BDE are decreased in the order of 103.7 (O_1-H_1) > 98.2 (C_1-H_3) ≈ 97.4 (C_1-H_4) > 87.2 (O_3-H_2) kcal mol^{-1}, which are in good agreement with the order of barrier heights of H-abstraction reactions. As indicated by their reaction free energy values, it can be found that the exothermicity of R4 is the largest among these four H-abstraction reactions. Based on the above discussions, it is concluded that H-abstraction from the $-O_2O_3H_2$ group resulting in formation of $HOCH_2OO$ radical (R4) is feasible on both thermodynamically and kinetically. If we assume that the spatial structure of RC is closed to identical in each H-abstraction reaction, it can be found that H-abstraction from $-CH_2$ group is competitive with that from the -OH group on $HOCH_2OOH$. The

result is contrary to the above-mentioned conclusion, implying that our hypothesis is incorrect.

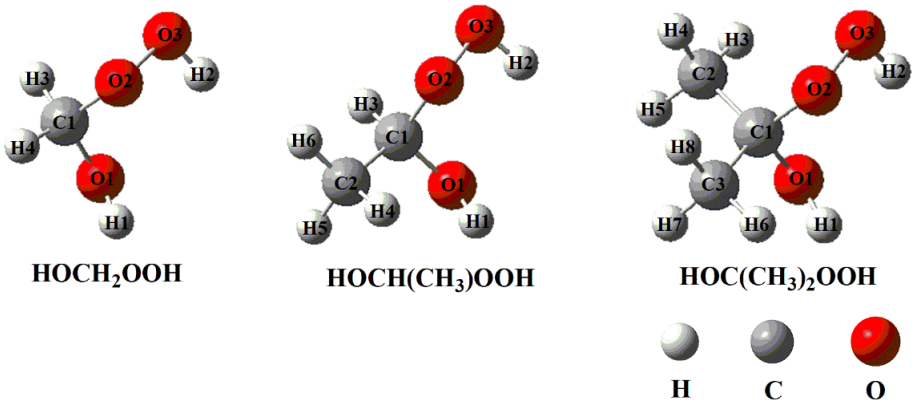

Figure 1. The structures of distinct HHPs

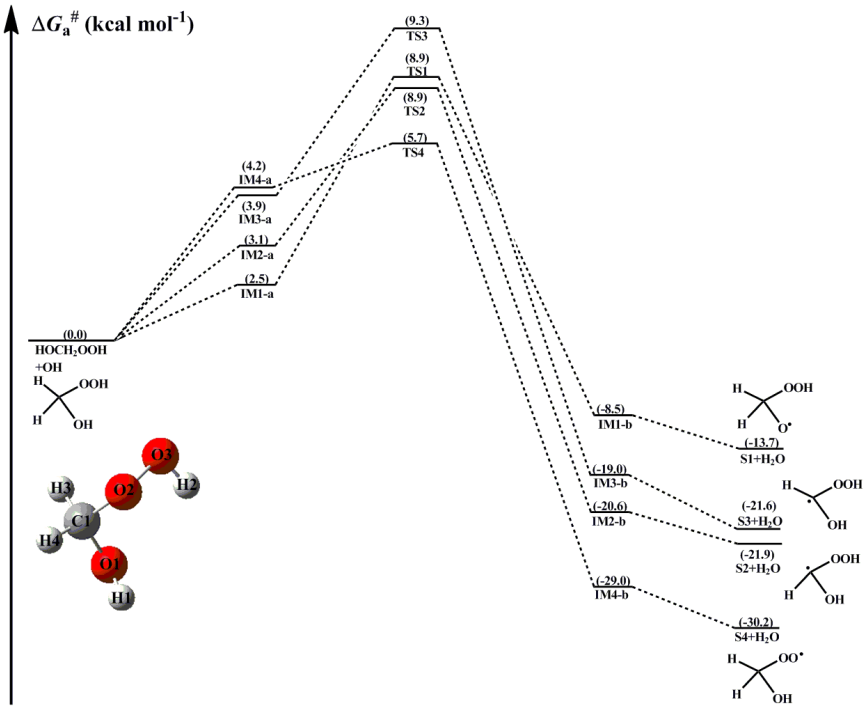

Figure 2. PES ($\Delta G_a^{\#}$) for the OH-initiated reactions of $HOCH_2OOH$ from the CH_2OO + H_2O reaction predicted at the M06-2X/ma-TZVP//M06-2X/6-311+G(2df,2p) level of theory (a and b represent the pre-reactive and post-reactive complexes)

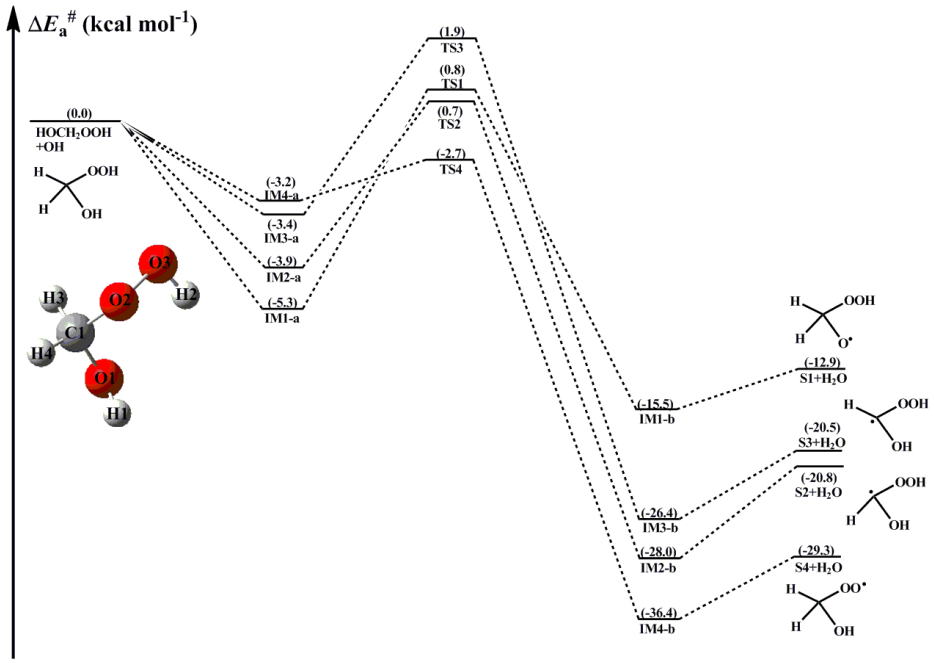

Figure S1. PES ($\Delta E_a^{\#}$) for the OH-initiated reactions of $HOCH_2OOH$ from the $CH_2OO + H_2O$ reaction predicted at the M06-2X/ma-TZVP//M06-2X/6-311+G(2df,2p) level of theory (a and b represent the pre-reactive and post-reactive complexes)

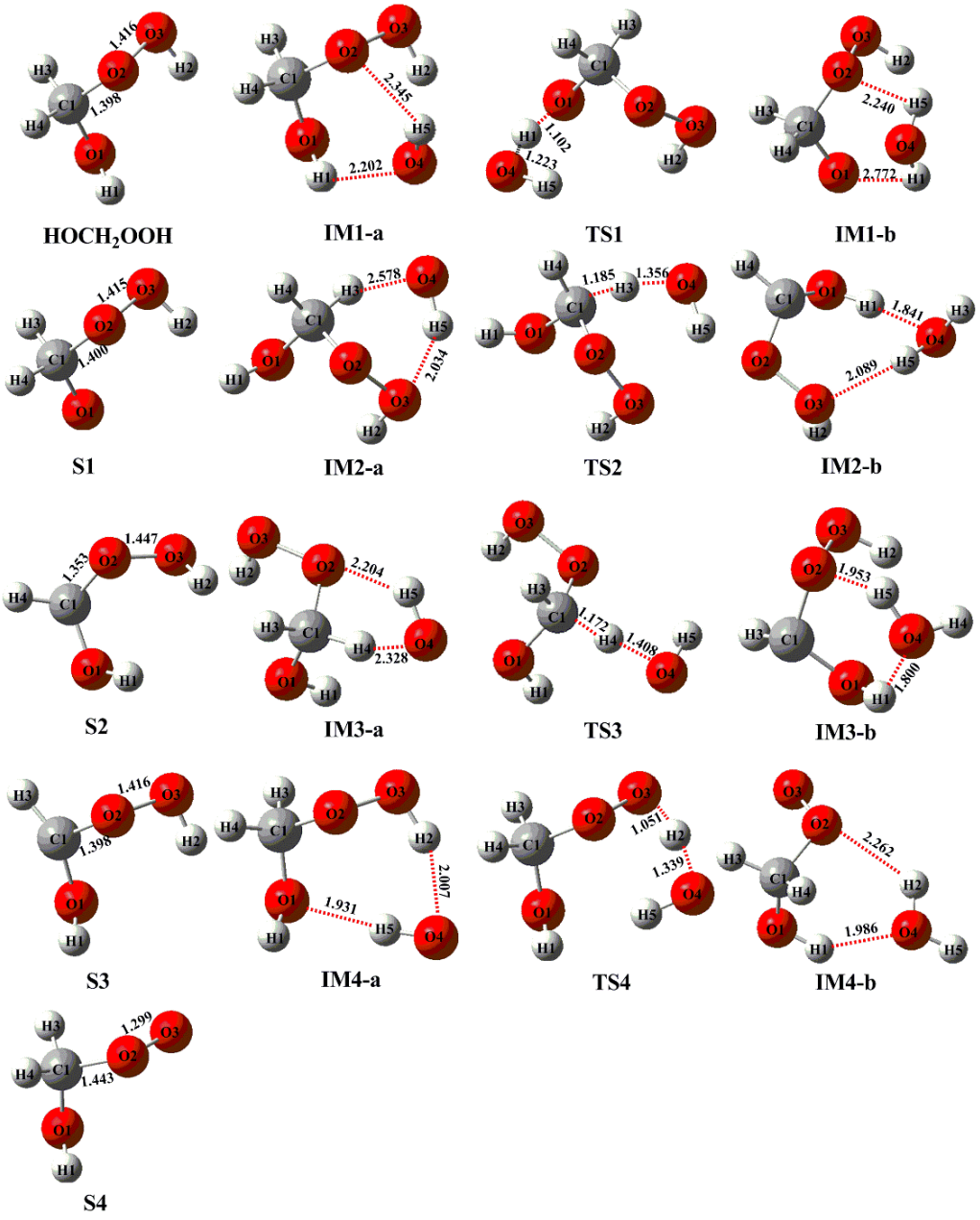

Figure S6. Geometries of all the stationary points for the initial reaction of $HOCH_2OOH$ with OH radical optimized at the M06-2X/6-311+G(2df,2p) level of theory

Corresponding descriptions have been added in the page 10 line 253-273 of the revised manuscript:

As can be seen in Figure 2, the reaction for $HOCH_2OOH$ with OH radical proceeds via four distinct pathways: H-abstraction from the $-O_1H_1$ (R1), $-C_1H_3$ (R2), $-C_1H_4$ (R3) and $-O_2O_3H_2$ groups (R4). For each pathway, a pre-reactive complex with a six- or seven-membered ring structure is formed in the entrance channel, which is stabilized by hydrogen bond interactions between the oxygen atom of OH radical and the abstraction hydrogen atom of $HOCH_2OOH$, and the remnant hydrogen atom of OH radical and one of oxygen atoms of $HOCH_2OOH$ (Figure S6).

Then, it surmounts modest barrier that is higher in energy than the reactants to reaction. The reaction barrier $\Delta G_a^{\#}$ are reduced in the order of 6.4 (R1) > 5.8 (R2) ≈ 5.4 (R3) > 1.5 (R4) kcal mol^{-1}, indicating that H-abstraction from the -$O_2O_3H_2$ group (R4) is more preferable than those from the -O_1H_1, -C_1H_3 and -C_1H_4 groups (R1-R3). Same conclusion is also derived from the energy barriers $\Delta E_a^{\#}$ that R4 is the most favorable H-abstraction pathway (Figure S1). The difference of barrier heights can be attributed to the bond dissociation energy (BDE) of different types of bonds in $HOCH_2OOH$ molecule. The BDE are decreased in the order of 103.7 (O_1-H_1) > 98.2 (C_1-H_3) ≈ 97.4 (C_1-H_4) > 87.2 (O_3-H_2) kcal mol^{-1}, which are in good agreement with the order of barrier heights of H-abstraction reactions. As indicated by their reaction free energy values, it can be found that the exothermicity of R4 is the largest among these four H-abstraction reactions. Based on the above discussions, it is concluded that H-abstraction from the -$O_2O_3H_2$ group resulting in formation of $HOCH_2OO$ radical (R4) is feasible on both thermodynamically and kinetically.

3. Furthermore, it feels a bit strange that in the methylated radicals, the C-H abstraction does not play a bigger role, as seen in some older work on OH + alcohols and OH + amines. From the same previous work it seems somewhat strange that abstraction from -OH is the next likely pathway, and still no C-H abstraction. Moreover, the conclusion that one methyl group substitution does not really matter, but two groups do, seem evenly strange as the methyl groups seem to be rather in the by-stander position, and are likely to influence little on what is occurring at the C-O-OH functionality. What type of sensitivity tests were made to ensure you have found the correct pathways? The IRC computation only ensures you are connecting the right reactants with the correct products, but it does not tell if you have found the most likely pathway or not.

Response: Based on the Reviewer's suggestion, all the H-abstraction pathways included in the initiation reactions of OH radical with $HOCH_2OOH$, $HOCH(CH_3)OOH$ and $HOC(CH_3)_2OOH$ have been recalculated in the revised manuscript. Owing to our carelessness, the conclusion that two methyl groups substitutions have a significant influence on the barrier of H-abstraction from the -OOH group is incorrect in the original manuscript. In the revised manuscript, a conformer search is employed to search the stable conformers of HHPs with OH radical. Based on the structures resulting from the conformer search, the transition states of various possible

H-abstraction reactions between OH radical and distinct HHPs are located at the M06-2X/6-311+G(2df,2p) level of theory. The intrinsic reaction coordinate (IRC) calculations are performed in both directions at the M06-2X/6-311+G(2df,2p) level of theory, and then the forward and reverse IRC endpoints are optimized at the same level. The single-point calculations are performed at the M06-2X/ma-TZVP level of theory based on the M06-2X/6-311+G(2df,2p) optimized geometries. By comparing the stability of pre-reactive complex and the barrier height of transition state, the most likely manner of each H-abstraction pathway is found. The corresponding free-energy and electronic-energy PESs for the OH-initiated oxidation of $HOCH_2OOH$, $HOCH(CH_3)OOH$ and $HOC(CH_3)_2OOH$ are presented in Figures 2-4 and S1-S3 of the revised manuscript. And the geometrical structures of all the stationary points are displayed in Figures S6-S8.

A schematic PES for the atmospheric transformation of $HOCH(CH_3)OOH$ initiated by OH radical is drawn in Figure 3. As shown in Figure 3, the reaction of OH radical with $HOCH(CH_3)OOH$ includes six kinds of H-abstraction pathways. Each H-abstraction reaction begins with the formation of a weakly bound hydrogen bonded pre-reactive complex with a six- or seven-membered ring structure in the entrance channel (Figure S7). Then it immediately transforms into the respective product via the corresponding transition state. The $\Delta G_a^{\#}$ of H-abstraction from the $-C_1H_3$ (R6) and $-O_2O_3H_2$ (R8) groups are 2.2 and 1.7 kcal·mol^{-1}, respectively, which are about 4-5 kcal·mol^{-1} lower than those from the $-O_1H_1$ (R5) and $-CH_3$ groups (R7). The result reveals that R6 and R8 have nearly identical importance in the atmosphere. Compared with the barriers of H-abstraction at the C_α (R6) and C_β (R7) positions, it can be found that the former case is more favourable than the latter case. This conclusion is further supported by Jara-Toro's study for the reactions of OH radical with linear saturated alcohols (methanol, ethanol and n-propanol) that H-abstraction at the C_α position is predominant (Jara-Toro et al., 2017, 2018).

From Figure 4, it can be seen that H-abstraction by OH radical from $HOC(CH_3)_2OOH$ includes eight possible H-abstraction pathways. All the H-abstraction reactions are strongly exothermic and spontaneous, signifying that they are thermodynamically feasible under atmospheric conditions. It deserves mentioning that the release of energy of R12 is significantly greater than those of R9-R11. For each H-abstraction pathway, a RC with a six- or

seven-membered ring structure is formed prior to the corresponding TS, which is more stable than the separate reactants due to the hydrogen bond interactions between $HOC(CH_3)_2OOH$ and OH radical. Then, the RC overcomes modest barrier to reaction. The $\Delta G_a^{\#}$ of H-abstraction from the $-O_2O_3H_2$ group (R12) is 2.7 kcal mol^{-1}, which is the lowest among these eight H-abstraction reactions. This result again shows that the H-abstraction from the $-O_2O_3H_2$ group is the dominant pathway.

In summary, the dominant pathway is the H-abstraction from the -OOH group in the initiation reactions of OH radical with $HOCH_2OOH$. H-abstraction from -CH group is competitive with that from the -OOH group in the reaction of OH radical with $HOCH(CH_3)OOH$. Compared the barriers of H-abstraction from the -OOH and $-CH_2$ groups in the OH + $HOCH_2OOH$ system with that for the analogous reactions in the OH + $HOCH(CH_3)OOH$ system. It can be found that the barrier of H-abstraction from the -CH group is reduced by 3.6 kcal mol^{-1}, whereas the barrier of H-abstraction from the -OOH group is increased by 0.2 kcal mol^{-1} when a methyl group substitution occurs at the C1-position of $HOCH_2OOH$. The dominant pathway is the H-abstraction from the -OOH group in the reaction of OH radical with $HOC(CH_3)_2OOH$, and the barrier height is increased by 1.2 kcal mol^{-1} compared to the OH + $HOCH_2OOH$ system. The barrier of H-abstraction from the -OOH group is slightly increased as the number of methyl group is increased.

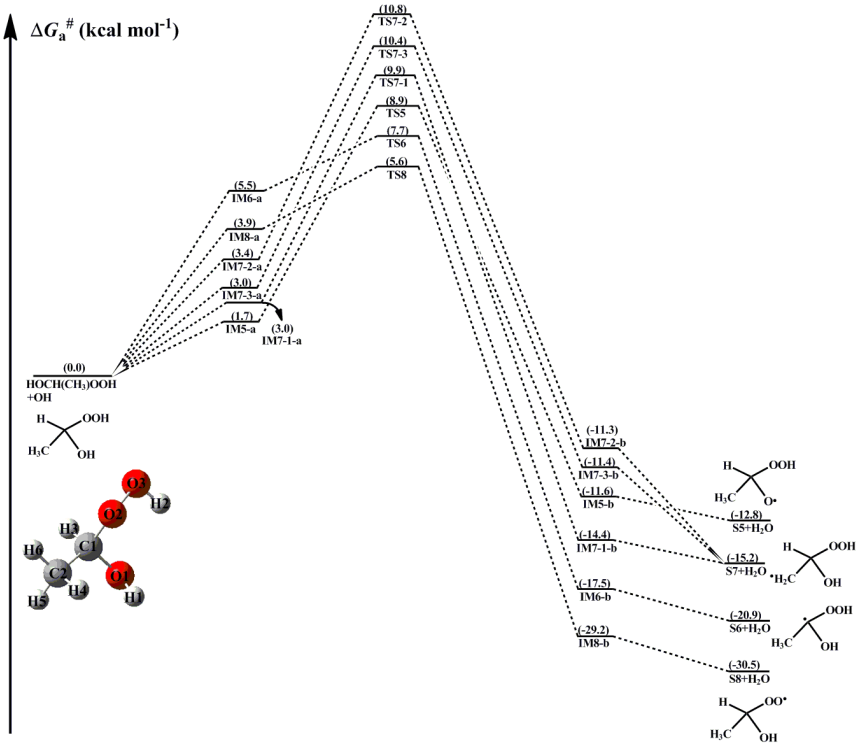

Figure 3. PES ($\Delta G_a^{\#}$) for the OH-initiated reactions of $HOCH(CH_3)OOH$ from the *anti*-CH_3CHOO + H_2O reaction predicted at the M06-2X/ma-TZVP//M06-2X/6-311+G(2df,2p) level of theory

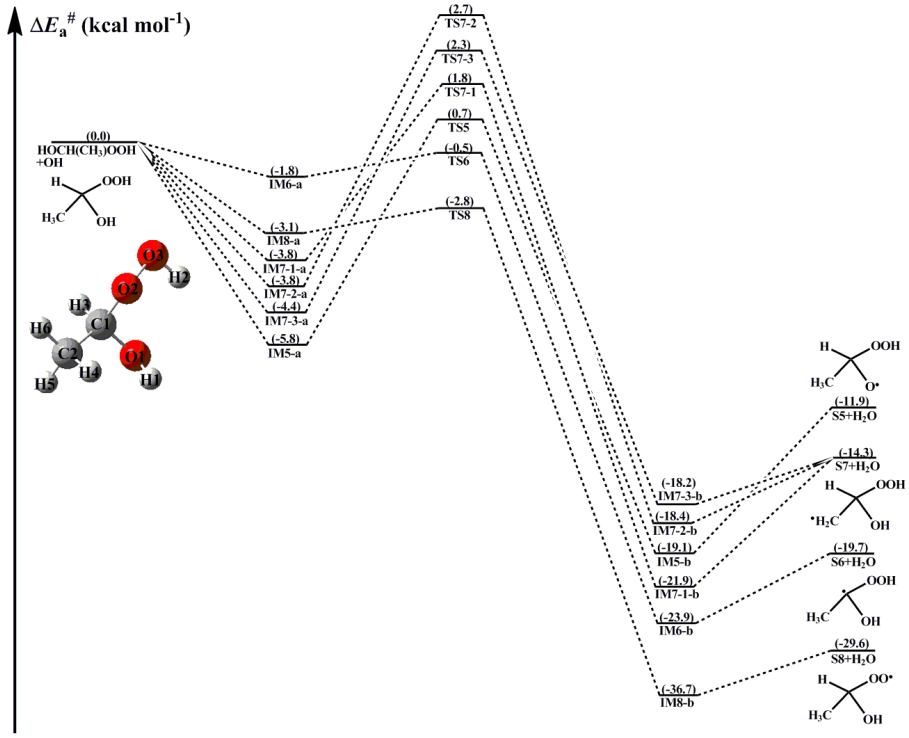

Figure S2. PES ($\Delta E_a^{\#}$) for the OH-initiated reactions of $HOCH(CH_3)OOH$ from the *anti*-CH_3CHOO + H_2O reaction predicted at the M06-2X/ma-TZVP//M06-2X/6-311+G(2df,2p) level of theory (a and b represent the pre-reactive and post-reactive complexes)

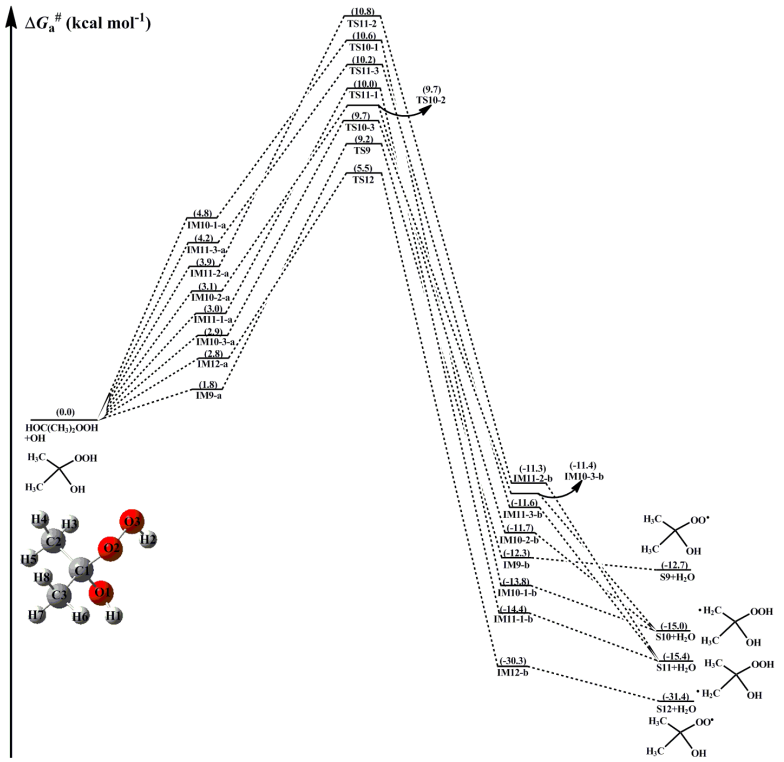

Figure 4. PES ($\Delta G_a^{\#}$) for the OH-initiated reactions of $HOC(CH_3)_2OOH$ from the $(CH_3)_2COO$ + H_2O reaction predicted at the M06-2X/ma-TZVP//M06-2X/6-311+G(2df,2p) level of theory (a and b represent the pre-reactive and post-reactive complexes)

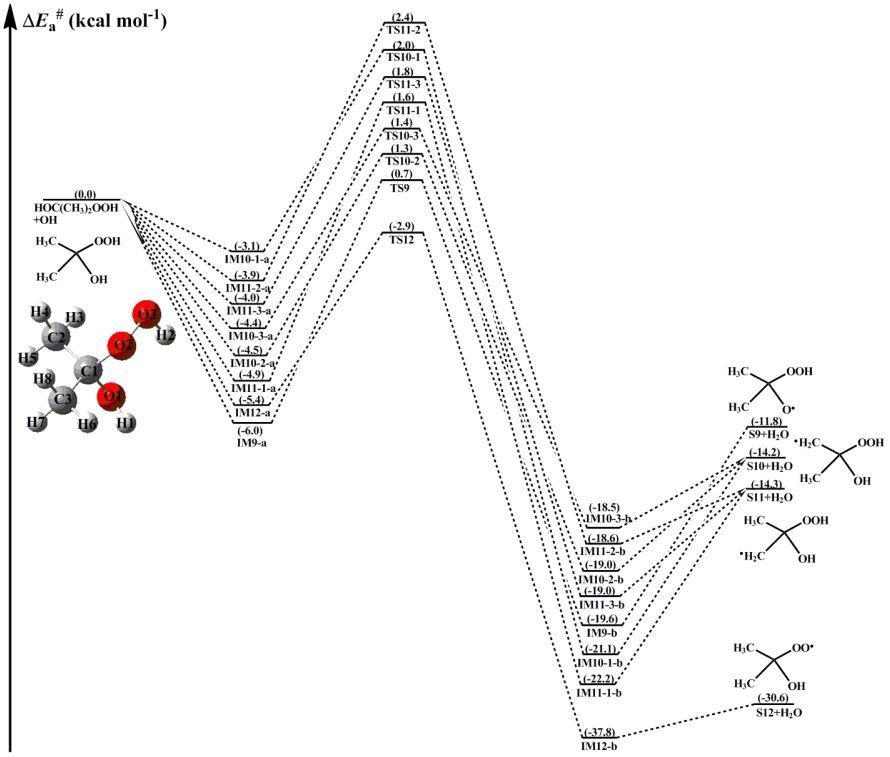

Figure S3. PES ($\Delta E_a^{\#}$) for the OH-initiated reactions of $HOC(CH_3)_2OOH$ from the $(CH_3)_2COO$ + H_2O reaction predicted at the M06-2X/ma-TZVP//M06-2X/6-311+G(2df,2p) level of theory (a and b represent the pre-reactive and post-reactive complexes)

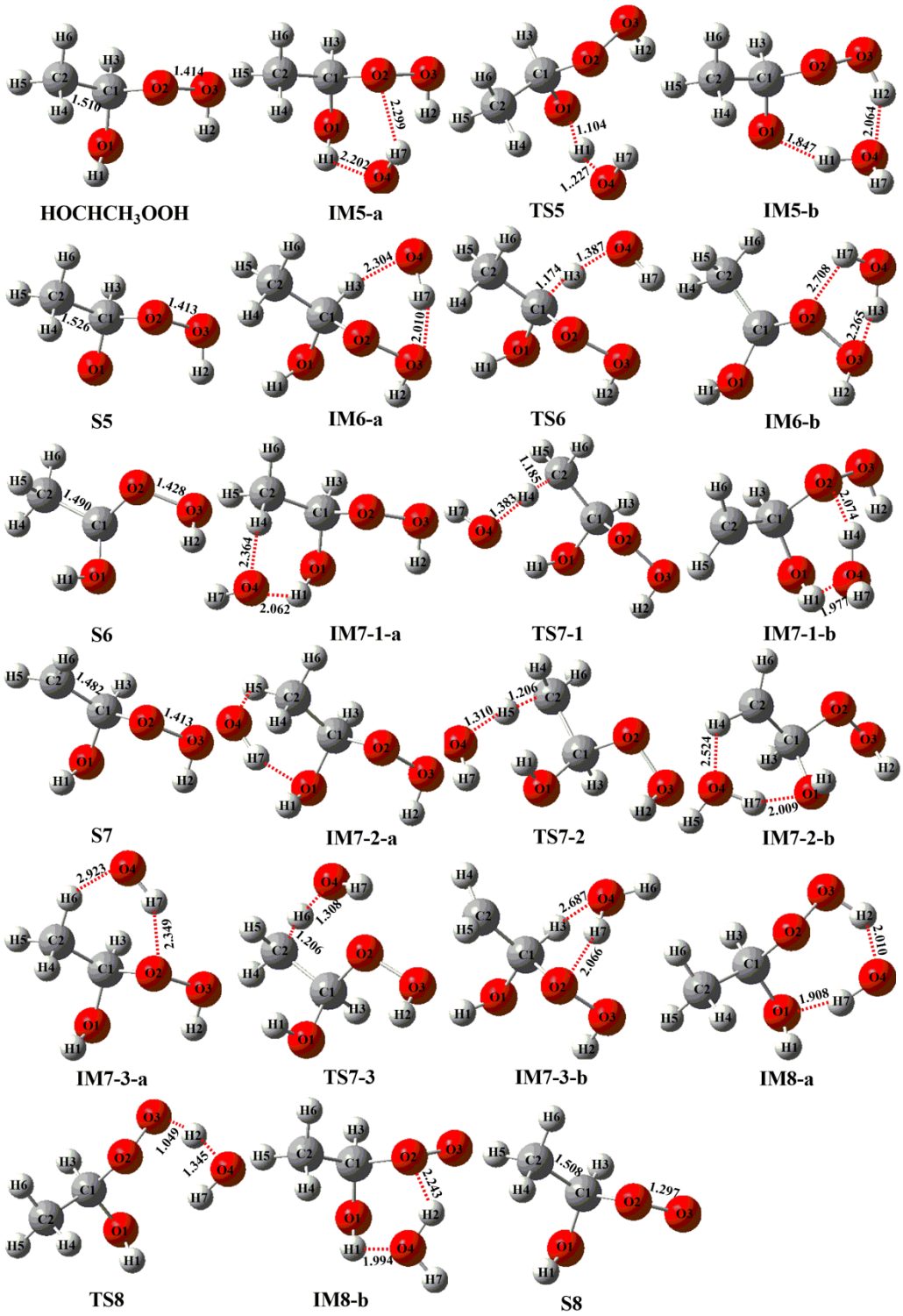

Figure S7. Geometries of all the stationary points for the initial reaction of HOCH(CH_3)OOH with OH radical optimized at the M06-2X/6-311+G(2df,2p) level of theory

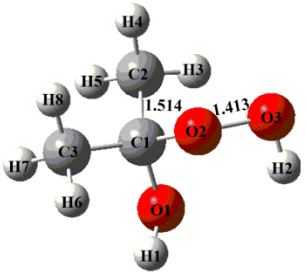

$HOC(CH_3)_2OOH$

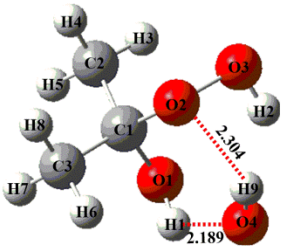

IM9-a

TS9

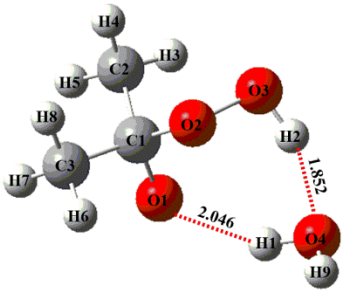

IM9-b

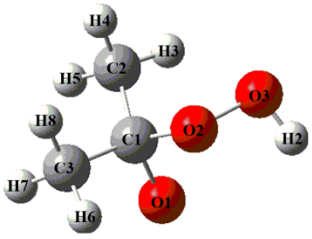

S9

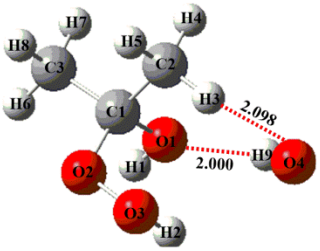

IM10-1-a

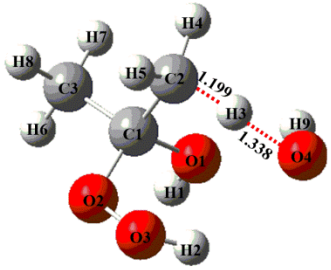

TS10-1

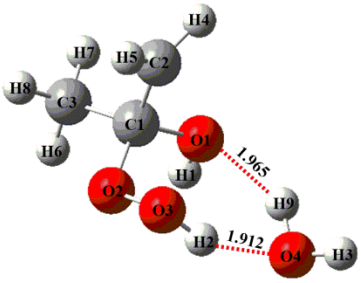

IM10-1-b

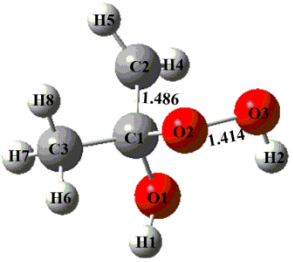

S10

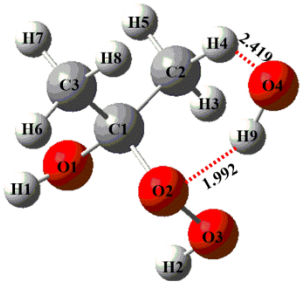

IM10-2-a

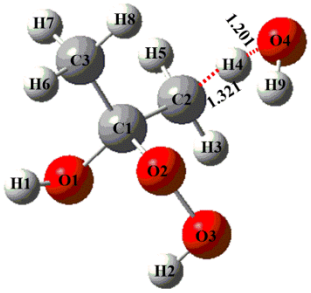

TS10-2

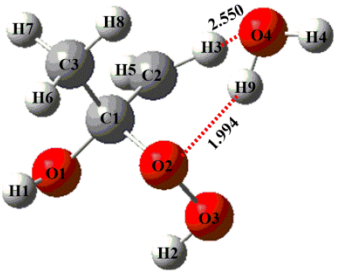

IM10-2-b

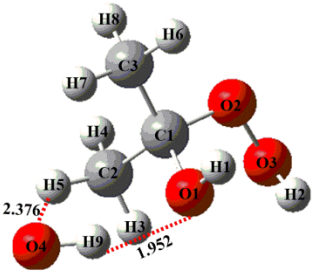

IM10-3-a

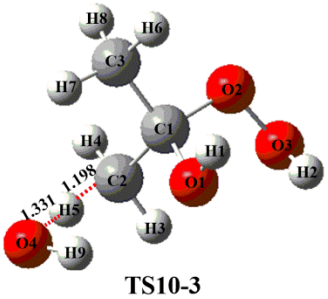

TS10-3

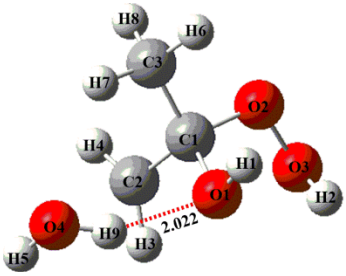

IM10-3-b

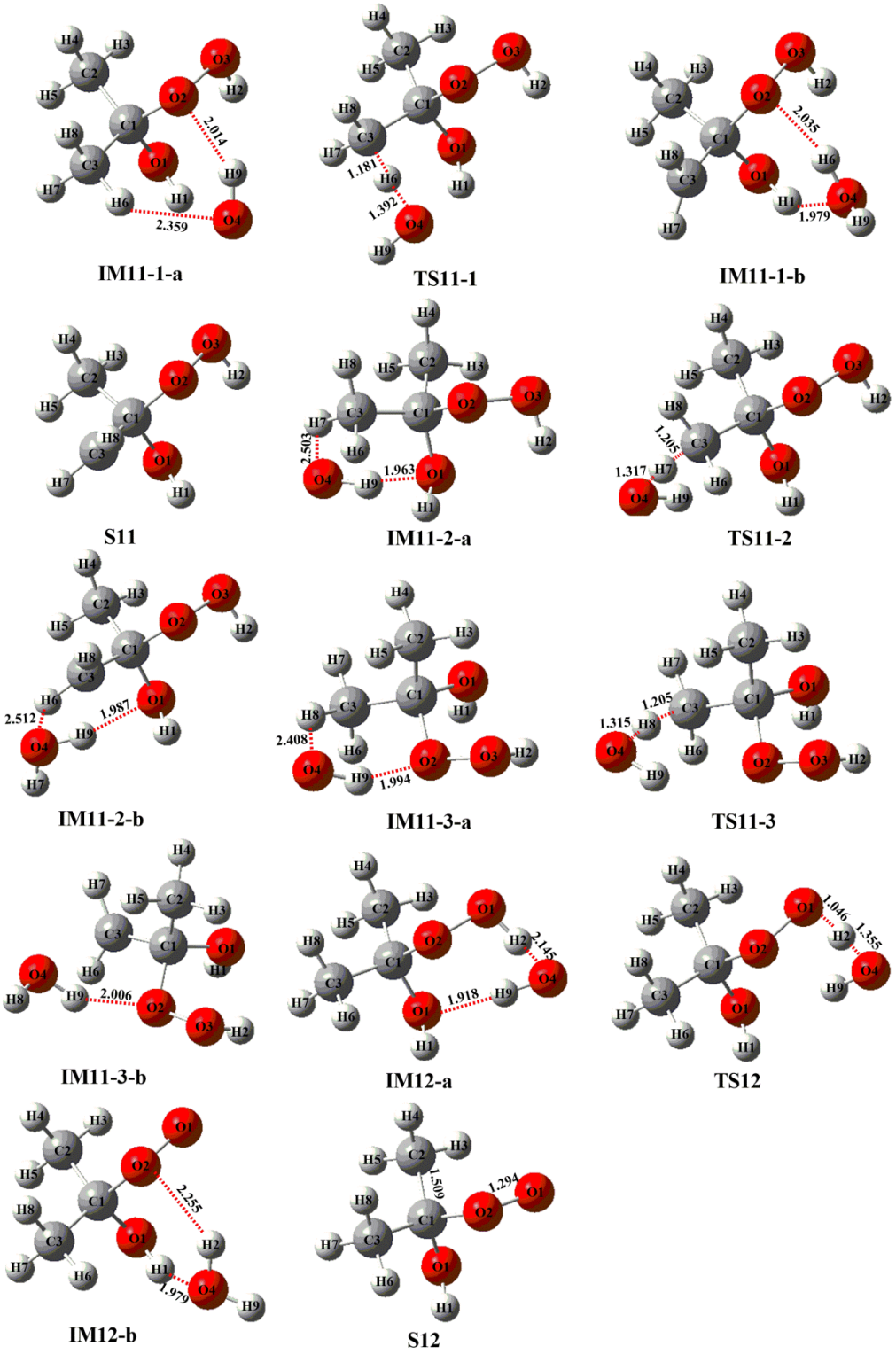

Figure S8. Geometries of all the stationary points for the initial reaction of $HOC(CH_3)_2OOH$ with OH radical optimized at the M06-2X/6-311+G(2df,2p) level of theory

Corresponding descriptions have been added in the page 10 line 274-288, page 11 line 309-320 and page 13 line 353-365 of the revised manuscript:

Considering the different reaction sites of hydrogen atoms, the atmospheric transformation of $HOCH(CH_3)OOH$ from the anti-CH_3CHOO + H_2O reaction should have six types of

H-abstraction pathways as presented in Figure 3. As shown in Figure 3, each H-abstraction reaction begins with the formation of a weakly bound hydrogen bonded pre-reactive complex with a six- or seven-membered ring structure in the entrance channel (Figure S7). Then it immediately transforms into the respective product via the corresponding transition state. The $\Delta G_a^{\#}$ of H-abstraction from the -C_1H_3 (R6) and -$O_2O_3H_2$ (R8) groups are 2.2 and 1.7 kcal mol^{-1}, respectively, which are ~ 4-5 kcal mol^{-1} lower than those from the -O_1H_1 (R5) and -CH_3 groups (R7). This result shows that R6 and R8 have nearly identical importance in the atmosphere. Compared with the barriers of H-abstraction at the C_α (R6) and C_β (R7) positions, it can be found that the former case is more favourable than the latter case. This conclusion is further supported by Jara-Toro's study for the reactions of OH radical with linear saturated alcohols (methanol, ethanol and n-propanol) that H-abstraction at the C_α position is predominant (Jara-Toro, R. A et al., 2017, 2018).

From Figure 4, it can be seen that H-abstraction from $HOC(CH_3)_2OOH$ includes eight possible H-abstraction pathways. All the H-abstraction reactions are strongly exothermic and spontaneous, signifying that they are thermodynamically feasible under atmospheric conditions. It deserves mentioning that the release of energy of R12 is significantly greater than those of R9-R11. For each H-abstraction pathway, a RC with a six- or seven-membered ring structure is formed prior to the corresponding TS, which is more stable than the separate reactants due to the hydrogen bond interactions between $HOC(CH_3)_2OOH$ and OH radical. Then, the RC overcomes modest barrier to reaction. The $\Delta G_a^{\#}$ of H-abstraction from the -$O_2O_3H_2$ group (R12) is 2.7 kcal mol^{-1}, which is the lowest among these eight H-abstraction reactions. This result again shows that the H-abstraction from the -$O_2O_3H_2$ group is the dominant pathway.

In summary, the dominant pathway is the H-abstraction from the -OOH group in the initiation reactions of OH radical with $HOCH_2OOH$. H-abstraction from -CH group is competitive with that from the -OOH group in the reaction of OH radical with $HOCH(CH_3)OOH$. Compared the barriers of H-abstraction from the -OOH and -CH_2 groups in the $\dot{O}H + HOCH_2OOH$ system with that for the analogous reactions in the $\dot{O}H + HOCH(CH_3)OOH$ system. It can be found that the barrier of H-abstraction from the -CH group is reduced by 3.6 kcal mol^{-1}, whereas the barrier of H-abstraction from the -OOH group is increased by 0.2 kcal mol^{-1} when a methyl group substitution occurs at the C1-position of $HOCH_2OOH$. The dominant pathway is the

H-abstraction from the -OOH group in the reaction of OH radical with $HOC(CH_3)_2OOH$, and the barrier height is increased by 1.2 kcal mol^{-1} compared to the OH + $HOCH_2OOH$ system. The barrier of H-abstraction from the -OOH group is slightly increased as the number of methyl group is increased.

4. Figures: Symbol fonts should be increased in all figures showing potential energy surfaces. Currently they are in many places unreadable. Moreover, the molecular figures are too small to follow the mechanism from the figures with this symbolism. To make matters worse, it is difficult to see what peroxy radicals are reacting to make the tetroxides in the figures, and there is no help from the captions. There must be a better way to make these readable. The easiest way is to split the figures in parts (i.e., Figure 3 becomes, for example, Figures 3a to 3c) and at the same time considerably increase the amount of text in the captions.

Response: Based on the Reviewer's suggestion, the symbol fonts and molecular structures in all figures have been redrawn in the revised manuscript. For clarity, the 2D drawings of some important species are labeled in the PESs of the initiation reactions of OH radical with $HOCH_2OOH$, $HOCH(CH_3)OOH$ and $HOC(CH_3)_2OOH$ (Figures 2-4 and S1-S3). And the optimized geometries of all the stationary points are displayed in Figures S6-S8. The PESs of the self-reactions of $HOCH_2OO$ and $HOCH(CH_3)OO$ radicals are divided into two parts (Figures 5a and 5b, Figures 6a and 6b). And the captions of all figures are reworded in the revised manuscript.

5. Figure 2 caption: Far more details of this figure should be included. Currently I am having very hard time understanding it based on the manuscript text. Why, for example, the RC is uphill in energy although you go from separated reactants into a pre-reactive (=favorable binding) complex? Currently the caption does not help.

Response: Based on the Reviewer's suggestion, the original Figure 2 has been divided into three figures in the revised manuscript. The free energy and electronic energy PESs for the initiation reactions of OH radical with $HOCH_2OOH$, $HOCH(CH_3)OOH$ and $HOC(CH_3)_2OOH$ are presented in Figures 2-4 and S1-S3, respectively. The energy of pre-reactive complex is higher than that of the separate reactants when the free energies are used to construct the PES. The energy of pre-reactive complex is lower than that of the separate reactants when the electronic energies

are employed to build the PES. The change in the position of pre-reactive complex relative to the initial reactants is due to the contribution of entropy effect in the free energy.

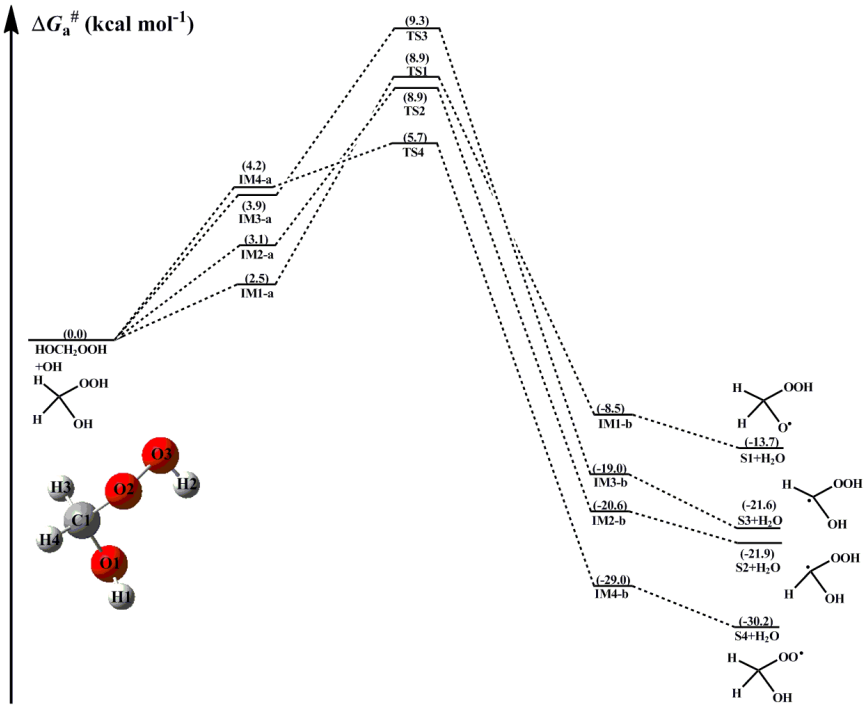

Figure 2. PES ($\Delta G_a^{\#}$) for the OH-initiated reactions of $HOCH_2OOH$ from the CH_2OO + H_2O reaction predicted at the M06-2X/ma-TZVP//M06-2X/6-311+G(2df,2p) level of theory (a and b represent the pre-reactive and post-reactive complexes)

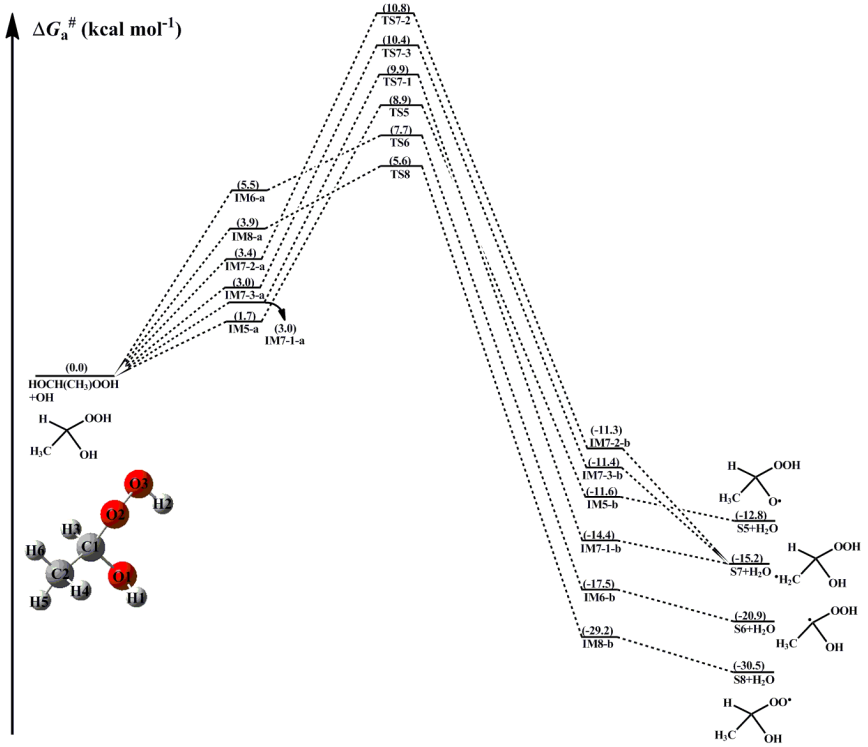

Figure 3. PES ($\Delta G_a^{\#}$) for the OH-initiated reactions of $HOCH(CH_3)OOH$ from the *anti*-CH_3CHOO + H_2O reaction predicted at the M06-2X/ma-TZVP//M06-2X/6-311+G(2df,2p) level of theory (a and b represent the pre-reactive and post-reactive complexes)

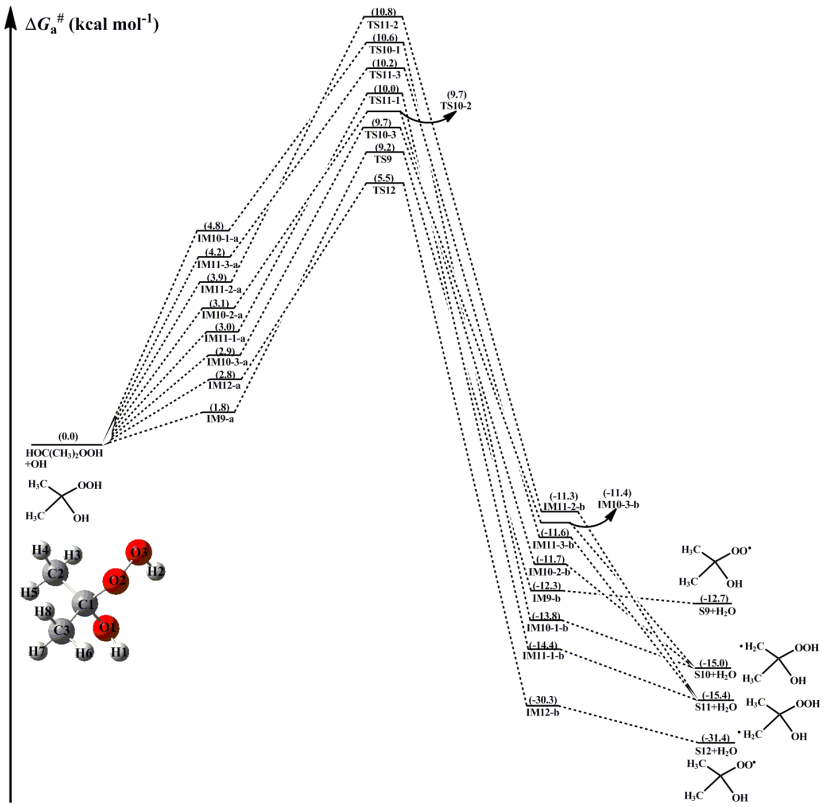

Figure 4. PES ($\Delta G_a^{\#}$) for the OH-initiated reactions of $HOC(CH_3)_2OOH$ from the $(CH_3)_2COO$ + H_2O reaction predicted at the M06-2X/ma-TZVP//M06-2X/6-311+G(2df,2p) level of theory (a and b represent the pre-reactive and post-reactive complexes)

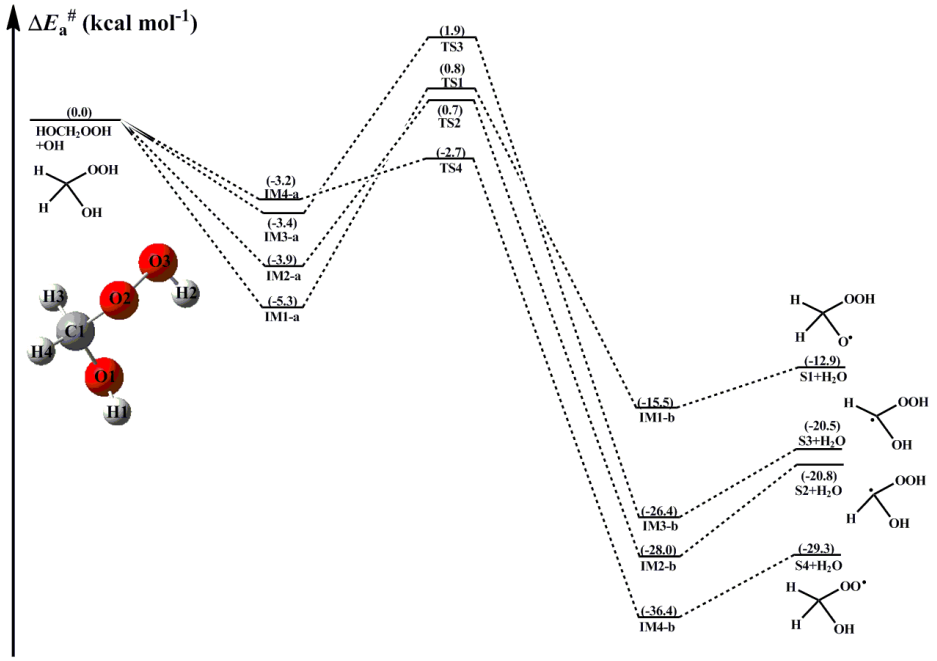

Figure S1. PES ($\Delta E_a^{\#}$) for the OH-initiated reactions of $HOCH_2OOH$ from the CH_2OO + H_2O reaction predicted at the M06-2X/ma-TZVP//M06-2X/6-311+G(2df,2p) level of theory (a and b represent the pre-reactive and post-reactive complexes)

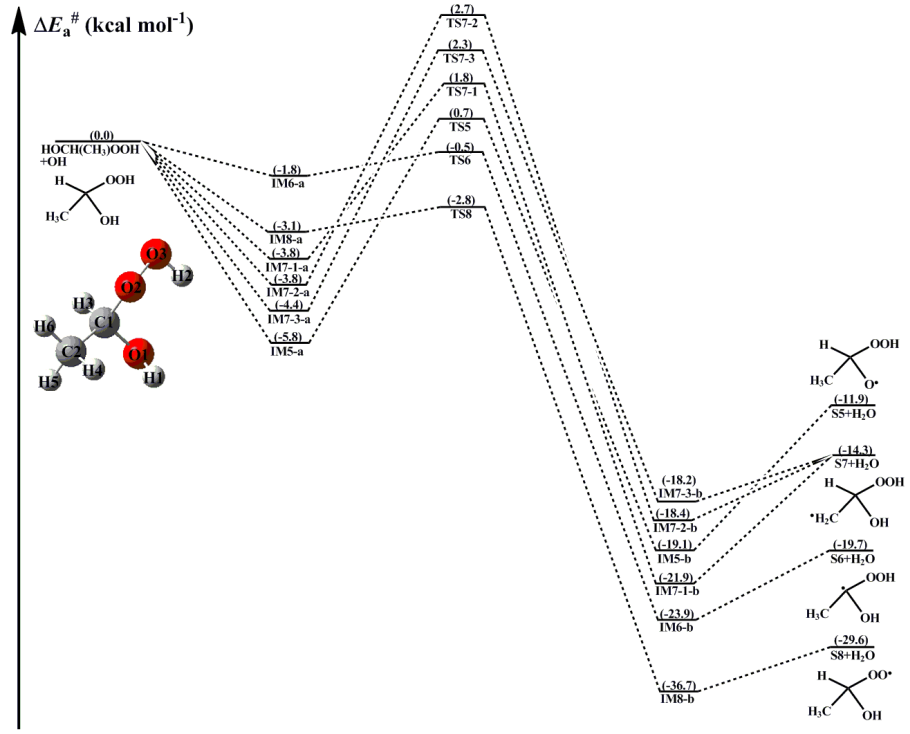

Figure S2. PES ($\Delta E_a^{\#}$) for the OH-initiated reactions of $HOCH(CH_3)OOH$ from the *anti*-CH_3CHOO + H_2O reaction predicted at the M06-2X/ma-TZVP//M06-2X/6-311+G(2df,2p) level of theory (a and b represent the pre-reactive and post-reactive complexes)

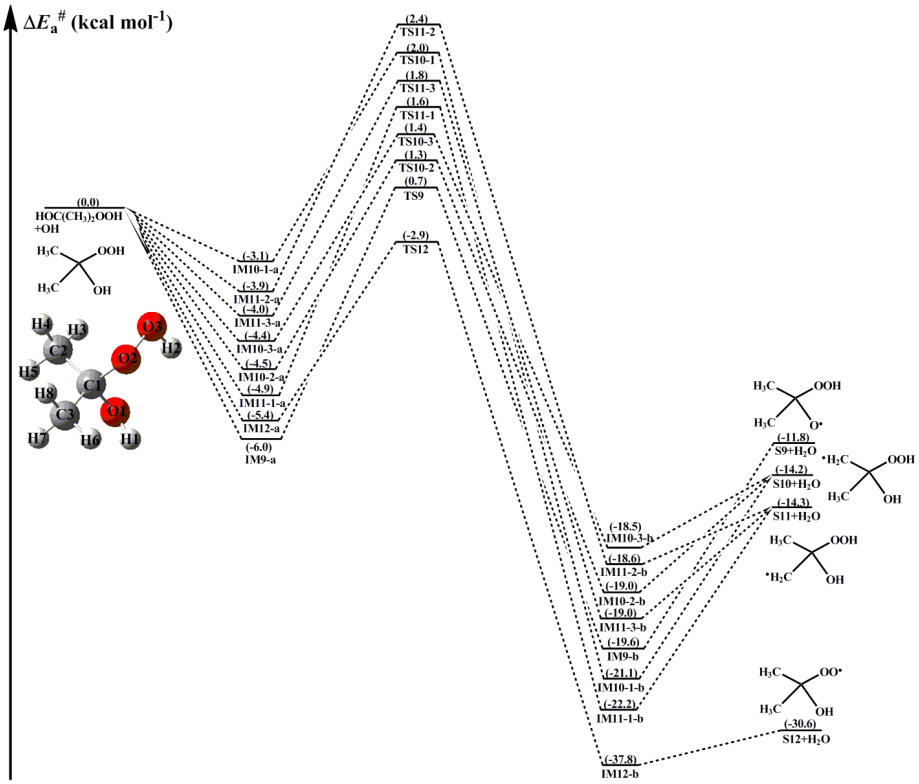

Figure S3. PES ($\Delta E_a^{\#}$) for the OH-initiated reactions of $HOC(CH_3)_2OOH$ from the $(CH_3)_2COO$ + H_2O reaction predicted at the M06-2X/ma-TZVP//M06-2X/6-311+G(2df,2p) level of theory (a and b represent the pre-reactive and post-reactive complexes)

6 Although the message comes “mostly clear” throughout the text, the text should be language edited. Again, I do understand it quite well being a non-native speaker, but I assume native speakers will not agree with me.

Response: Based on the Reviewer’s suggestion, the revised manuscript has been corrected carefully, and the sentences and grammar have been proofread detailedly by some native English speakers.

7 Hydroxyalkyl hydroperoxides (HHPs) are formed in several other reactions too, especially in OH addition initiation with subsequent HO_2 termination. This could be mentioned in the intro too.

Response: Based on the Reviewer’s suggestion, the HHPs formed from the initiation OH-addition with subsequent HO_2-termination reactions have been added in the Introduction of the revised manuscript. Hydroxyalkyl hydroperoxides (HHPs), formed in the reactions of Criegee intermediates (CIs) with water vapour and in the initiation OH-addition with subsequent HO_2-termination reactions, play important roles in the formation of secondary organic aerosol (SOA).

Corresponding descriptions have been revised in the page 3 line 58-61 of the revised manuscript:

Hydroxyalkyl hydroperoxides (HHPs), formed in the reactions of Criegee intermediates (CIs) with water vapour and in the initiation OH-addition with subsequent HO_2-termination reactions, play important roles in the formation of secondary organic aerosol (SOA) (Qiu et al., 2019; Kumar et al., 2014).

8 Line 69: What is the difference between vapor pressure and volatility?

Response: In general, at a given temperature, the higher the saturated vapor pressure of compound, the stronger the volatility. At different temperatures, the saturated vapor pressure of the same compound is different. HHPs, due to the presence of both hydroxyl and perhydroxy moieties, have relatively low volatility contributing substantially to the formation of SOA.

Corresponding descriptions have been revised in the page 3 line 76-78 of the revised manuscript:

HHPs, due to the presence of both hydroxyl and perhydroxy moieties, have relatively low

volatility contributing substantially to the formation of SOA (Qiu et al., 2019).

9 In the Abstract, please reword the following sentence: "In urban environments, the rate-limiting step is the hydrogen abstraction by O_2 in the processes of $HOCH_2OO$ radical reaction with NO, while it becomes the O-O bond scission when one or two methyl substitutions occur at the C1-position of $HOCH_2OO$ radical." I think I know what this means, but I can't be sure.

Response: Based on the Reviewer's suggestion, the mentioned sentence has been reworded as "In urban environments, reaction with O_2 forming formic acid and HO_2 radical is the dominant removal pathway for $HOCH_2O$ radical formed from the reaction of $HOCH_2OO$ radical with NO. The β-site C-C bond scission is the dominate pathway in the dissociation of $HOCH(CH_3)O$ and $HOC(CH_3)_2O$ radicals formed from the $HOCH(CH_3)OO\cdot$ + NO and $HOC(CH_3)_2OO\cdot$ + NO reactions."

Corresponding descriptions have been revised in the page 2 line 48-536 of the revised manuscript:

In urban environments, reaction with O_2 forming formic acid and HO_2 radical is the dominant removal pathway for $HOCH_2O$ radical formed from the reaction of $HOCH_2OO$ radical with NO. The β-site C-C bond scission is the dominate pathway in the dissociation of $HOCH(CH_3)O$ and $HOC(CH_3)_2O$ radicals formed from the $HOCH(CH_3)OO\cdot$ + NO and $HOC(CH_3)_2OO\cdot$ + NO reactions.

10 The sentence: "Previous literatures have been confirmed that the energies obtained from unrestricted DFT are comparable to the multi-reference CASSCF method (Lee et al., 2016; Bach et al., 2005)." seems to indicate that "unrestricted DFT" gives similar results to "CASSCF". Is this really the case, and why it is so? Does not the choice of active space factor in?

Response: The tetroxide intermediate formed from the self-reaction of RO_2 radical proceeds through the asymmetric two step O-O bond scission to produce a caged tetroxide intermediate of overall singlet multiplicity comprising two same-spin alkoxyl radicals (spin down) and triplet oxygen (spin up). This type of reaction mechanism can be described by the broken symmetry unrestricted DFT (UDFT) and multi-reference CASSCF methods (Lee et al., 2016; Bach et al., 2005). Previous studies have demonstrated that the UDFT method is suitable to identify the

metastable singlet caged radical complex minimum and is successfully located the transition states of O-O bond homolysis, and the energies are comparable to the more accurate and expensive CASSCF method (Lee et al., 2016; Bach et al., 2005). In the present study, the UDFT method is selected to study the asymmetric O-O bond scission and represents a compromise between the computational accuracy and efficiency. The broken symmetry UM06-2X method is applied to generate the initial guesses of the tetroxide intermediate and transition state geometries with mixed HOMO and LUMO ($S^2 \approx 1$) by using the guess = mix keyword. The single-point energies are refined at the UM06-2X/ma-TZVP level of theory.

Corresponding descriptions have been revised in the page 6 line 155-170 of the revised manuscript:

The tetroxide intermediate formed from the self-reaction of RO_2 radical proceeds through the asymmetric two step O-O bond scission to produce a caged tetroxide intermediate of overall singlet multiplicity comprising two same-spin alkoxyl radicals (spin down) and triplet oxygen (spin up). This type of reaction mechanism can be described by the broken symmetry unrestricted DFT (UDFT) and multi-reference CASSCF methods (Lee et al., 2016; Bach et al., 2005). Previous studies have demonstrated that the UDFT method is suitable to identify the metastable singlet caged radical complex minimum and is successfully located the transition states of O-O bond homolysis, and the energies are comparable to the more accurate and expensive CASSCF method (Lee et al., 2016; Bach et al., 2005). In the present study, the UDFT method is selected to study the asymmetric O-O bond scission and represents a compromise between the computational accuracy and efficiency. The broken symmetry UM06-2X/6-311+G(2df,2p) method is applied to generate the initial guesses of the tetroxide intermediate and transition state geometries with mixed HOMO and LUMO ($S^2 \approx 1$) by using the guess = mix keyword. The single-point energies are refined at the UM06-2X/ma-TZVP level of theory.

11 Please embed figures into text. It helps no one if they are positioned after the text.

Response: Based on the Reviewer's suggestion, all figures have been embedded into the revised manuscript.

12 Why is there four reactions in Figure 2, although there are 3 title reactions handled in the paper?

In fact, the fourth option is hinted in the text “Considering the different chemical environments of hydrogen atoms, the atmospheric transformation of HHPs initiated by OH radical should have four types of H-abstraction pathways as presented in Figure 2.” but I did not observe an explanation what is meant by it. In any case it would be good to break the Figure 2 into several separate figures - one for each reaction.

Response: Based on the Reviewer’s suggestion, the Figure 2 has been divided into three separate figures in the revised manuscript. The free-energy PESs for the initiation reactions of OH radical with $HOCH_2OOH$, $HOCH(CH_3)OOH$ and $HOC(CH_3)_2OOH$ are presented in Figures 2-4, respectively. As can be seen in Figure 2, the reaction for $HOCH_2OOH$ with OH radical proceeds via four distinct pathways: H-abstraction from the $-O_1H_1$ (R1), $-C_1H_3$ (R2), $-C_1H_4$ (R3) and $-O_2O_3H_2$ groups (R4). For each pathway, a pre-reactive complex with a six- or seven-membered ring structure is formed in the entrance channel, which is stabilized by hydrogen bond interactions between the oxygen atom of OH radical and the abstraction hydrogen atom of $HOCH_2OOH$, and the remnant hydrogen atom of OH radical and one of oxygen atoms of $HOCH_2OOH$. Then, it surmounts modest barrier that is higher in energy than the reactants to reaction. The reaction barrier $\Delta G_a^{\#}$ are reduced in the order of 6.4 (R1) > 5.8 (R2) $\approx$ 5.4 (R3) > 1.5 (R4) kcal $\cdot$mol^{-1}, indicating that H-abstraction from the $-O_2O_3H_2$ group (R4) is more preferable than those from the $-O_1H_1$, $-C_1H_3$ and $-C_1H_4$ groups (R1-R3). The difference of barrier heights can be attributed to the bond dissociation energy (BDE) of different types of bonds in $HOCH_2OOH$ molecule. The BDE are decreased in the order of 103.7 (O_1-H_1) > 98.2 (C_1-H_3) $\approx$ 97.4 (C_1-H_4) > 87.2 (O_3-H_2) kcal $\cdot$mol^{-1}, which are in good agreement with the order of barrier heights of distinct H-abstraction reactions. As indicated by their reaction free energy values, it can be found that the exothermicity of R4 is the largest among these four H-abstraction reactions. Based on the above discussions, it is concluded that H-abstraction from the $-O_2O_3H_2$ group resulting in formation of $HOCH_2OO$ radical (R4) is feasible on both thermodynamically and kinetically.

Considering the different reaction sites of hydrogen atoms, the atmospheric transformation of $HOCH(CH_3)OOH$ from the *anti*-CH_3CHOO + H_2O reaction should have six types of H-abstraction pathways as presented in Figure 3. As shown in Figure 3, each H-abstraction reaction begins with the formation of a weakly bound hydrogen bonded pre-reactive complex with a six- or seven-membered ring structure in the entrance channel. Then it immediately transforms

into the respective product via the corresponding transition state. The $\Delta G_a^{\#}$ of H-abstraction from the -C_1H_3 (R6) and -$O_2O_3H_2$ (R8) groups are 2.2 and 1.7 kcal mol^{-1}, respectively, which are ~ 4-5 kcal mol^{-1} lower than those of R5 and R7. This result shows that R6 and R8 have nearly identical importance in the atmosphere. Compared with the barriers of H-abstraction at the C_α (R6) and C_β (R7) positions, it can be found that the former case is more favourable than the latter case. This conclusion is further supported by Jara-Toro's study for the reactions of OH radical with linear saturated alcohols (methanol, ethanol and n-propanol) that H-abstraction at the C_α position is predominant (Jara-Toro et al., 2017, 2018).

From Figure 4, it can be seen that H-abstraction from $HOC(CH_3)_2OOH$ includes eight possible pathways. All the H-abstraction reactions are strongly exothermic and spontaneous, signifying that they are thermodynamically feasible under atmospheric conditions. It deserves mentioning that the release of energy of R12 is significantly greater than those of R9-R11. For each H-abstraction pathway, a RC with a six- or seven-membered ring structure is formed prior to the corresponding TS, which is more stable than the separate reactants due to the hydrogen bond interactions between $HOC(CH_3)_2OOH$ and OH radical. Then, the RC overcomes modest barrier to reaction. The $\Delta G_a^{\#}$ of H-abstraction from the -$O_2O_3H_2$ group (R12) is 2.7 kcal mol^{-1}, which is the lowest among these eight H-abstraction reactions. This result again shows that the H-abstraction from the -$O_2O_3H_2$ group leading to the formation of $HOC(CH_3)_2OO$ radical is the dominant pathway.

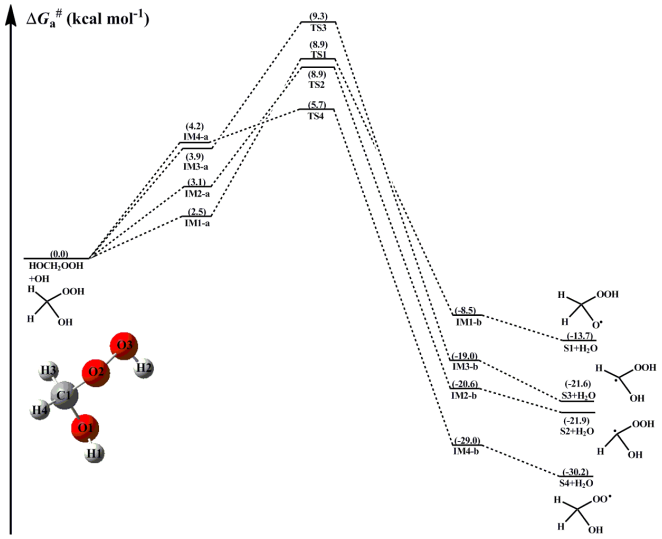

Figure 2. PES ($\Delta G_a^{\#}$) for the OH-initiated reactions of $HOCH_2OOH$ from the CH_2OO + H_2O reaction predicted at the M06-2X/ma-TZVP//M06-2X/6-311+G(2df,2p) level of theory (a and b represent the pre-reactive and post-reactive complexes)

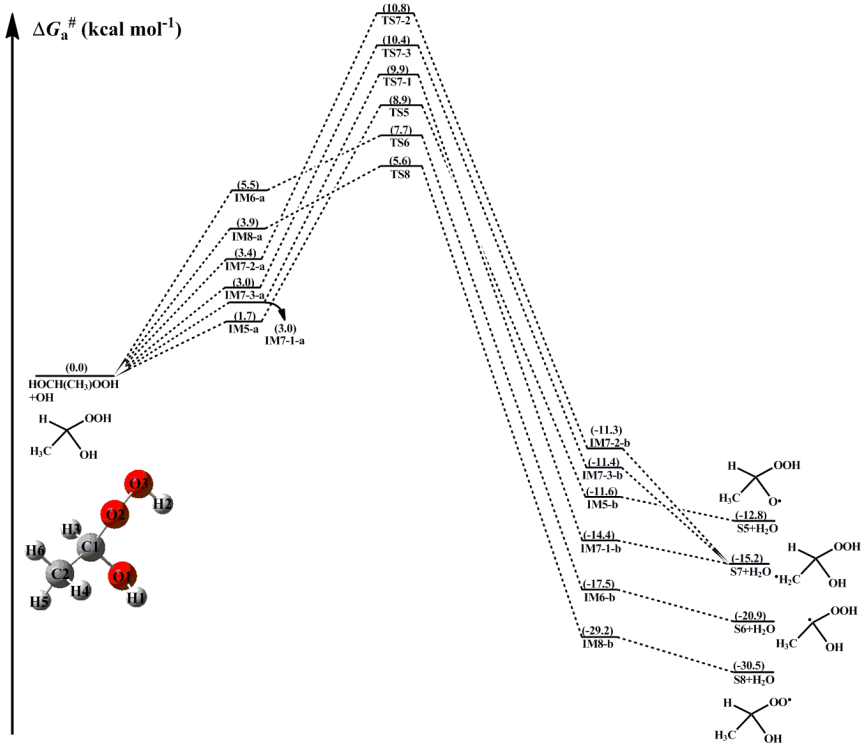

Figure 3. PES ($\Delta G_a^{\#}$) for the OH-initiated reactions of $HOCH(CH_3)OOH$ from the *anti*-CH_3CHOO + H_2O reaction predicted at the M06-2X/ma-TZVP//M06-2X/6-311+G(2df,2p) level of theory (a and b represent the pre-reactive and post-reactive complexes)

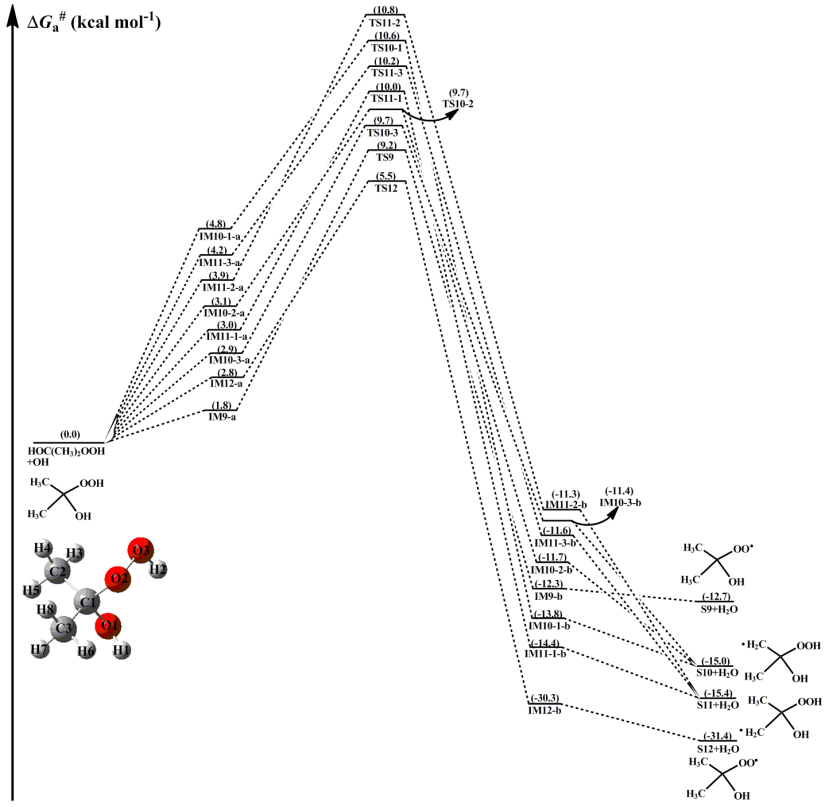

Figure 4. PES ($\Delta G_a^{\#}$) for the OH-initiated reactions of $HOC(CH_3)_2OOH$ from the $(CH_3)_2COO$ + H_2O reaction predicted at the M06-2X/ma-TZVP//M06-2X/6-311+G(2df,2p) level of theory (a and b represent the pre-reactive and post-reactive complexes)

Corresponding descriptions have been revised in the page 10 line 253-280, page 11 line 281-288 and page 12 line 309-320 of the revised manuscript:

As can be seen in Figure 2, the reaction for $HOCH_2OOH$ with OH radical proceeds via four distinct pathways: H-abstraction from the -O_1H_1 (R1), -C_1H_3 (R2), -C_1H_4 (R3) and -$O_2O_3H_2$ groups (R4). For each pathway, a pre-reactive complex with a six- or seven-membered ring structure is formed in the entrance channel, which is stabilized by hydrogen bond interactions between the oxygen atom of OH radical and the abstraction hydrogen atom of $HOCH_2OOH$, and the remnant hydrogen atom of OH radical and one of oxygen atoms of $HOCH_2OOH$. Then, it surmounts modest barrier that is higher in energy than the reactants to reaction. The reaction barrier $\Delta G_a^{\#}$ are reduced in the order of 6.4 (R1) > 5.8 (R2) $\approx$ 5.4 (R3) > 1.5 (R4) kcal mol^{-1}, indicating that H-abstraction from the -$O_2O_3H_2$ group (R4) is more preferable than those from the -O_1H_1, -C_1H_3 and -C_1H_4 groups (R1-R3). The difference of barrier heights can be attributed to the bond dissociation energy (BDE) of different types of bonds in $HOCH_2OOH$ molecule. The BDE are decreased in the order of 103.7 (O_1-H_1) > 98.2 (C_1-H_3) $\approx$ 97.4 (C_1-H_4) > 87.2 (O_3-H_2) kcal mol^{-1}, which are in good agreement with the order of barrier heights of distinct H-abstraction reactions. As indicated by their reaction free energy values, it can be found that the exothermicity of R4 is the largest among these four H-abstraction reactions. Based on the above discussions, it is concluded that H-abstraction from the -$O_2O_3H_2$ group resulting in formation of $HOCH_2OO$ radical (R4) is feasible on both thermodynamically and kinetically.

Considering the different reaction sites of hydrogen atoms, the atmospheric transformation of $HOCH(CH_3)OOH$ from the anti-CH_3CHOO + H_2O reaction should have six types of H-abstraction pathways as presented in Figure 3. As shown in Figure 3, each H-abstraction reaction begins with the formation of a weakly bound hydrogen bonded pre-reactive complex with a six- or seven-membered ring structure in the entrance channel. Then it immediately transforms into the respective product via the corresponding transition state. The $\Delta G_a^{\#}$ of H-abstraction from the -C_1H_3 (R6) and -$O_2O_3H_2$ (R8) groups are 2.2 and 1.7 kcal mol^{-1}, respectively, which are ~ 4-5 kcal mol^{-1} lower than those of R5 and R7. This result shows that R6 and R8 have nearly identical importance in the atmosphere. Compared with the barriers of H-abstraction at the C_α (R6) and C_β (R7) positions, it can be found that the former case is more favourable than the latter case. This conclusion is further supported by Jara-Toro's study for the reactions of OH radical with linear

saturated alcohols (methanol, ethanol and n-propanol) that H-abstraction at the C_α position is predominant (Jara-Toro et al., 2017, 2018).

From Figure 4, it can be seen that H-abstraction from $HOC(CH_3)_2OOH$ includes eight possible pathways. All the H-abstraction reactions are strongly exothermic and spontaneous, signifying that they are thermodynamically feasible under atmospheric conditions. It deserves mentioning that the release of energy of R12 is significantly greater than those of R9-R11. For each H-abstraction pathway, a RC with a six- or seven-membered ring structure is formed prior to the corresponding TS, which is more stable than the separate reactants due to the hydrogen bond interactions between $HOC(CH_3)_2OOH$ and OH radical. Then, the RC overcomes modest barrier to reaction. The $\Delta G_a^{\#}$ of H-abstraction from the $-O_2O_3H_2$ group (R12) is 2.7 kcal mol^{-1}, which is the lowest among these eight H-abstraction reactions. This result again shows that the H-abstraction from the $-O_2O_3H_2$ group leading to the formation of $HOC(CH_3)_2OO$ radical is the dominant pathway.

13 The following statement:" pseudo-first-order rate constant k'_{HO2} of ~ 10^{-2} s^{-1} in the forest environments" is completely condition dependent and cannot be represented by a single value. A range of values would be equally ambiguous, yet still better.

Response: Based on the Reviewer's suggestion, the range of pseudo-first-order rate constant k'_{HO2} is given in the revised manuscript. The rate coefficients of distinct RO_2 radicals reactions with HO_2 radical exhibit a weakly negative temperature dependence, translating into the pseudo-first-order rate constant k'_{HO2} of 1-5 × 10^{-2} s^{-1} in the forest environments.

Corresponding descriptions have been revised in the page 30 line 710-712 of the revised manuscript:

The calculated rate coefficients exhibit a weakly negative temperature dependence, translating into the pseudo-first-order rate constant k'_{HO2} of 1-5 × 10^{-2} s^{-1} in the forest environments.

14 I am not sure if I can follow what is meant by this: "(e) The rate-limiting step is the hydrogen abstraction by O_2 in the processes of $HOCH_2OO$ radical reaction with NO, while it becomes the C-C bond scission when one or two methyl substitutions occur at the C1-position of $HOCH_2OO$

radical." Please clarify and reword the statement.

Response: Based on the Reviewer's suggestion, the statement on the mentioned sentence has been reworded in the revised manuscript. The $HOCH_2O$ radical formed from the reaction of $HOCH_2OO$ radical with NO has two kinds of pathways (Figure 10): (1) it directly decomposes into CH_2O and OH radical (R40) via β-site C_1-O_1 bond scission with the barrier of 52.4 kcal mol^{-1}; (2) it converts into HCOOH and HO_2 radical (R41) through H-abstraction by O_2 with the barrier of 26.4 kcal mol^{-1}. This result reveals that R41 is the most feasible channel in the fragmentation of $HOCH_2O$ radical. The resulting $HOCH(CH_3)O$ radical from the $HOCH(CH_3)OO\cdot$ + NO reaction has three types of pathways (Figure 11). The first one is β-site C_1-C_2 bond scission leading to the formation of HCOOH + CH_3 (R45) with the barrier of 8.3 kcal mol^{-1}. The second one is β-site C_1-O_1 bond cleavage resulting in formation of CH_3COH + OH (R46) with the barrier of 26.7 kcal mol^{-1}. The third one is H-abstraction by O_2 leading to CH_3COOH + $HO_2\cdot$ (R47) with the barrier of 26.2 kcal mol^{-1}. Based on the calculated reaction barriers, it can be found that β-site C_1-C_2 bond scission is the dominant pathway in the fragmentation of $HOCH(CH_3)O$ radical. The $HO(CH_3)_2CO$ radical formed from the $HOC(CH_3)_2OO\cdot$ + NO reaction can either dissociate to CH_3COOH + $CH_3\cdot$ (R51) via the C_1-C_3 bond scission with the barrier of 8.2 kcal mol^{-1}, or decompose into CH_3COCH_3 + OH (R52) through the C_1-O_1 bond breaking with the barrier of 24.3 kcal mol^{-1} (Figure 12). The result again shows that the β-site C-C bond scission is the dominate pathway.

In summary, reaction with O_2 forming formic acid and HO_2 radical is the dominant removal pathway for $HOCH_2O$ radical formed from the reaction of $HOCH_2OO$ radical with NO. The β-site C-C bond scission is the dominate pathway in the dissociation of $HOCH(CH_3)O$ and $HOC(CH_3)_2O$ radicals formed from the $HOCH(CH_3)OO\cdot$ + NO and $HOC(CH_3)_2OO\cdot$ + NO reactions.

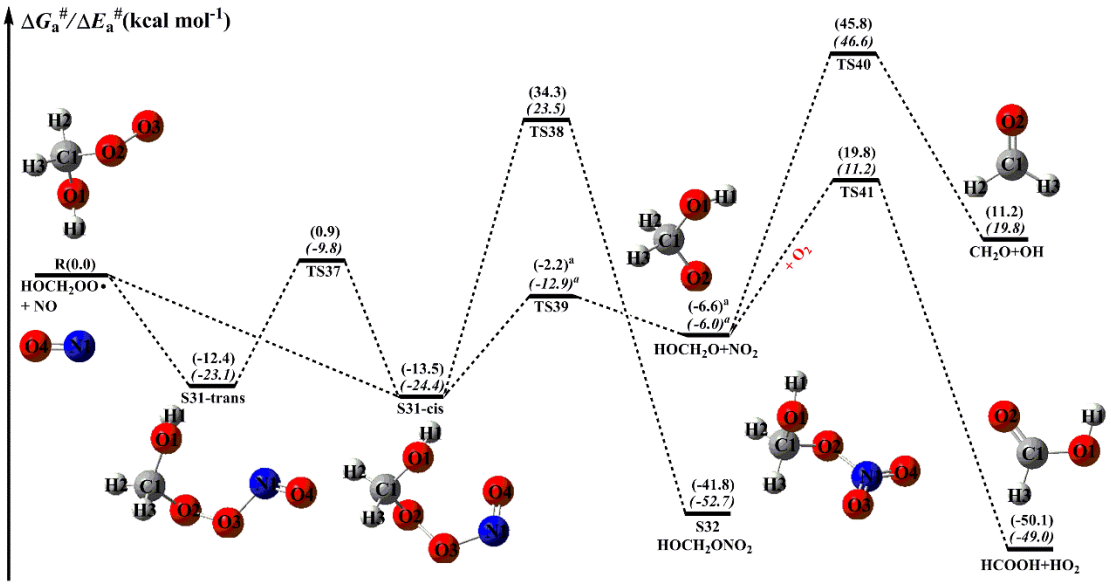

Figure 10. PES ($\Delta G_a^{\#}$ and $\Delta E_a^{\#}$, in italics) for the reaction of $HOCH_2OO$ radical with NO predicted at the M06-2X/ma-TZVP//M06-2X/6-311+G(2df,2p) level of theory (the superscript a is calculated at the MP2/ma-TZVP//MP2/6-311+G(2df,2p) level)

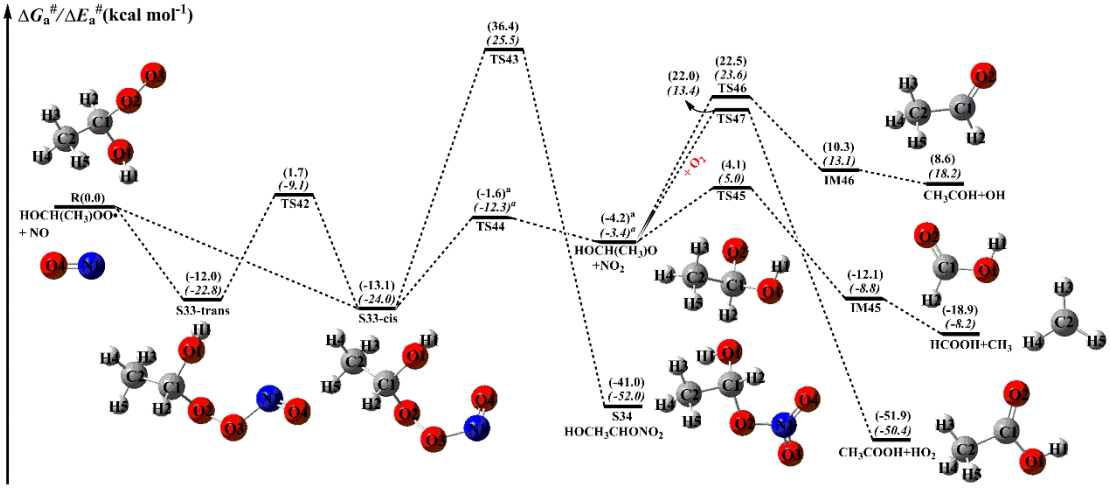

Figure 11. PES ($\Delta G_a^{\#}$ and $\Delta E_a^{\#}$, in italics) for the reaction of $HOCH(CH_3)OO$ radical with NO predicted at the M06-2X/ma-TZVP//M06-2X/6-311+G(2df,2p) level of theory (the superscript a is calculated at the MP2/ma-TZVP//MP2/6-311+G(2df,2p) level)

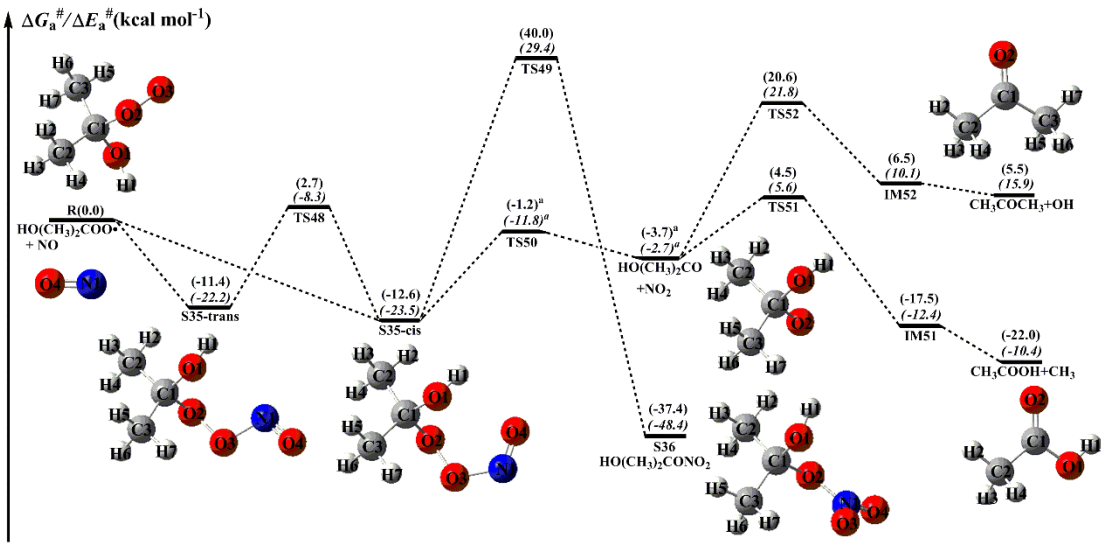

Figure 12. PES ($\Delta G_a^{\#}$ and $\Delta E_a^{\#}$, in italics) for the reaction of $HO(CH_3)_2COO$ radical with NO predicted at the M06-2X/ma-TZVP//M06-2X/6-311+G(2df,2p) level of theory (the superscript a is calculated at the MP2/ma-TZVP//MP2/6-311+G(2df,2p) level)

Corresponding descriptions have been revised in the page 26 line 624-629, page 27 line 633-640, page 27 line 648-652 and page 30 line 713-717 of the revised manuscript:

The formed $HOCH_2O$ radical has two kinds of pathways: (1) it directly decomposes into CH_2O and OH radical (R40) via β-site C_1-O_1 bond scission with the barrier of 52.4 kcal mol^{-1}; (2) it converts into HCOOH and HO_2 radical (R41) through H-abstraction by O_2 with the barrier of 26.4 kcal mol^{-1}. This result reveals that R41 is the most feasible channel in the fragmentation of $HOCH_2O$ radical.

The resulting $HOCH(CH_3)O$ radical has three types of pathways. The first one is β-site C_1-C_2 bond scission leading to the formation of HCOOH + CH_3 (R45) with the barrier of 8.3 kcal mol^{-1}. The second one is β-site C_1-O_1 bond cleavage resulting in formation of CH_3COH + OH (R46) with the barrier of 26.7 kcal mol^{-1}. The third one is H-abstraction by O_2 leading to CH_3COOH + HO_2 ·(R47) with the barrier of 26.2 kcal mol^{-1}. Based on the calculated reaction barriers, it can be found that β-site C_1-C_2 bond scission is the dominant pathway in the fragmentation of $HOCH(CH_3)O$ radical.

The formed $HO(CH_3)_2CO$ radical can either dissociate to CH_3COOH + CH_3 ·(R51) via the C_1-C_3 bond scission with the barrier of 8.2 kcal mol^{-1}, or decompose into CH_3COCH_3 + OH (R52) through the C_1-O_1 bond breaking with the barrier of 24.3 kcal mol^{-1}. The result again shows that the β-site C-C bond scission is the dominate pathway.

Reaction with O_2 forming formic acid and HO_2 radical is the dominant removal pathway for $HOCH_2O$ radical formed from the reaction of $HOCH_2OO$ radical with NO. The β-site C-C bond scission is the dominate pathway in the dissociation of $HOCH(CH_3)O$ and $HOC(CH_3)_2O$ radicals formed from the $HOCH(CH_3)OO$ ·+ NO and $HOC(CH_3)_2OO$ ·+ NO reactions.

15 It is unclear what is meant by the following statement "One reason for the barrier difference could lie in the fact that the bond dissociation energies (BDE) of different types of bonds are significantly different in the $HOCH_2OOH$ molecule."

Response: The free-energy and electronic-energy PESs for the initiation reactions of OH radical with $HOCH_2OOH$ are displayed in Figure 2 and S1, respectively. As can be seen in Figure 2, the reaction for $HOCH_2OOH$ with OH radical proceeds via four distinct pathways: H-abstraction from the $-O_1H_1$ (R1), $-C_1H_3$ (R2), $-C_1H_4$ (R3) and $-O_2O_3H_2$ groups (R4). The reaction barrier $\Delta G_a^{\#}$ are reduced in the order of 6.4 (R1) > 5.8 (R2) ≈ 5.4 (R3) > 1.5 (R4) kcal mol^{-1}, indicating that H-abstraction from the $-O_2O_3H_2$ group (R4) is more preferable than those from the $-O_1H_1$, $-C_1H_3$ and $-C_1H_4$ groups (R1-R3). Same conclusion is also derived from the energy barriers $\Delta E_a^{\#}$ that R4 is the most favorable H-abstraction pathway (Figure S1). The difference of barrier heights can be attributed to the bond dissociation energy (BDE) of different types of bonds in $HOCH_2OOH$ molecule. The BDE are decreased in the order of 103.7 (O_1-H_1) > 98.2 (C_1-H_3) ≈ 97.4 (C_1-H_4) > 87.2 (O_3-H_2) kcal mol^{-1}, which are in good agreement with the order of barrier heights of H-abstraction reactions.

Corresponding descriptions have been revised in the page 10 line 253-269 of the revised manuscript:

As can be seen in Figure 2, the reaction for $HOCH_2OOH$ with OH radical proceeds via four distinct pathways: H-abstraction from the $-O_1H_1$ (R1), $-C_1H_3$ (R2), $-C_1H_4$ (R3) and $-O_2O_3H_2$ groups (R4). The reaction barrier $\Delta G_a^{\#}$ are reduced in the order of 6.4 (R1) > 5.8 (R2) ≈ 5.4 (R3) > 1.5 (R4) kcal mol^{-1}, indicating that H-abstraction from the $-O_2O_3H_2$ group (R4) is more preferable than those from the $-O_1H_1$, $-C_1H_3$ and $-C_1H_4$ groups (R1-R3). Same conclusion is also derived from the energy barriers $\Delta E_a^{\#}$ that R4 is the most favorable H-abstraction pathway (Figure S1). The difference of barrier heights can be attributed to the bond dissociation energy (BDE) of different types of bonds in $HOCH_2OOH$ molecule. The BDE are decreased in the order of 103.7

(O_1-H_1) > 98.2 (C_1-H_3) ≈ 97.4 (C_1-H_4) > 87.2 (O_3-H_2) kcal mol^{-1}, which are in good agreement with the order of barrier heights of H-abstraction reactions.

16 I would like to see the rates obtained (k vs T) also in Figures in relation to each other, and not just as Tables. I think this could be very useful to the reader, as the tabular format is more difficult to compare.

Response: Based on the Reviewer's suggestion, the rate coefficients versus temperature have been plotted in figures of the revised manuscript.

17 I find it a bit odd to state that a single channel of hydroxymethylperoxy radical oxidation giving HO_2 radical is "a new source of HO_2 radical in the troposphere". I mean, can this specific radical have even a minute influence on the tropospheric HO_2 burden?

Response: Kumar and Francisco investigated the gas phase decomposition of α-hydroxymethylperoxy radical $HOCH_2OO$ by using quantum chemical method (Kumar et al., 2015). It was found that the $HOCH_2OO$ radical decomposition represents a new source of HO_2 radical in the troposphere. This finding may help in understanding the discrepancy between the modeled and measured concentrations of HO_2 radical in the troposphere. However, to the best of our knowledge, the contribution of the $HOCH_2OO$ radical decomposition to the tropospheric HO_2 radical burden is still unknown. In the future work, we will adopt the combination of quantum chemistry and numerical simulation to estimate the contribution of the $HOCH_2OO$ radical decomposition to the tropospheric HO_2 radical burden.

18 In the beginning of chapter 3.2., you are missing the second RO produced in the reaction.

Response: Based on the Reviewer's suggestion, the second RO radical formed from the self-reaction of RO_2 radicals has been added in the revised manuscript. The self-reactions of RO_2 radicals can either produce RO ·+ R'O ·+ O_2 (propagation channel), or generate ROH + R'(-H, =O) + O_2 or produce ROOR + O_2 (termination channel) that has been recognized as an important SOA precursor.

Corresponding descriptions have been revised in the page 15 line 387-390 of the revised manuscript:

The self-reactions of RO_2 radicals can either produce $RO\cdot + R'O\cdot + O_2$ (propagation channel), or generate ROH + R'(-H, =O) + O_2 or produce ROOR + O_2 (termination channel) that has been recognized as an important SOA precursor (Berndt et al., 2018; Zhang et al., 2012)

19 Chapter 3.2.1: Mark all radicals the same way (i.e., with similar dot).

Response: Based on the Reviewer's suggestion, the dot is applied to mark all radicals in the revised manuscript.

20 Chapter 3.2.1: It is rather disappointing to hear that "It is worth noting that the termination products are not found in the $HO(CH_3)_2COO$ radical reaction system owing to the absence of alpha hydrogen atom." when it was just in previous sentence stated that:" is not discussed in detail to avoid redundancy." Please explain further these currently missing channels.

Response: Based on the Reviewer's suggestion, the missing pathways for the self-reaction of $HO(CH_3)_2COO$ radical have been added in the revised manuscript. Figure 7 depicts a schematic PES for the self-reaction of $HOC(CH_3)_2OO$ radical. As shown in Figure 7, the dominant pathway for the self-reaction of $HO(CH_3)_2COO$ radical begins with the formation of tetroxide intermediate S24 via an oxygen-to-oxygen coupling transition state TS28 with the barrier of 20.4 kcal·mol^{-1}; then it transforms into the caged tetroxide intermediate S26 of overall singlet spin multiplicity through the asymmetric two-step O-O bond cleavage with the barriers of 22.0 and 3.4 kcal·mol^{-1}; finally, S26 can either produce two $HO(CH_3)_2CO$ radicals with the exoergicity of 10.3 kcal·mol^{-1}, or generate dimer S27 with the exothermicity of 31.5 kcal·mol^{-1}. Different the self-reactions of $HOCH_2OO$ and $HOCH(CH_3)OO$ radicals, the termination product of the self-reaction of $HOC(CH_3)_2OO$ radical is exclusively dimer S27. The reason is due to the absence of alpha hydrogen atom in $HOC(CH_3)_2OO$ radical.

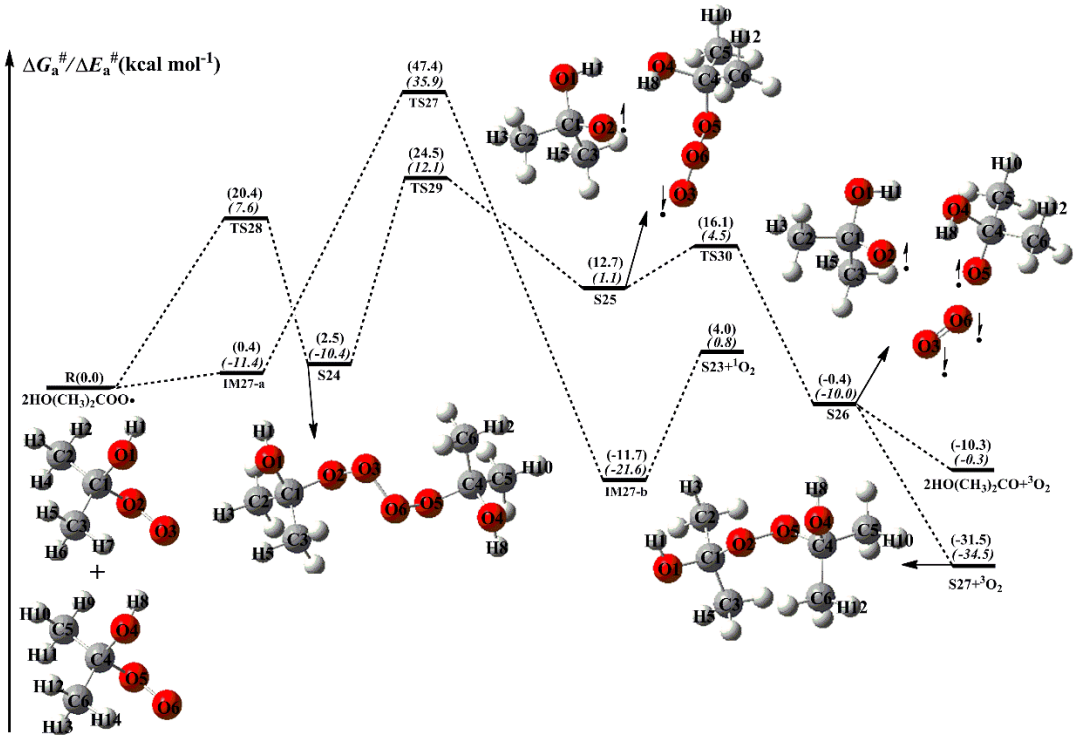

Figure 7. PES ($\Delta G_a^{\#}$ and $\Delta E_a^{\#}$, in italics) for the self-reaction of $HO(CH_3)_2COO$ radicals predicted at the M06-2X/ma-TZVP//M06-2X/6-311+G(2df,2p) level of theory

Corresponding descriptions have been revised in the page 18 line 465-475 of the revised manuscript:

As shown in Figure 7, the dominant pathway for the self-reaction of $HO(CH_3)_2COO$ radical begins with the formation of tetroxide intermediate S24 via an oxygen-to-oxygen coupling transition state TS28 with the barrier of 20.4 kcal mol^{-1}; then it transforms into the caged tetroxide intermediate S26 of overall singlet spin multiplicity through the asymmetric two-step O-O bond cleavage with the barriers of 22.0 and 3.4 kcal mol^{-1}; finally, S26 can either produce two $HO(CH_3)_2CO$ radicals with the exoergicity of 10.3 kcal mol^{-1}, or generate dimer S27 with the exothermicity of 31.5 kcal mol^{-1}. Different the self-reactions of $HOCH_2OO$ and $HOCH(CH_3)OO$ radicals, the termination product of the self-reaction of $HOC(CH_3)_2OO$ radical is exclusively dimer S27. The reason is due to the absence of alpha hydrogen atom in $HOC(CH_3)_2OO$ radical.

21 It is stated that "The main primary sources of HO_2 radical in the atmosphere are from the photolysis of CH_2O and OVOCs, and the ozonolysis reactions". I guess the authors meant "photo-oxidation" rather than "photolysis" here.

Response: Based on the Reviewer's suggestion, the word "photolysis" has been replaced by

"photo-oxidation" in the revised manuscript. The main sources of HO_2 radical involve the photo-oxidation of oxygenated volatile organic compounds (OVOCs) and the ozonolysis reaction.

Corresponding descriptions have been revised in the page 21 line 496-498 of the revised manuscript:

The main sources of HO_2 radical involve the photo-oxidation of oxygenated volatile organic compounds (OVOCs) and the ozonolysis reaction.

22 I wonder if you could find a better reference for [HO_2] (and other atmospheric concentrations) than Bianchi et al. 2019. To me it seems that those numbers are somewhat questionable, or perhaps better to say that it feels odd that you can give such a "common value" for a whole type-of-an-environment. Is single value really realistic?

Response: Based on the Reviewer's suggestion, the concentrations of HO_2 radical have been corrected in the revised manuscript. The atmospheric concentration of HO_2 radical is 1.5-10 $\times 10^8$ molecules cm^{-3} at ground level in polluted urban environments (Stone et al., 2012).

Corresponding descriptions have been revised in the page 21 line 502-503 of the revised manuscript:

The atmospheric concentration of HO_2 radical is 1.5-10 $\times$ 10^8 molecules cm^{-3} at ground level in polluted urban environments (Stone et al., 2012).

23 According to "HOM review" by Bianchi et al, almost none of the compounds in the work of Noziere and Vereecken would be labelled HOMs, and thus I would strongly advice to change the referencing of the following sentence: "…one after the other, and the resulting finally HOMs (Nozière and Vereecken, 2019; Vereecken and Nozière, 2020)."

Response: Based on the Reviewer's suggestion, the references of the formation mechanism of HOMs have been changed in the revised manuscript. The autoxidation mechanism includes an intramolecular H-shift from the $-CH_3$ or $-CH_2-$ groups to the -OO ·site, resulting in formation of a hydroperoxyalkyl radical QOOH, followed by O_2 addition to form a new peroxy radical ($HOOQO_2$), one after the other, and the resulting finally HOMs (Berndt et al., 2015; Rissanen et al., 2014).

Corresponding descriptions have been revised in the page 23 line 541-545 of the revised manuscript:

The autoxidation mechanism includes an intramolecular H-shift from the -CH_3 or -CH_2- groups to the -OO ·site, resulting in formation of a hydroperoxyalkyl radical QOOH, followed by O_2 addition to form a new peroxy radical ($HOOQO_2$), one after the other, and the resulting finally HOMs (Rissanen et al., 2014; Berndt et al., 2015).

24 What is meant by: "It deserves mentioning that the conformers $HOCH_2OO$-c and $HOCH_2OO$-d are not proceed H-shift reactions."

Response: For the H-shift reactions of RO_2 radical, reactants, transition states and products have multiple conformers. Previous literatures have demonstrated that the reaction kinetics of multiconformers involvement are more precisely than that of the single conformer approximation (Møller et al., 2016, 2020). Herein, the multiconformers treatment is performed to investigate the H-shift reactions of RO_2 radical. A conformer search within the Molclus program is employed to generate a pool of conformers for RO_2 radicals. The selected conformers are further optimized at the M06-2X/6-311+G(2df,2p) level of theory, followed by single-point energies calculations at the M06-2X/ma-TZVP level of theory. Based on the calculated results, it can be found that $HOCH_2OO$ radical has four energetically similar conformers ($HOCH_2OO$-a, $HOCH_2OO$-b, $HOCH_2OO$-c and $HOCH_2OO$-d). The relative free energy and Boltzmann population (w_i) of individual conformer are listed in Table S6. As shown in Table S6, the Boltzmann populations of these four conformers are 46.39, 46.31, 2.99 and 4.32%, respectively.

A schematic PES for the H-shift reactions of $HOCH_2OO$ radical is drawn in Figure 9. As can be seen in Figure 9, the lowest-energy conformer $HOCH_2OO$-a can proceed via a 1,3-H shift from the -CH_2 group to the terminal oxygen leading to the formation of S28-a (HO·CHOOH) with the barrier of 41.6 kcal·mol^{-1}. $HOCH_2OO$-b can isomerize to S28-b1 and S28-b2 via the four-membered ring transition states TS34-b1 and TS34-b2 (1,3-H shifts) with the barriers of 41.6 and 45.0 kcal·mol^{-1}. But these three 1,3-H shift reactions have comparatively high barrier, making them irrelevant in the atmosphere. Despite many attempts, the transition states of H-shift reactions of $HOCH_2OO$-c and $HOCH_2OO$-d are not located. The result implies that the H-shift reactions of these two conformers are inhibited, which is consistent with the previous study that

not all reactants will be in a conformation with a path across the barrier to reaction in the H-shift reactions of RO_2 radicals (Møller et al., 2016).

Corresponding descriptions have been revised in the page 7 line 195-203 and page 23 line 547-564 of the revised manuscript:

For the H-shift reactions of peroxy radicals RO_2, reactants, transition states and products have multiple conformers. Previous literatures have demonstrated that the reaction kinetics of multiconformers involvement are more precisely than that of the single conformer approximation (Møller et al., 2016, 2020). Herein, the multiconformers treatment is performed to investigate the H-shift reactions RO_2 radicals. A conformer search within the Molclus program is employed to generate a pool of conformers for RO_2 radicals (Lu, 2020). The selected conformers are further optimized at the M06-2X/6-311+G(2df,2p) level of theory, followed by single-point energies calculations at the M06-2X/ma-TZVP level of theory.

Based on the calculated results, it can be found that $HOCH_2OO$ radical has four energetically similar conformers ($HOCH_2OO$-a, $HOCH_2OO$-b, $HOCH_2OO$-c and $HOCH_2OO$-d). The relative free energy and Boltzmann population (w_i) of individual conformer are listed in Table S6. As shown in Table S6, the Boltzmann populations of these four conformers are 46.39, 46.31, 2.99 and 4.32%, respectively. A schematic PES for the H-shift reactions of $HOCH_2OO$ radical is displayed in Figure 9. As can be seen in Figure 9, the lowest-energy conformer $HOCH_2OO$-a can proceed via a 1,3-H shift from the -CH_2 group to the terminal oxygen leading to the formation of S28-a (HO CHOOH) with the barrier of 41.6 kcal mol^{-1}. $HOCH_2OO$-b can isomerize to S28-b1 and S28-b2 via the four-membered ring transition states TS34-b1 and TS34-b2 (1,3-H shifts) with the barriers of 41.6 and 45.0 kcal mol^{-1}. But these three 1,3-H shift reactions have comparatively high barriers, making them irrelevant in the atmosphere. Despite many attempts, the transition states of H-shift reactions of $HOCH_2OO$-c and $HOCH_2OO$-d are not located. The result implies that the H-shift reactions of these two conformers are inhibited, which is consistent with the previous study that not all reactants will be in a conformation with a path across the barrier to reaction in the H-shift reactions of RO_2 radicals (Møller et al., 2016).

25 Where is the SAR mentioned in the title?

Response: Based on the Reviewer's suggestion, the structure-activity relationship on the

initiation reactions of OH radicals with distinct HHPs has been added in the revised manuscript. The dominant pathway is the H-abstraction from the -OOH group in the initiation reactions of OH radical with $HOCH_2OOH$. H-abstraction from -CH group is competitive with that from the -OOH group in the reaction of OH radical with $HOCH(CH_3)OOH$. Compared the barriers of H-abstraction from the -OOH and $-CH_2$ groups in the OH + $HOCH_2OOH$ system with that for the analogous reactions in the OH + $HOCH(CH_3)OOH$ system. It can be found that the barrier of H-abstraction from the -CH group is reduced by 3.6 kcal mol^{-1}, whereas the barrier of H-abstraction from the -OOH group is increased by 0.2 kcal mol^{-1} when a methyl group substitution occurs at the C1-position of $HOCH_2OOH$. The dominant pathway is the H-abstraction from the -OOH group in the reaction of OH radical with $HOC(CH_3)_2OOH$, and the barrier height is increased by 1.2 kcal mol^{-1} compared to the OH + $HOCH_2OOH$ system. The barrier of H-abstraction from the -OOH group is slightly increased as the number of methyl group is increased. It is interesting to compare the rate coefficient of dominant pathway in the OH + $HOCH_2OOH$ system with that for the analogous reactions in the OH + $HOCH(CH_3)OOH$ and OH + $HOC(CH_3)_2OOH$ reactions. It can be found that the rate coefficient is almost identical when a methyl group substitution occurs at the C_1-position, whereas the rate coefficient reduces by a factor of 2-5 when two methyl groups introduce into the C_1-position.

Corresponding descriptions have been added in the page 13 line 353-371 of the revised manuscript:

The dominant pathway is the H-abstraction from the -OOH group in the initiation reactions of OH radical with $HOCH_2OOH$. H-abstraction from -CH group is competitive with that from the -OOH group in the reaction of OH radical with $HOCH(CH_3)OOH$. Compared the barriers of H-abstraction from the -OOH and $-CH_2$ groups in the OH + $HOCH_2OOH$ system with that for the analogous reactions in the OH + $HOCH(CH_3)OOH$ system. It can be found that the barrier of H-abstraction from the -CH group is reduced by 3.6 kcal mol^{-1}, whereas the barrier of H-abstraction from the -OOH group is increased by 0.2 kcal mol^{-1} when a methyl group substitution occurs at the C1-position of $HOCH_2OOH$. The dominant pathway is the H-abstraction from the -OOH group in the reaction of OH radical with $HOC(CH_3)_2OOH$, and the barrier height is increased by 1.2 kcal mol^{-1} compared to the OH + $HOCH_2OOH$ system. The barrier of H-abstraction from the -OOH group is slightly increased as the number of methyl

group is increased. It is interesting to compare the rate coefficient of dominant pathway in the $\dot{O}H + HOCH_2OOH$ *system with that for the analogous reactions in the* $\dot{O}H + HOCH(CH_3)OOH$ *and* $\dot{O}H + HOC(CH_3)_2OOH$ *reactions. It can be found that the rate coefficient is almost identical when a methyl group substitution occurs at the* C_1*-position, whereas the rate coefficient reduces by a factor of 2-5 when two methyl groups introduce into the* C_1*-position.*

References

Bach, R. D., Dmitrenko, O., and Estévez, C. M.: Chemical behavior of the biradicaloid (HO ··ONO) singlet states of peroxynitrous acid. the oxidation of hydrocarbons, sulfides, and selenides, J. Am. Chem. Soc., 127, 3140-3155, https://doi.org/10.1021/ja044245d, 2005.

Berndt, T., Richters, S., Kaethner, R., Voigtländer, J., Stratmann, F., Sipilä, M., Kulmala, M., and Herrmann, H.: Gas-phase ozonolysis of cycloalkenes: formation of highly oxidized RO_2 radicals and their reactions with NO, NO_2, SO_2, and Other RO_2 radicals, J. Phys. Chem. A, 119, 10336-10348, https://doi.org/10.1021/acs.jpca.5b07295, 2015.

Berndt, T., Scholz, W., Mentler, B., Fischer, L., Herrmann, H., Kulmala, M., and Hansel, A.: Accretion product formation from self- and cross-reactions of RO_2 radicals in the atmosphere, Angew. Chem. Int. Ed., 57, 3820-3824, https://doi.org/10.1002/anie.201710989, 2018.

Bianchi, F., Kurten, T., Riva, M., Mohr, C., Rissanen, M. P., Roldin, P., Berndt, T., Crounse, J. D., Wennberg, P. O., Mentel, T. F., Wildt, J., Junninen, H., Jokinen, T., Kulmala, M., Worsnop, D. R., Thornton, J. A., Donahue, N., Kjaergaard, H. G., and Ehn, M.: Highly oxygenated organic molecules (HOM) from gas-phase autoxidation involving peroxy radicals: a key contributor to atmospheric aerosol, Chem. Rev., 119, 3472-3509, https://doi.org/10.1021/acs.chemrev.8b00395, 2019.

Crounse, J. D., Nielsen, L. B., Jørgensen, S., Kjaergaard, H. G., and Wennberg, P. O.: Autoxidation of organic compounds in the atmosphere, J. Phys. Chem. Lett., 4, 3513-3520, https://doi.org/10.1021/jz4019207, 2013.

Ehn, M., Berndt, T., Wildt, J., and Mentel, T.: Highly oxygenated molecules from atmospheric autoxidation of hydrocarbons: a prominent challenge for chemical kinetics studies, Int. J. Chem. Kinet., 49, 821-831, https://doi.org/10.1002/kin.21130, 2017.

Jara-Toro, R. A., Hernández, F. J., Garavagno, M. A., Taccone, R. A., and Pino, G. A.: Water catalysis of the reaction between hydroxyl radicals and linear saturated alcohols (ethanol and n-propanol) at 294 K, Phys. Chem. Chem. Phys., 20, 27885-27896, https://doi.org/10.1039/C8CP05411H, 2018.

Jara-Toro, R. A., Hernández, F. J., Taccone, R. A., Lane, S. I., and Pino, G. A.: Water catalysis of the reaction between methanol and OH at 294 K and the atmospheric implications, Angew. Chem., Int. Ed., 56, 2166-2170, https://doi.org/10.1002/anie.201612151, 2017.

Kumar, M., and Francisco, J. S.: Red-light-induced decomposition of an organic peroxy radical: a new source of the HO_2 radical, Angew. Chem. Int. Ed., 54, 15711-15714, https://doi.org/10.1002/anie.201509311, 2015.

Lee, R., Gryn'ova, G., Ingold, K. U., and Coote, M. L.: Why are sec-alkylperoxyl bimolecular self-reactions orders of magnitude faster than the analogous reactions of tert-alkylperoxyls? The unanticipated role of CH hydrogen bond donation, Phys. Chem. Chem. Phys., 18, 23673-23679, https://doi.org/10.1039/C6CP04670C, 2016.

Liang, Y. N., Li, J., Wang, Q. D., Wang, F., and Li, X. Y.: Computational study of the reaction mechanism of the methylperoxy self-reaction, J. Phys. Chem. A, 115, 13534-13541, https://doi.org/10.1021/jp2048508, 2011.

Møller, K. H., Berndt, T., and Kjaergaard, H. G.: Atmospheric autoxidation of amines, Environ. Sci. Technol., 54, 11087-11099, https://doi.org/10.1021/acs.est.0c03937, 2020.

Møller, K. H., Otkjær, R. V., Hyttinen, N., Kurtén, T., and Kjaergaard, H. G.: Cost-effective implementation of multiconformer transition state theory for peroxy radical hydrogen shift

reactions, J. Phys. Chem. A, 120, 10072-10087, https://doi.org/10.1021/acs.jpca.6b09370, 2016.

Nozière, B., and Vereecken, L.: Direct observation of aliphatic peroxy radical autoxidation and water effects: an experimental and theoretical study, Angew. Chem. Int. Ed., 58, 13976-13982, https://doi.org/10.1002/anie.201907981, 2019.

Rissanen, M. P., Kurtén,T., Sipila, M., Thornton, J. A., Kangasluoma, J., Sarnela, N., Junninen, H., Jørgensen, S., Schallhart, S., Kajos, M. K., Taipale, R., Springer, M., Mentel, T. F., Ruuskanen, T., Petäjä, T., Worsnop, D. R., Kjaergaard, H. G., and Ehn M.: The formation of highly oxidized multifunctional products in the ozonolysis of cyclohexene, J. Am. Chem. Soc., 136, 15596-15606, https://doi.org/10.1021/ja507146s, 2014.

Stone, D., Whalley, L. K., and Heard, D. E.: Tropospheric OH and HO_2 radicals: field measurements and model comparisons, Chem. Soc. Rev., 41, 6348-6404, https://doi.org/10.1039/c2cs35140d, 2012.

Zhang, P., Wang, W., Zhang, T., Chen, L., Du, Y., Li, C., and Lv, J.: Theoretical study on the mechanism and kinetics for the self-reaction of $C_2H_5O_2$ radicals, J. Phys. Chem. A, 116, 4610-4620, https://doi.org/10.1021/jp301308u, 2012.